

Cation Diffusion in Silicate Melts
Kationendiffusion in Silikatschmelzen

Vom Fachbereich Geowissenschaften und Geographie

der Universität Hannover

zur Erlangung des Grades

DOKTOR DER NATURWISSENSCHAFTEN

Dr. rer. nat.

genehmigte Dissertation

von

DIPL. MIN. ASTRID SABINE TEGGE-SCHÜRING

geboren am 19.07.1971 in Twistringen

2003

Referent: Prof. Dr. François Holtz, Universität Hannover

Koreferent: Prof. Dr. Youxue Zhang, University of Michigan

Tag der Promotion: 10. Juli 2002

Datum der Veröffentlichung: Juli 2003

DANKSAGUNG

Die vorliegende Arbeit wurde unter der Leitung von Prof. Dr. F. Holtz am Institut für Mineralogie der Universität Hannover angefertigt und von Dr. H. Behrens und Dr. J. Koepke betreut. Insbesondere Harald Behrens möchte ich für die endlosen Korrekturarbeiten, zahlreichen Anregungen und intensiven Diskussionen danken, die wesentlich zur Fertigstellung dieser Arbeit beigetragen haben. Ebenso sei Jürgen Koepke für Diskussionen und sein immer offenes Ohr für Mikrosonden- und SYRFA-Probleme gedankt. Herrn Prof. Youxue Zhang danke ich für die Übernahme des Koreferats und vor allem dafür, dass er mich während meines Aufenthalts in den USA in seiner Arbeitsgruppe an der University of Michigan aufgenommen und intensiv betreut und motiviert hat. Gerald Falkenberg und Karen Rickers möchte ich für die Betreuung an der SYRFA danken, sowie Michael Wiedenbeck für die Unterstützung an der SIMS. Max Wilke, Frank Schulze und auch dem gesamten Werkstattpersonal in Hannover gilt mein Dank für die Einweisung und Hilfe an den Gasdruckanlagen und der technischen Unterstützung bei experimentellen Problemen. Vor allem Otto Diedrich danke ich für die zahlreichen Präparationen meiner Versuchsprodukte, die gerade für die SYRFA sehr arbeitsintensiv waren. Tony Withers, Yang Liu und Melroy Borges möchte ich danken für den Erfahrungsaustausch bei Piston-Zylinder Experimenten und IR-Analysen und ganz besonders für die ständige Hilfsbereitschaft und der schönen Zeit in Ann Arbor. Kerstin, Susi, Jasper und vor allem Melli und Matthi möchte ich für den ständigen moralischen Beistand und die vielen motivierenden Worte während der harten Stunden dieser Arbeit danken und auch Marcus und Kevin sei für die Hilfe bei Computerproblemen und die witzigen Kommentare in unserem Büro gedankt.

HG danke ich einfach für alles.

CONTENTS

1. Introduction	7
1.1. Theoretical Background (Tracer vs. Chemical Diffusion)	9
1.2. Analytical Background (SYXRF vs SIMS)	11
2. Experimental Techniques	13
2.1. Sample Description	13
2.2. Experimental Setup	15
2.3. Pressure Apparatus and Run Conditions	17
3. Analytical Techniques	21
3.1. Sample Preparation	21
3.2. KFT and FTIR	21
3.3. Microprobe Analysis	24
3.4. SYXRF	24
3.5. SIMS	26
4. Results	29
4.1. Evaluation of Diffusion Profiles	30
4.2. Influence of non-diffusive Transport	30
4.3. Trace Element Diffusion	32
4.4. Diffusion Profiles evaluated by SYXRF and SIMS	35
4.5. Chemical Diffusion	37
4.6. Precision of Diffusion Data	38
4.7. Enhancement of Diffusivities by adding H ₂ O	39

4.8. Temperature Dependence of Diffusion in Rhyolitic Melts	41
4.9. Pressure Dependence of Diffusion in Dacitic Melts	43
5. Discussion	46
5.1. Comparison of SYXRF and SIMS Analyses	46
5.2. Effect of H ₂ O on Diffusion	47
5.3. Effect of Pressure on Diffusion	48
5.3.1. Comparison to other Diffusion Studies on Rhyolitic Melts	49
5.3.2. Hydrous Melts (> 0.5 wt% H ₂ O)	51
5.4. Comparison to other Melt Compositions	52
5.5. Speciation and Effect of Redox Conditions on Trace Element Diffusion	53
5.6. Predicting Trace Element Diffusivity	56
5.7. Relation of Diffusivities to Viscosity	59
6. Conclusion	63
7. References cited	65
8. Tables	77

ABSTRACT

Chemical diffusion of major components and trace element diffusion of a large variety of cations were studied in dacitic and rhyolitic melts. Dacitic glasses similar in composition to a dacite erupted from Unzen Volcano in Japan and rhyolitic glasses with compositions close to the natural obsidian of the Erevan Dry Fountain of Armenia (EDF) were synthesized for this study. To examine both diffusion processes simultaneously, the classical diffusion couple technique was modified by combining two diffusion couples of synthetic glass cylinders to one diffusion triple. In these experiments one end of the triple was enriched by 5 wt% SiO₂ and 0.3 wt% TiO₂ relative to the middle part in order to measure chemical diffusion of major components SiO₂ and Al₂O₃. The other end was doped with up to 23 trace elements belonging to different geochemical groups. Since small amounts of dissolved water may enhance the diffusion of elements, in addition to nominally anhydrous melts, hydrous melts containing up to 5 wt% H₂O were also investigated. Triple experiments were performed at 500 MPa in internally heated pressure vessels (1100-1400°C) and cold seal pressure vessels (800°C) for rhyolitic melts. Triple experiments with dacitic melts were performed at 100, 250 and 500 MPa in internally heated pressure vessels at 1200°C and in a piston cylinder at 1 GPa (1200-1400°C) with traditional diffusion couples.

Concentration profiles of major and trace elements were determined by electron microprobe and synchrotron x-ray fluorescence microanalysis, respectively. On some experimental run products diffusion profiles of trace elements were also measured by secondary ion mass spectrometry to certify diffusion data and to compare analytical techniques. Water distribution along the diffusion profiles was analyzed by infrared microspectroscopy. Diffusion profiles determined by both methods are in excellent agreement for the most elements, except for the transition metal elements Ni and Cu and the high field strength element Ta.

In rhyolitic melts trace element diffusivities of high valenced cations are close to the effective binary diffusion coefficients of the major components SiO₂ and Al₂O₃. This indicates that the network dynamics, which are related to viscosity, determine the mobility of these elements.

Trace element diffusivities systematically decrease at constant pressure, temperature and water content with ionic charge of the cation, except of Co, which was found to migrate faster than the other transition metal elements, whereas diffusivities of Cu are close to the diffusivities of the high valenced cations. Especially in rhyolitic melts the mobility of Eu is faster compared to the other rare earth elements, Sn migrates significant faster than Ge and Nb is faster than its neighbor element Zr. The relatively high mobility of Eu in rhyolitic melts compared to neighbor elements Sm and Gd may be attributed to contributions of divalent Eu. The ratio of Eu²⁺/Eu_{tot} derived from D_{Eu}, D_{Sr} and the average of D_{Gd} and D_{Sr}, has a minimum in rhyolitic melts close to 2 wt% water independent of temperature. Because the OH/H₂O ratio increases with water content, an explanation for this trend could be that complexes with OH groups stabilizes Eu³⁺ whereas complexes with H₂O molecules stabilizes Eu²⁺ in the melt. In general, the enhancing effect of water increases with the charge of the cation. A relatively strong dependence of diffusivity on water content was observed for Sn at 1200°C. This can be explained by a change in valence of Sn from 4+ at low water to 2+ at high water contents.

In rhyolitic melts activation energies calculated from simple Arrhenius relationships increase from Rb to Zr by about 100 kJ/mole at both 2 and 5 wt% H₂O. Activation energies for the water-poor rhyolitic melts increase from 100 kJ/mole for low field strength elements to about 470 kJ/mole for high field strength elements. Calculated apparent activation volumes for elements in dacitic melts with 5 wt% H₂O increases from 12 cm³/mole for Ni to 18 cm³/mole for Ba to 43 cm³/mole for the REE's and Sn to about 80 cm³/mole for Hf in the pressure range of 100-500 MPa at 1200 °C.

Keywords: trace element diffusion, chemical diffusion, EBDC, diffusion triple, rhyolite, dacite, H₂O, SYXRF, SIMS

ZUSAMMENFASSUNG

In der vorliegenden Arbeit wurde mit einer subaluminösen Rhyolitschmelze die Abhängigkeit der Kationendiffusion von der Temperatur (800–1400 °C) bei 500 MPa experimentell bestimmt. Der Einfluss von chemischer Zusammensetzung auf die Kationendiffusion wurde durch den Vergleich mit einer Daziterschmelze bei Temperaturen von 1200-1400 °C und Drucken von 0.1-1 GPa untersucht. Da bereits geringe Mengen von Wasser zu einer Beschleunigung von Transportvorgängen in Silikatschmelzen führen können, wurde besonders der Effekt von H₂O auf die Diffusion herausgearbeitet, indem Schmelzen mit H₂O-Gehalten von ca. 0,1- 5 Gew.% H₂O verwendet wurden. Bei 1 GPa wurde mit traditionellen Diffusionspaaren in der Piston Zylinder Apparatur der University of Michigan in Ann Arbor (USA) gearbeitet, während bei niedrigeren Drucken in der Gasdruckanlage in Hannover (kleinerer Temperaturgradient, grösseres Probenvolumen) diese Methode zu Diffusionstriplen modifiziert wurde. Mit den Diffusionstriplen konnten unter gleichen experimentellen Bedingungen sowohl die chemische Diffusion von Hauptelementen (SiO₂ und Al₂O₃) als auch die Diffusion von bis zu 23 verschiedenen Spurenelementen (Rb, Sr, Ba, Cr, Co, Ni, Cu, Zn, Y, La, Ce, Nd, Sm, Eu, Gd, Er, Yb, V, Zr, Nb, Hf, Ta, Ge, Sn) untersucht werden.

Die Diffusionsprofile der Spurenelemente wurden routinemässig mit der orts aufgelösten Synchrotron-Röntgenfluoreszenz-Analyse (SYXRF) im Hamburger Synchrotron Labor (HASYLAB) aufgenommen. Damit konnten für die Vielzahl der Elemente Unterschiede in den Diffusionsgeschwindigkeiten herausgearbeitet werden. An ausgewählten Proben (D18, D22 und PC11) wurden Diffusionsdaten mit der Sekundärionen Massenspektrometrie (SIMS) im Geoforschungszentrum (GFZ) Potsdam ermittelt, um beide analytischen Methoden anhand der Diffusionsdaten zu vergleichen. Die in experimentellen Studien oft nachgewiesene Uphill Diffusion von Hauptelementen in Multikomponenten-Schmelzen (Diffusion einer Komponente gegen seinen eigenen Konzentrationsgradienten) konnte in dieser Arbeit nicht beobachtet werden. Die chemische Diffusion von SiO₂ und Al₂O₃, die durch Profilmessungen an der Mikrosonde ermittelt wurde konnte daher mit dem Konzept der sogenannten effektiven binären Diffusionskoeffizienten (EBDK) beschrieben werden.

Die Diffusionsdaten zeigen, dass mit zunehmender Kationenladung die Diffusion der Kationen bei konstanten Temperatur-Druckbedingungen in Rhyolithen und Daziten abnimmt. Mit zunehmendem Wassergehalt nimmt die Kationendiffusion zu. In Rhyolithen wurde für Eu eine relativ hohe Mobilität im Vergleich zu den Nachbarkationen Sm und Gd beobachtet, was auf ein Vorliegen von sowohl zwei- als auch dreiwertigem Eu zurückgeführt werden kann. Das Verhältniss von Eu^{2+}/Eu_{total} , dass durch die vorliegenden Diffusionskoeffizienten von Eu, Sr und einem Mittelwert von D_{Gd} und D_{Sm} abgeschätzt wurde, zeigt ein Minimum bei einem Wassergehalt von ca. 2 Gew.% H₂O. Da das OH/H₂O-Verhältniss mit zunehmendem Wassergehalt ansteigt, könnte Eu³⁺ durch OH-Gruppen und Eu²⁺ durch H₂O-Molekülgruppen in der Schmelze stabilisiert werden. Obwohl generell die Beschleunigung durch Wasser mit der Ladung des Kations zunimmt, zeigt Sn eine stärkere Abhängigkeit der Beschleunigung vom Wassergehalt als man es vom Ladungszustand erwarten würde. Dafür könnte ein Ladungswechsel von Sn⁴⁺ für niedrige Wassergehalte zu Sn²⁺ für höhere Wassergehalte die Ursache sein. Die Temperaturabhängigkeit konnte für alle Elemente mit einer einfachen Arrheniusbeziehung beschrieben und aus der Steigung Aktivierungsenergien berechnet werden. Diese zeigen für rhyolithische Schmelzen eine Zunahme mit der Kationenladung und -grösse und eine Abnahme mit dem Wassergehalt. Scheinbare Aktivierungsvolumen für Kationen in dazitischen Schmelzen (berechnet aus den Diffusion-Druck-Beziehungen) zeigen eine Zunahme von einwertig geladenen zu den mehrwertig geladenen Kationen.

Schlagnworte: Spurenelementdiffusion, Chemische Diffusion, EBDK, Diffusionstriple, Rhyolit, Dazit, H₂O, SYXRF, SIMS

1. INTRODUCTION

The diffusion of elements in silicate melts and glasses is of fundamental interest for understanding and quantifying transport related phenomena in petrologic processes. For example, crystal growth or dissolution from and in the melt phase (Lasaga, 1982; Ghiorso, 1987; Zhang et al., 1989), melt/rock interactions, and mixing and contamination of magma bodies (e.g. Watson, 1982; Trial and Spera, 1990; Baker, 1990 and 1991) are affected by diffusion. Information about melt structure and dynamics of silicate melts may be obtained by investigating diffusion of particles differing in charge and size (Jambon, 1982; Roselieb and Jambon, 1997) and comparing diffusivities of elements belonging to different geochemical groups (i.e. low field strength elements (LFSE), transition metal elements (TME), rare earth elements (REE) and high field strength elements (HFSE)). These experiments can provide insight into the mechanisms of cation diffusion in melts (Chakraborty, 1995; Mungall and Dingwell, 1997; Koepke and Behrens, 2001).

Diffusion coefficients for trace elements in simple and natural silicate melts have been measured by several investigators over a wide p-T-range, though predominantly for anhydrous systems (e.g., Hofmann, 1980; Watson and Baker, 1991; Lesher, 1994; Brady, 1995; LaTourrette et al., 1996). Although it has been shown, that H₂O is a major constituent of natural magmas and strongly influences chemical and physical properties of silicate melts, only a few studies have been performed on hydrous systems (see reviews by Watson, 1994 and Chakraborty, 1995 and studies of Linnen et al., 1996; Mungall and Dingwell, 1997; Mungall et al., 1999; Koepke and Behrens, 2001). Substantial research has been accomplished on the diffusion of H₂O and on the mechanisms of H₂O diffusion in melts (Jambon, 1979; Stolper, 1982; Lapham et al., 1984; Wasserburg, 1988; Doremus, 1995; Behrens et al., 1996; Behrens and Nowak, 1997; Nowak and Behrens, 1997; Zhang and Behrens, 1998, 2000; Zhang, 1999). Also well known is that dissolved water decreases glass and melt density

(Lange, 1994; Ochs and Lange, 1997; Richet et al., 2000), reduces liquidus temperatures (Holtz et al., 2000) and melt viscosity (Persikov et al., 1990; White and Montana, 1990; Baker and Vaillancourt, 1995; Hess and Dingwell, 1996; Richet et al., 1996; Schulze et al., 1996), and enhances diffusion of cations and volatiles in silicate melts (Watson, 1991; Behrens and Nowak, 1997; Mungall and Dingwell, 1997; Zhang and Behrens, 2000; Koepke and Behrens, 2001). Comparatively little research is focussed on the effects of water on diffusion of elements (e.g. Watson, 1994; Mungall and Dingwell, 1997; Mungall et al., 1997, 1999; Koepke and Behrens, 2001). The present study is designed to obtain new experimental diffusion data for major and trace element diffusion in nominally anhydrous and rhyolitic melts and hydrous dacitic to (i) characterize differences in transport mechanisms of the geochemical elemental groups, and (ii) determine the effects of melt composition including dissolved H₂O on cation diffusion of trace elements in silicate melts. Using a new experimental arrangement (diffusion triple) chemical and tracer diffusion are studied in a single experiment. Systematic differences in diffusion behavior of elements with regards to temperature, pressure and melt composition can be reliably obtained. To avoid a complicated diffusion path in compositional space, a chemical diffusion couple with the compositional difference being close to a main eigen vector of the haplogranite system (Mungall et al. 1998) was chosen. One half of the couple was enriched in SiO₂ so that during the diffusion experiment silica was exchanged by alumina and an associated flux of alkali components (Chakraborty, 1995, Mungall et al. 1998).

Since in this study the used method synchrotron x-ray fluorescence microanalysis (SYXRF) is proved for measuring trace element diffusion profiles, a second goal of this experimental study is to combine and compare results with secondary ion mass spectrometry (SIMS), which is a common method for measuring trace elements in geoscience. Therefore typical diffusion experiments differing in melt composition (SiO₂ and FeO in particular) and dissolved water content were chosen (i) to identify analytical problems of both methods, which may be specific for selected elements and (ii) to clarify possible matrix effects during analysis. The

whole set of diffusion data obtained in this study is useful to model magmatic processes, e.g., fractionation of elements during differentiation of magmas and redistribution of elements during magma mixing (see e.g., Grove et al., 1988; Allen, 1991; Blichert-Toft et al., 1992; Snyder and Tait, 1998). Implications for melt structure and properties are discussed.

1.1. Theoretical Background (Tracer vs. Chemical Diffusion)

In tracer diffusion experiments thermal motion of elements in absence of driving forces such as chemical or thermal potential gradients is measured. If concentrations of trace elements are low, the composition of the system (i.e., rhyolitic and dacitic melts as used in this study) does not vary significantly along the diffusion profile and, in first approximation, the medium can be considered as chemically homogeneous. Thus, tracer diffusion coefficients are constant in the experimental charge, however, their values depend on the specific composition and the run conditions. To predict tracer diffusivities for other compositions either the mechanisms of diffusion must be well known or additional data must be available to describe the compositional dependence of tracer diffusivities.

In contrast to tracer diffusion, chemical diffusion in multi-component systems is a complex process driven by chemical potential and/or temperature gradients. The flux of each component may depend on the concentration gradients of the other components, and a multi-component diffusion matrix is required to fully describe diffusive mass transport. A quantitative approach for such processes must include a theory of the thermodynamics of irreversible processes. In recent years, several papers have addressed the application of irreversible thermodynamics to multi-component diffusion in simple systems of three or four components (Kubicki et al., 1990; Kress and Ghiorso, 1993; Chakraborty et al., 1995a, 1995b; Liang et al., 1996). However, an accurate estimate of diffusion matrices in multi-component systems requires at least as many different diffusion couples as components in the system (Gupta and Cooper, 1971). This means an application to natural melts (such as rhyolite or

basalt) is practically impossible due to the large number of components. An attempt was made by Mungall et al. (1998) to quantify eigenvalues for a simplified granitic melt composition $K_2O-Na_2O-Al_2O_3-SiO_2-H_2O$. The authors found that the diffusion matrix has a highly degenerated set of real, positive eigenvalues that show a regular relation to melt viscosity on an Arrhenius diagram. In agreement with Chakraborty et al. (1995b), Mungall et al. (1998) inferred that the exchange of alkalis is independent of alumina, whereas the exchange of alumina for silica always produces an associated flux of the alkali components.

In a simpler approach, the process of multi-component diffusion is modeled using a single effective binary diffusion coefficient (EBDC) for each element. The concept, developed by Cooper (1968), considers all elements other than the diffusing element as an effective solvent, such that the chemical exchange process can be treated as an effective interdiffusion of a single melt component with all other melt components. This concept gives meaningful diffusion coefficients provided (i) concentration gradients of all elements are in the same direction in compositional space (quasibinary interdiffusion, no uphill diffusion) and (ii) the system is semi-infinite or infinite. The concept of EBDC was successfully applied to major element diffusion (e.g., rhyolite/dacite, Baker, 1990; diopside/anorthite, Kubicki et al., 1990; rhyolite/basalt, Leshner, 1994; rhyolite/rhyolite and rhyolite/andesite, van der Laan et al., 1994) and minor element diffusion in chemically complex melt systems (e.g., Sr in dacite/rhyolite pairs, Baker, 1989; F and Cl in peralkaline intermediate and silicic melts, Baker, 1993; Sn in haplogranite, Linnen et al., 1996). The advantage of using EBDC is the simple application to diffusion couple experiments. Further, using the Boltzmann-Matano analysis (Crank, 1975), compositional variation of EBDC along a diffusion profile may be characterized for each element (Baker, 1989, 1990, 1993). However, the effects of diffusive coupling are absorbed in the EBDC and consequently, these coefficients are strong functions of composition, and more notably of concentration gradients (Chakraborty, 1995). This means that measured diffusion

coefficients are not transferable unless the concentration gradients to be modeled are similar to those used in the experiments.

The approach of EBDC of Cooper (1968) is unable to describe chemical diffusion in systems showing strong coupling of element fluxes (indicated for instance by curved diffusion paths in compositional space) and uphill diffusion of elements. As an improvement, Chakraborty and Ganguly (1992) suggest incorporation of a thermodynamic factor into the EBDC for such systems. An alternative may be to use activity gradients instead of concentration gradients for evaluating the diffusion profiles (Zhang, 1993). However, assumptions on the compositional dependence of the activity coefficients must be made. For the experiments of this study the chemical diffusion couple was chosen align parallel to a main eigen vector of the granite system (Mungall et al. 1998) so that the concept of EBDC is a suitable approach to describe the diffusion process.

1.2. Analytical Background (SYXRF vs SIMS)

During the past decade, there has been an increasing interest in the development of microanalytical techniques for the analysis of elements at trace and ultra trace concentrations. For many years SIMS was the only microanalytical technique commonly available, and it is still the most widely accepted and established instrument in geoscience and geochemical research (for detailed geological applications of SIMS, see Metson et al. (1988) and Hinton (1995)).

In recent times SYXRF has become a well-established and powerful microanalytical technique, because of the intrinsic characteristics of synchrotron radiation (SR) such as high intensity, polarization and externe low divergence provide the potential for analysing a wide range of petrologically important trace elements. It is well established, that SR induced X-Ray fluorescence (SYXRF) can obtain detection limits under the ppm level for many elements. Also the development of X-Ray optics and glass capillaries enables lateral resolution in the

μm range. In the early seventies Horowitz and Howell produced a 2 μm X-Ray beam with a cylindrical mirror to focus the synchrotron beam. Applications to measure trace element concentrations in geological materials such as in fluid inclusions (Vanco et al., 2001), in lunar rocks (Tarasov et al., 1998), in atmospheric aerosols (Khodzher et al., 2000) and in natural and synthetic minerals (Dalpé and Baker, 1995) demonstrate the SYXRF as a complementary tool for geochemical analysis. Baker (1990) successfully used the SYXRF for trace element analysis in silicate glasses. However, a very time-consuming wavelength dispersive technique was used and only a few elements were analyzed. The more recent development of SYXRF as a tool for high-precision and local multi-elemental analysis in geological relevant glasses (Baker, 1990, Koepke and Behrens, 2001) has introduced an easy and fast method to analyze a wide variety of different elements (for further details see Smith and Rivers (1995), Haller and Knöchel (1996) and references therein). First applications of SYXRF for analyzing simultaneously a broad set of trace elements in hydrous andesitic melts were given by Koepke and Behrens (2001).

2. EXPERIMENTAL TECHNIQUES

2.1. Sample Description

Diffusion couple experiments were performed using synthetic rhyolitic glasses with compositions close to a natural obsidian from Erevan Dry Fountain flow (EDF) of Armenia (Bagdassarov and Dingwell, 1993; Stevenson et al., 1995) or synthetic dacitic glasses similar to dacite erupted from Unzen Volcanos (Chen et al., 1993). The EDF obsidian is metaluminous and contains only small amounts of iron (~0.7 wt% FeO) compared to the dacite composition (~4.7 wt% FeO). This compositional difference can be taken to specify the effects of iron on spectral resolution of fluorescence lines of transition metal elements in SYXRF and on matrix effects of SIMS.

In this study synthetic analogues were used to avoid experimental and analytical problems due to initially present trace elements in natural glasses. Concentrations of trace elements in the EDF obsidian and Unzen dacite are not known. However, natural melts may contain several hundreds to thousands ppm of various trace elements (e.g. for rhyolites see Fogel and Rutherford, 1990; Blank et al., 1993, for dacites see Chen et al., 1993). To investigate the diffusion of these elements, about the same quantity of trace elements has to be added. Using a large number of trace elements as in this study, the total amount of added oxides must be in the range of wt%. In this case, it can not be excluded that the difference in composition of doped and undoped sample impose chemical gradients on the trace element profiles.

The starting materials were synthesized in three steps. (1) synthesis of the basic glass (A1, central piece of the triple), (2) synthesis of glasses doped with either 5 wt% of SiO₂ and 0.3 wt% of TiO₂ (A2, second half of the chemical diffusion couple) or with 300 to 500 ppm of selected trace elements (A3, second half of the tracer diffusion couple), (3) synthesis of hydrous glasses.

To (1): Reagent oxides and carbonates were dried at 110 °C overnight before weighing. The oxides and carbonates were grinded and intensively mixed for one hour in a ball mill. The so-obtained powder was annealed in a platinum crucible at 1600 °C for 3 h in an electric muffle furnace. After three cycles of grinding and re-melting a homogeneous glass was obtained for rhyolitic composition. Since the viscosity of dacitic melts are lower than of rhyolitic melts homogeneous glasses were obtained already after two cycles for dacitic glasses.

To (2): A part of the A1 glass was ground in an agate mortar. One third of the glass powder was doped with 300-500 ppm of Rb, Sr, Ba, Co, Cr, V, La, Ce, Nd, Sm, Eu, Gd, Y, Er, Yb, Sn, Ge, Hf, Zr, Nb and Ta as oxides or carbonates (A3 glass), another third with SiO₂ and TiO₂ (A2 glass). In a second charge 300 ppm of Zn, Ni and Cu were added to the A3 glass. TiO₂ was not doped in the A3 glass because of peak overlapping of Ti with other trace elements in SYXRF measurements. Further, using Ti in the chemical diffusion couple may provide information on effects of chemical gradients on trace element diffusion by comparing with other HFSE used in the trace element couple. Added amounts of SiO₂ (5.0 wt%) and TiO₂ (0.3 wt%) are large enough to measure well-resolved diffusion profiles. The anhydrous glasses were synthesized as described under (1).

To (3): Glass powder (< 200 µm) and doubly distilled water were inserted in a platinum capsule (40 mm long, 3 mm in diameter, 0.2 mm wall thickness) in three to five portions to get a homogeneous distribution of water in the whole sample. The powder was compacted with a steel piston to produce a sample with cylindrical shape. For the dacite composition AuPd-capsules were used to minimize an iron loss through the capsule walls (Johannes and Bode, 1978; Sisson and Grove; 1993a; Ratajeski and Sisson, 1999). Synthesis were carried out in internally heated pressure vessels (IHPV) at 1200°C and 500 MPa for 48 hours for rhyolitic and a shorter run duration of 4 hours for the dacitic glasses. After turning of the heating power, experiments were quenched isobarically by automatic pumping for rhyolitic glasses. The initial cooling rate was about 200 °C/min, decreasing to about 100°C/min in the

range of glass transition. To avoid quench crystals in the dacitic glasses a rapid quench device described by Roux and Lefevre (1992) was used. With this methods almost bubble-free glass cylinders (15-40 mm long, 2.6-3 mm in diameter) with H₂O contents from 1.9 to 5.2 wt% H₂O for rhyolitic glasses and with H₂O contents from 2.3 to 5.1 wt% H₂O for dacite glasses were synthesized.

2.2. Experimental Setup

A suitable experimental method to study cation diffusion is the diffusion couple technique, where two polished glass cylinders differing in composition are contacted. This design was modified to determine the diffusion of trace elements and the chemical diffusion of SiO₂, Al₂O₃ and TiO₂ in one single experiment under the same conditions. The setup may be designated as a double diffusion couple or a diffusion triple. It is noteworthy that this method only can be applied in an experimental apparatus such as an IHPV which has a relatively large volume with almost constant temperature. The upper pressure limit of the IHPV's in Hannover is at 800 MPa. Experiments at higher pressures of 1 GPa were performed in a piston cylinder apparatus (PCA). Since temperature gradients in the PCA are much higher than in the IHPV an acceptable capsule length is limited to at most 7 mm to minimize temperature differences within the experimental charge. This is too small for diffusion triple experiments so traditional diffusion couple experiments were performed with trace element diffusion couples at 1GPa. The experimental arrangements of diffusion triples within an IHPV and diffusion couples in a PCA are sketched in Fig. 1.

Only homogeneous samples regard to the major elements without bubbles and crystals were used in diffusion couples or diffusion triples. For diffusion experiments with nominally anhydrous rhyolitic melts, cylindrical cores of 3 mm in diameter were drilled out of the glass body synthesized at 1 atm. The dacite glasses tend to build bubbles by the reaction Fe₂O₃ to FeO and O₂ at 1 atm. To avoid bubbles nominally anhydrous dacitic glasses were synthesized

in IHPV's at 1200 °C and 500 MPa for 4 h using a rapid quench device with an estimated cooling rate of about 200 °C/s.

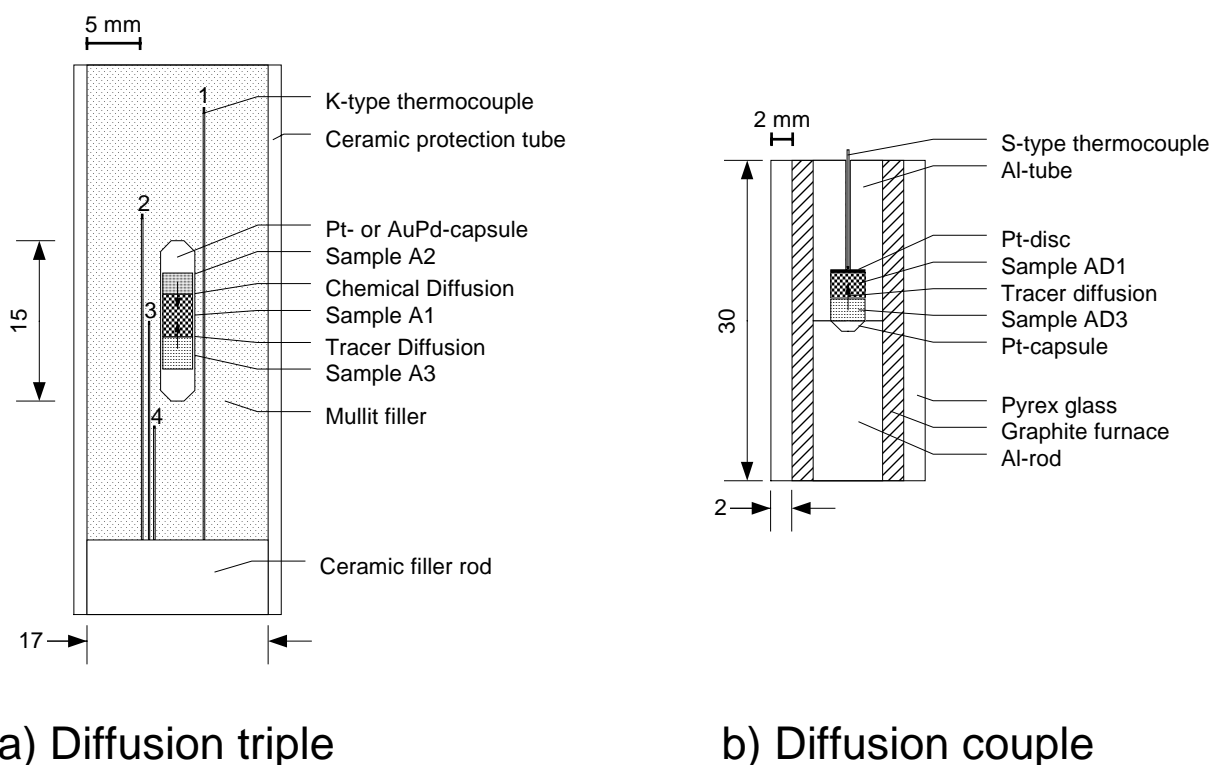


Fig. 1: Schematic scetch of assembled diffusion experiments in the IHPV or PCA.

Anhydrous dacitic samples as well as hydrous rhyolitic and dacitic samples were cut directly from the synthesis cylinders. The basic planes of cylinders were polished for the diffusion experiments. Three glasses with the same water content were aligned in a Pt- or AuPd-capsule with polished planes in contact for diffusion triple experiments. The capsules were carefully squeezed to minimize the free volume before welding shut. The cylinders varied in length between 2 and 4 mm to avoid an overlap of diffusion profiles in any part of the triple. Since diffusion profiles of the fast trace elements (e.g. Rb) are significantly longer than profiles resulting from chemical diffusion, cylinders differed in length like 4 mm for A3, 2 mm for A2 and the length of A1 was to be about the sum of both others.

For PCA experiments two glass cylinders (2–2.5 mm long, 2.8–3 mm in diameter) with a polished contact plane were inserted tightly in a specially formed Pt-container (5–7 mm long,

3.2 mm in diameter). The bottom of a 12 mm long Pt capsule was firstly welded and then pressed with a piston into a container with a bore hole matching the size of the capsule. Thus it is insured that at least at one side the sample fits exactly in the capsule so that a movement of the melt in the capsule under experimental conditions is avoided. The carefully squeezed container was welded at the top in a 4-fin-crimp shape. The capsules were enclosed in crushable alumina sleeves and then encased in a graphite heater (3 cm long, 0.65 cm inner diameter). To insulate the furnace from the carbide core of the PCA, Pyrex glass or BaCO₃ tubes were mounted over the graphite heater.

2.3. Pressure Apparatus and Run Conditions

Diffusion triple experiments with rhyolitic melts were performed at 500 MPa in two different pressure vessels: (1) IHPV at 1100-1400°C and (2) in cold seal pressure vessel (CSPV) at 800°C. Experiments with dacitic melts were carried out in (1) IHPV at pressures of 100, 250 and 500 MPa and temperatures of 1200-1400°C (diffusion triple) and (2) in a solid-media ½ inch PCA at 1 GPa at 1200-1400°C in the Department of Geoscience in Ann Arbor, Michigan. Since the diffusivities of the cations differ widely, long and short term runs at identical conditions were chosen. Furthermore by using different run durations it is possible to control whether any kind of non-diffusive processes such as convection has an influence on the experiments. To avoid convection driven by density differences, the more denser melt was always placed at the base (in IHPV's A3 was placed at the base and A2 on top of the triple). The run durations varied from 15 days to 15 minutes for rhyolitic melts and from 60 hours to 5 minutes for dacitic melts depending on pressure, temperature and water content.

Diffusion triples were vertically orientated in the IHPV and pressurized with argon to 500 MPa (for technical details see Becker et al., 1998). Experiments were heated to run temperature at a constant rate of 30°C/min using a programmable Eurotherm 900 controller. Temperature was controlled in the sample chamber of the IHPV by 4 NiCr-Ni thermocouples

(K-type) calibrated against a certified thermocouple over a length of about 4 cm. The temperature gradient at the sample position was less than 1°C/mm. Pressure was measured with a strain gauge manometer leading to an accuracy of ± 5 MPa. The accuracy of temperature determination in the diffusion zone is estimated to be within $\pm 10^\circ\text{C}$. At an average rate of 200 °C/min experiments were isobarically quenched to below 100°C while constant pressure was maintained by automatic pumping.

Experiments above 1250 °C were performed in a high T rapid quench apparatus using S-type thermocouples. Experiments at 800 °C and 500 MPa were performed in horizontal direction in the CSPV pressurized with water. Temperature at the sample position was calibrated to an external thermocouple by using a calibration vessel and is estimated to be accurate within $\pm 8^\circ\text{C}$ (details see Puziewicz and Johannes, 1988). Pressure was measured also with a strain gauge manometer with an accuracy of ± 5 MPa. Samples were quenched isobarically in a flux of compressed air with a cooling rate of about 150°C/min.

Assemblies in the PCA were pressurized to 1 GPa and with a roughly constant pressure (piston-in method) heated to run temperature while maintaining pressure. Temperatures were raised to conditions of the experiment at a rate of about 400 K/min. To prevent an overshoot of the desired temperature, experiments were heated slowly through the final 20°C at a rate of 10°C/min. Temperature was controlled with an S-type thermocouple calibrated against the melting point of gold. Experiments were quenched roughly isobarically by manual pumping while turning of the furnace for short term runs (5-15 min) with a cooling rate of about 200 °C/s. To minimize dilation cracks in the sample long term runs were “warm quenched” by cooling down to 300 °C in one step (about 15 s) and then slowly to room temperature in 100°C/min. During experiments temperatures were monitored with an Eurotherm 984 control system and fluctuations in temperature at the set point were usually less than 5°C.

Temperature gradients inside the capsule were determined by measuring the OH/H₂O ratios along the axis of an rhyolitic glass body (6.5 mm long, 4.1 mm in diameter) wrapped in gold

foil and heated to 600°C at 500 MPa for 30 min in the PCA. The used rhyolitic glass contained about 1 wt% H₂O. With an Perkin–Elmer GX FTIR spectrometer in the Department of Geoscience in Ann Arbor, Michigan (USA)) concentrations of H₂O molecules and OH groups were quantified by the absorption bands at 5230 cm⁻¹ and 4520 cm⁻¹, respectively. With the determined OH/H₂O ratios over the whole sample temperature distribution was calculated with a new calibrated model after Zhang et. al (1997). The resulting temperature gradient is about 10°C±1.5/mm for experimental conditions of 600°C at 500 MPa (see Fig. 2).

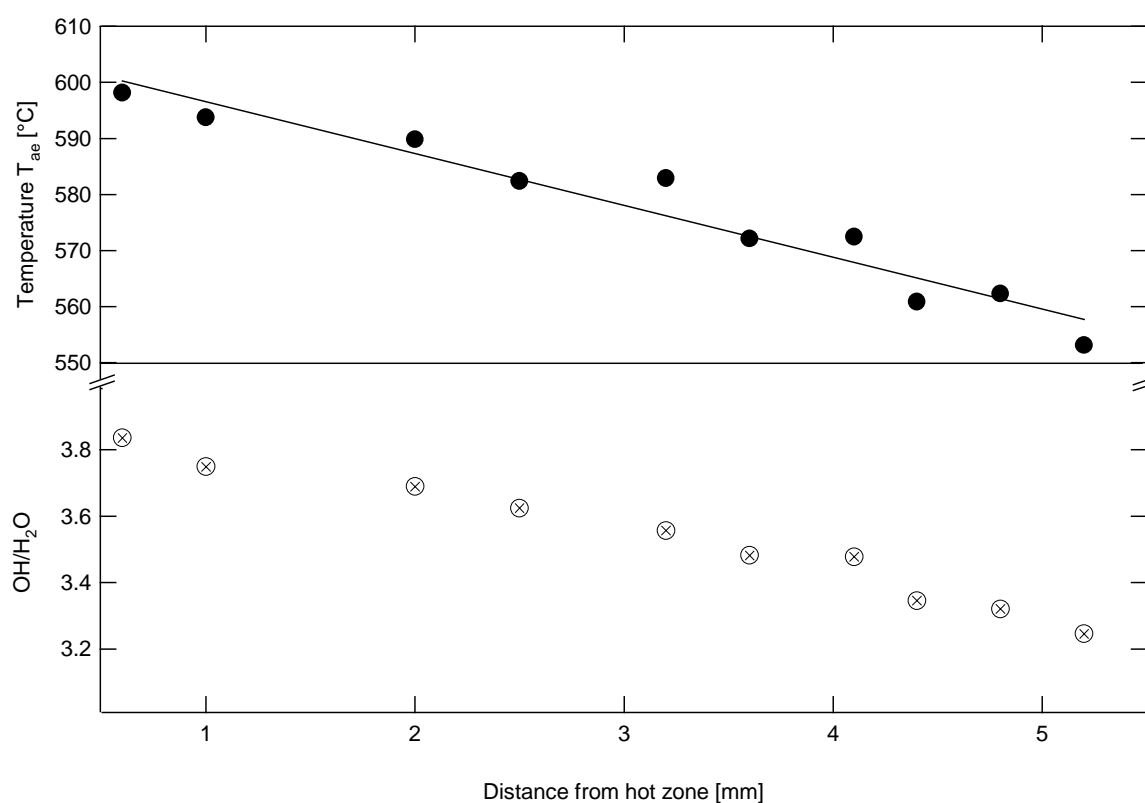


Fig. 2: Temperature distribution (T_{ae}) along the axis of rhyolitic glass body calculated from OH/H₂O ratios after a model by Zhang et. al (1997) with a resulting temperature gradient of about 10°C/mm. The thermocouple is placed about 2.5 mm away from the hot zone.

Temperature differences at 1400°C and 1 GPa were calibrated by the two-pyroxene thermometry after Nickel et al. (1985). A mixture of pyrope, enstatite and diopside were loaded into a Pt-capsule (6 mm long, 3 mm in diameter) together with pre-synthesized glass (6 wt% CaO, 30 wt% MgO, 18 wt% Al₂O₃ and 46 wt% SiO₂) and welded shut. The starting point of the mechanical mixture is at low Ca/low Al orthopyroxen (opx) and high Ca/low Al

clinopyroxen (cpx). The glassy starting material converts under pressure and temperature rapidly into pyroxen, low in Ca in respect to cpx and high in Ca in respect to opx. The Pt capsule was loaded into the PCA and run for 5 hours at 1400 °C and 1GPa. The Ca and Al contents in the resulting opx and cpx minerals of the synthesis products were analyzed with a microprobe after the experimental run. From the Ca and Al concentrations in wt % K_D was calculated after Nickel et al. (1985) with

$$K_D = ((1-Al/2)*(1-Ca)^{cpx}) / ((1-Al/2)*(1-Ca)^{opx}). \quad (1)$$

Since the dependency of T on $\ln K_D$ derived also by Nickel et al. (1985) is given by

$$T(^{\circ}C) = 1616.67 (\pm 14.7) + 287.935 (\pm 5.5) * \ln K_D + 2.933 (\pm 0.25) * P(\text{kbar}) \quad (2)$$

temperature gradients over the whole sample could be calculated with a resulting gradient of about 14°C/mm.

Oxygen fugacity was not controlled in the experiments. Redox conditions in the IHPV apparatus are $\Delta NNO + 3.5$ at 1100 °C, 500 MPa and $\Delta NNO + 2.3$ at 850 °C, 500 MPa for water saturated experiments as measured by NiPd sensors (Wilke and Behrens, 1999; Tamic et al., 2001). Oxygen fugacity in the CSPV is buffered by the stainless, Ni-rich steel of the autoclave and is close to that of the NNO buffer. Conditions in the PCA are estimated to be $\Delta NNO - 2$ at 1200°C and 1 GPa (pers. com. by Zhang and Withers).

3. ANALYTICAL TECHNIQUES

3.1. Sample Preparation

Along the cylindrical axis of the experimental runs double polished sample sections (thickness: 50-80 μm) were prepared for trace element analysis with SYXRF. Parallel to this first section a glass plate of 0.3-0.5 mm thickness polished on both sides was prepared for IR spectroscopy and SIMS. For SIMS analysis, sample sections were embedded in epoxy disks, polished, ultrasonically cleaned in ethanol and after drying at 75 °C for 1 hour and coated with a conducting gold film. For measuring the diffusion profiles of major elements with electron microprobe analysis, samples used for IR analysis or SIMS were polished down to 100 μm , and covered with a carbon film. The plane analyzed by electron microprobe always was that near the cylindrical axis.

3.2. KFT and FTIR

Water contents at both ends of the starting glasses were determined by both Karl Fischer titration (KFT) (more details in Behrens et al., 1996) and FTIR (Fourier transform infrared) microspectroscopy. IR spectra of doubly polished plates were collected in the mid-infrared (MIR) for glasses with up to 2 wt% H_2O and in the near-infrared (NIR) for glasses with higher water contents.

Measurements were performed using an IR microscope A590 coupled with a Bruker IFS 88 FTIR spectrometer. MIR measurement conditions were: 80–200 μm sample thickness, glowbar source, KBr beamsplitter, HgCdTe detector, spectral resolution of 4 cm^{-1} . NIR measurement conditions were: 300–500 μm sample thickness, tungsten white light source, CaF_2 beamsplitter, HgCdTe detector, spectral resolution of 2 cm^{-1} . The thickness of samples was measured by a digital Mitutoyo micrometer with a precision of $\pm 2 \mu\text{m}$. For each spectrum 100 scans were accumulated. 20-50 spectra were measured along the diffusion

profiles. A slit aperture located between objective and detector was used to limit the analysis sample volume, resulting in a spatial resolution of about 30 μm (Zhang and Behrens, 2000). Errors in peak heights based on repeated measurements at different points of the sample are estimated as ± 0.003 for OH peaks and ± 0.002 for H_2O peaks.

Simple tangents through the minima on both sides of the water-related absorption bands in the spectra of rhyolitic compositions were fitted for baseline correction. Total water (MIR spectra) and water species (NIR spectra) were determined from the heights of the absorption bands using the Lambert-Beer law. In the MIR absorption spectra, the fundamental OH stretching vibration band at 3550 cm^{-1} was evaluated using a linear molar absorption of $78\text{ l mole}^{-1}\text{cm}^{-1}$ as determined for a haplogranitic composition by Behrens and Schmidt (1998). Concentrations of H_2O molecules and OH groups were quantified by the absorption bands at 5230 cm^{-1} and 4520 cm^{-1} , respectively. Total water was calculated as the sum of both species. To evaluate the NIR spectra of glasses containing about 5 wt% water, linear molar absorption coefficients determined by Withers and Behrens (1999) for the same rhyolite of Armenia ($\epsilon_{4500} = 1.52\text{ l mole}^{-1}\text{cm}^{-1}$; $\epsilon_{5200} = 1.72\text{ l mole}^{-1}\text{cm}^{-1}$) were used.

Water contents of the dacitic glasses were measured using a new IR microscope (IR-scope II) coupled with a Bruker IFS 88 FTIR spectrometer. The detector is a narrow band MCT detector with NIR equipment and the objective is a cassegranian 15x. Due to broad intensive iron-related bands with a maxima at around 5700 cm^{-1} the linear baseline under the H_2O combination bands intersects the absorbance curve at 5400 cm^{-1} . To account effects of iron-related bands influencing the spectra by determining water species in this case, the background of OH and H_2O combination bands is modeled by the two gaussian fit to the iron-related band at 5770 cm^{-1} and the water-related band at 3931 cm^{-1} . The procedure of this baseline correction is described in detail by Ohlhorst et al. (2001). For evaluation of the spectra molar absorption coefficients determined by Ohlhorst et al. (2001) for the same Unzen Volcano

dacite ($\epsilon_{4500} = 1.04 \text{ l mole}^{-1} \text{ cm}^{-1}$; $\epsilon_{5200} = 1.18 \text{ l mole}^{-1} \text{ cm}^{-1}$) were used. Since the setup of the IR spectrometer changed (new microscope, new objective, new CaF_2 beamsplitter, condensor lense instead of a mirror, slit aperture instead of an aperture hole) and a new detector with a much better signal to noise ratio was used, the calculated water contents for the dacitic glasses are expect to be 2-10 % to high by using the molar absorption coefficients determined by Ohlhorst et al. (2001) for the old setup of the IR spectrometer (pers. comm. by Ohlhorst). Also Behrens et al. (1996) observed a variation of up to 10 % relative in peakintensities by using different FTIR spectrometers for the same sample.

To consider compositional variation in the chemical diffusion couple, the relationship between absorption coefficients and SiO_2 content derived by Ohlhorst et al. (2001) for basaltic to rhyolitic composition was extrapolated to higher SiO_2 -contents (for rhyolitic compositions to $\epsilon_{4500} = 1.49 \text{ l mole}^{-1} \text{ cm}^{-1}$ and $\epsilon_{5200} = 1.81 \text{ l mole}^{-1} \text{ cm}^{-1}$ at 82 wt% SiO_2 and interpolated dacitic compositions to $\epsilon_{4500} = 1.39 \text{ l mole}^{-1} \text{ cm}^{-1}$ and $\epsilon_{5200} = 1.55 \text{ l mole}^{-1} \text{ cm}^{-1}$ at 72 wt% SiO_2).

Densities required for evaluation of the spectra were calculated by the linear density-total H_2O -content relationship derived for EDF compositions by Withers and Behrens (1999) as

$$\rho = (2390 \pm 12) - (17.0 \pm 2.3) * c_{\text{water}} \quad (3)$$

and derived for dacite of the Unzen Volcano by Ohlhorst et al. (2001) as

$$\rho = (2517 \pm 5) - (12.1 \pm 1.7) * c_{\text{water}} \quad (4)$$

where ρ is the density of the hydrous glass in g/l and c_{water} is the total water content in wt%.

Using this relationship for the silica-rich compositions gives only a minor error. Density measurements on selected starting glasses by the buoyancy method (measuring the sample weight in water and in air) agree within 2 % with calculated densities independent on anhydrous composition.

3.3. Microprobe Analysis

Compositions of anhydrous and hydrous starting glasses were analyzed with an electron microprobe (Cameca Camebax). Raw data were corrected following the PAP procedure (Pouchou and Pichoir, 1988). For checking the composition of the starting materials analysis conditions of 15 kV accelerating voltage, 5 nA beam current, 5 s acquisition time for Si, Al, Mg, Ca, Fe and 2 s for Na and K were used to avoid migration of the alkalis. Analysis on the samples were done with a defocused beam (spot size 20 μm). An average of 10-20 electron microprobe analysis collected for anhydrous and hydrous starting material is listed in Tab. 1 and compared to natural composition of the EDF from Armenia and Unzen Volcano dacite.

Chemical diffusion profiles of SiO_2 , Al_2O_3 and TiO_2 in the couple A1/A2 were measured with different operating conditions compared to the standard glass analysis to achieve a higher analytical precision. Beam conditions varied but best results for the major elements SiO_2 and Al_2O_3 were obtained using an accelerating voltage of 15 kV, a beam current of 20 nA and a beam spot of 5 μm . Counting time were 30 s for SiO_2 and Al_2O_3 , and 50 s for TiO_2 and FeO.

To minimize alkali loss during analysis the profiles of Na_2O and K_2O were measured separately in the diffusion samples with analysis conditions as used for the starting materials. Accurate diffusivities for the components Na_2O , K_2O , CaO and MgO could not be evaluated from the profiles due to high signal to noise ratios and small concentration gradients.

3.4. SYXRF

Trace element diffusion profiles were routinely analyzed at the beamline L (SYXRF) at the Hamburger Synchrotron Labor (HASYLAB) of the Deutsches Elektronen-Synchrotron Labor (DESY) in Hamburg, Germany. The SYXRF beam arises from deflection of a 4.5 GeV electron beam around the DORIS III bending magnet ring, yielding a white spectrum with a maximum flux at 16.6 keV and a usable spectrum in the range of 2 – 80 keV. Theoretical

concepts and general principles of operation of SYXRF are reviewed in detail elsewhere (e.g. Haller and Knöchel, 1996; Lechtenberg et al., 1996; Koepke and Behrens, 2001).

The thin section prepared along the cylindrical axis was mounted with epoxy on a slit of an Al holder so that the synchrotron beam only passes through the sample. The middle part of doubly polished 50-80 μm thin sample sections were centered on 1.0-1.5 mm slits cutted in an Al holder, which is mounted on a XYZ table (reproducible positioning 0.5 μm).

Fluorescent X-Rays from the K-shell lines of the elements have been measured for concentration-distance profiles by using the white and lineary polarized fluorescent excitation of the highly brilliant SR source (white beam technique). To suppress intense K fluorescence lines of major elements such as Ca and Fe in the used samples and to avoid thermal damage of beamline components due to the very high white beam intensity, Al absorber of 1-4 mm thickness (depends on sample material) must be used. Dead-time for the EDS detector was maintained in the range of 10–30 % and live-time was selected to be 170-180 s for analysis, yielding a real acquisition time of 240 s for every point, while EDS spectra were accumulated in a 2048-bit multichannel analyzer. K-spectra of all elements could be measured simultaneously by acquisition of only one spectrum (multi-element spectra) and with a high local resolution (10-25 μm point distance). To achieve a smaller and focused beam spot calibrated glass capillaries of 8 μm (only for very short diffusion profiles) or 20 μm in diameter were used. To observe the sample position and orientation the SYXRF is equipped with a CCD camera (3 μm resolution) and a long distance microscope with a magnification of 40–1200x. To minimize Raleigh and Compton scattering, samples were aligned at 45° and the fluorescence spectrum was detected at 90° to the incident beam. The sample was moved perpendicular to the diffusion trend (along Y direction) and in the plane parallel to the surface. Thus, one dimensional line scans were surveyed remote controlled from the outside of the microprobe set-up. Fluorescence signals are recorded by an energy-dispersive HPGe

semiconductor, 30 mm² in diameter and 5 mm thick. The resulting spectra were fitted with the AXIL-software (van Espen et al., 1977). Net intensities were normalized to an internal standard (Fe in this study) to correct analytical fluctuations caused by the synchrotron beam and variations in sample orientation and thickness. The set-up of SYXRF at beamline L is sketched in Fig. 3.

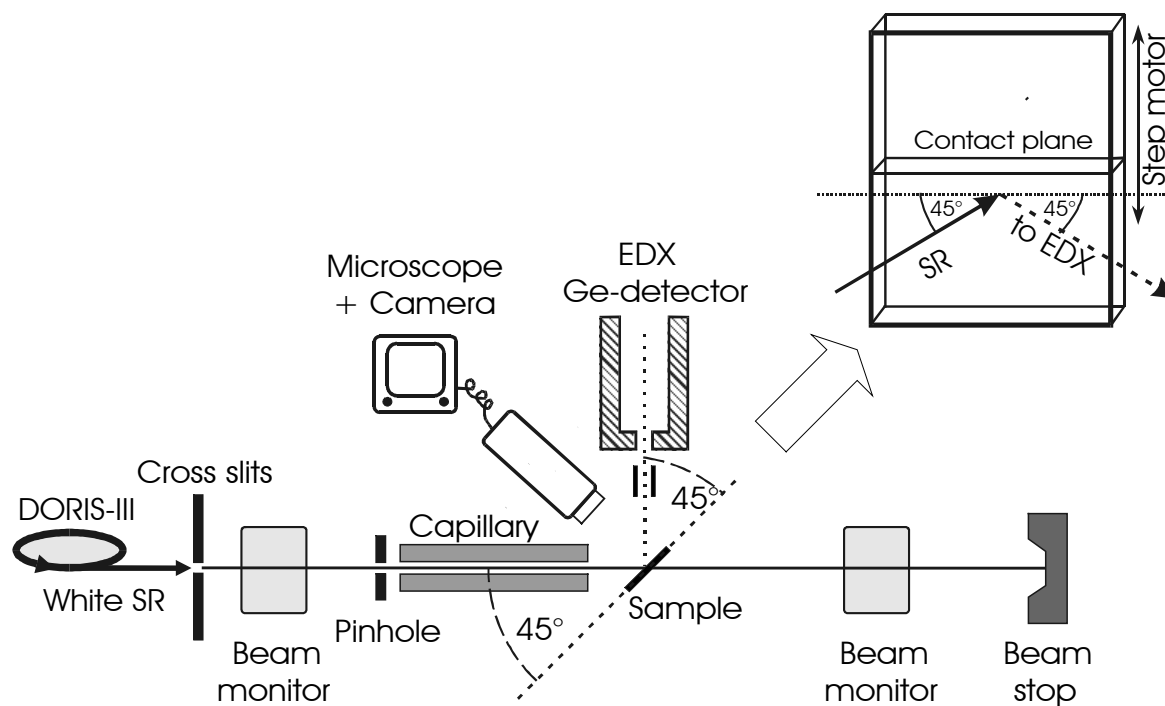


Fig. 3: Set-up of the SYXRF at the beamline L in the HASYLAB of DESY in Hamburg.

3.5. SIMS

Trace element diffusion profiles were measured also by SIMS using the Cameca ims 6f SIMS of the Geoforschungs Zentrum (GFZ) in Potsdam. Relative concentration profiles of trace elements were measured in three selected diffusion couples differing in (1) bulk composition at the same H₂O contents (rhyolitic (D18) and dacitic (PC 11), 5 wt% H₂O) and (2) water content at the same bulk composition (rhyolitic with either 2 (D22) or 5 wt% of H₂O (D18)).

During analysis the sample surface is bombarded with a focused primary beam of high energy ions generated by an ion column. The impact of primary ions sputters atoms from the sample (secondary ions). An extraction system transfers the secondary ions to an entrance slit of a

mass spectrometer where they are accelerated by an electrostatic field for the mass spectrometric analysis. Since no chemical separation is made prior to analysis, the secondary ion beam may also contain polyatomic ion combinations or ionized molecular combinations (especially with oxygen in the positive ion mass spectrum) of elements present in the sample-matrix including trace elements. However, there are small differences in interfering masses of the fragments which can be used for separation.

An $^{16}\text{O}^-$ -ion beam was used for the SIMS analysis of the diffusion samples with energies of about 12.5 kV and 2 or 8 nA (depended on the diameter of the beam). This source was preferred to a $^{133}\text{Cs}^+$ -ion or Ar beam to analyse the positive species in the glasses. The resulting minimum spot size by using these conditions is 10 to 25 μm and depends on the initial source brightness and the optical alignment of the primary column.

The determination of the relative distribution profiles of selected 'heavy metals' and REE's required the tuning of the instrument to operate at the minimum mass resolution of $M/\delta M =$ circa 350. A primary beam intensity of circa 8 nA was focussed to a circa 20 μm diameter spot (98% of beam); 18 mass stations were included in the peak stepping sequence such as ^{30}Si , ^{58}Ni , ^{63}Cu , ^{85}Rb , ^{88}Sr , ^{90}Zr , ^{93}Nb , ^{133}Cs , ^{138}Ba , ^{140}Ce , ^{147}Sm , ^{151}Eu , ^{153}Eu , ^{158}Gd , ^{174}Yb , ^{180}Hf and ^{181}Ta . The background was measured for 0.1 s, ^{63}Cu for 5 s, ^{133}Cs and ^{181}Ta for 10 s and the other isotopes for 2 s. Four cycles were conducted, resulting in a total analytical time of 7 minutes including a 3 minute presputter. A -100 V energy offset was applied to nominal 10 kV secondary ion extraction potential, the instrument was operated with a 25 V energy bandpass. Profiles were measured automatically using a 50 μm stage stepping distance. Secondly profiles for slowly diffusing isotopes such as ^{28}Si , ^{90}Zr , ^{93}Nb , ^{89}Y , ^{59}Co , ^{64}Zn , ^{66}Zn , ^{74}Ge , ^{139}La , ^{180}Hf and ^{181}Ta were measured with a smaller point distance of 20 or 25 μm parallel to the first measured profile. Therefore a primary beam intensity of circa 2 nA was used focussed to a circa 10 μm diameter spot (98% of beam). Decreasing the intensity of the primary beam reduces the crater size but also results in longer counting times in order to

observe sufficient secondary ions. Therefore a longer analytical time of 13 min for each point, including 5 min presputter was necessary to reach an acceptable number of observed ions.

To correct fluctuations in the secondary ion production and transmission, the secondary ion intensities were rationed to those of ^{30}Si , which is a major isotope (60-80 wt% of SiO_2) in the used silicate glasses. As the Si concentration is constant across the length of the sample measured data reflect the relative variation in the element concentration as a function of diffusion distance.

4. RESULTS

Small difference in the concentrations of Na₂O and K₂O between the undoped (A1) and the doped glasses (A2 and A3) resulting from melting at 1600°C on air were detected. Especially the SiO₂-enriched glass (A2), which had to be grinded and re-melted three times to become homogeneous, was depleted in alkalis and thus became slightly peraluminous (NBO/T = 0.04). To check, if the initial inhomogeneity in the diffusion triple influence the trace element diffusion and the interdiffusion of Al and Si, electron microprobe traverses were measured along the cylindrical axis of selected samples after short and long term runs (run D2, D4, D9 and D11) demonstrated for D4 and D11 in Fig. 4.

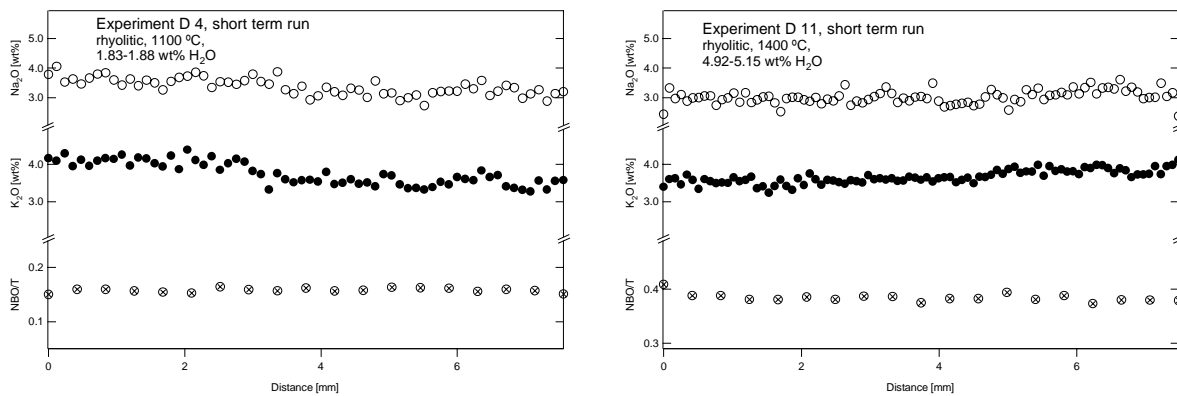


Fig. 4a,b: Alkali distribution after the experimental run and calculated NBO/T.

Homogeneous distribution of Na₂O and K₂O in all samples were found and even in the short term runs no alkali gradients were measured. NBO/T were calculated over the whole length of the diffusion triples on 10-15 microprobe analysis with the water contents given in Tab. 2 and 3 for each part of the triple. After the experiments NBO/T became 0.08 to 0.14 for D2, 0.15 to 0.16 for D4, 0.32 to 0.33 for D9 and 0.39 to 0.41 for D11 compared to the NBO/T of the starting materials of 0.01 for A1, 0.04 for A2 and 0.03 for A3 (see Tab.1) Thus, the diffusion of Na and K must be significant faster than the diffusion of the other cations. This is consistent with observations in other studies (e.g. Jambon, 1982).

4.1. Evaluation of Diffusion Profiles

Crystal- and bubble-free glasses were obtained from all diffusion experiments performed in the IHPV except of one experiment with anhydrous samples at 1200°C (D30). The SiO₂-rich part of this triple was completely crystallized. However, EBDCs for SiO₂ and Al₂O₃ evaluated from the chemical diffusion profiles of the crystallized part of this experiment agree very well with Eyring diffusivities $D\eta$ (see Tab. 2 and 3) calculated using the viscosity model after Hess and Dingwell (1996). Diffusion profiles from PCA experiments show crystallization in the tracer diffusion couple at 1200°C and about 2 wt% H₂O (PC12). From PC12 and also from PC5, PC8 and PC11, which show strong deformation of the samples in diffusion direction no diffusion data could be evaluated and possible matrix effects during analysis with SYXRF and SIMS could not be clarified because PC11 was one of the chosen sample.

Diffusion coefficients for trace and major elements were determined by fitting the measured concentration-distance profiles to the appropriate solution of Fick's second law. Assuming concentration-independent diffusion coefficients, the solution for one-dimensional diffusion between two semi-infinite media is after Crank (1975):

$$\frac{(C_{(x,t)} - C_0)}{(C_1 - C_0)} = \frac{1}{2} \cdot \left[1 - \operatorname{erf} \left(\frac{x-a}{2 \cdot \sqrt{Dt}} \right) \right], \quad (5)$$

where $C_{(x,t)}$ is the concentration at a distance x after run time t , a is the inflection point of the diffusion profile, C_0 and C_1 are the initial concentrations in both halves of the diffusion couple and D is the diffusion coefficient. The calculated diffusion coefficients and experimental conditions are summarized in Tab. 2 and 3 for rhyolitic and in Tab. 5 for dacitic melts.

4.2. Influence of non-diffusive Transport

To ensure that the concentration distance profiles are exclusively due to diffusion, experiments under identical conditions for different run durations were performed. It is convenient to normalize concentrations against \sqrt{t} to make the profiles invariant in time. The

time-dependence for cations with very high diffusivities such as Rb could not be analyzed because in the long term runs profiles were reflected at one end of the diffusion couple.

Normalized diffusion profiles of Co, Nd and Zr are plotted in Fig. 5 a-e.

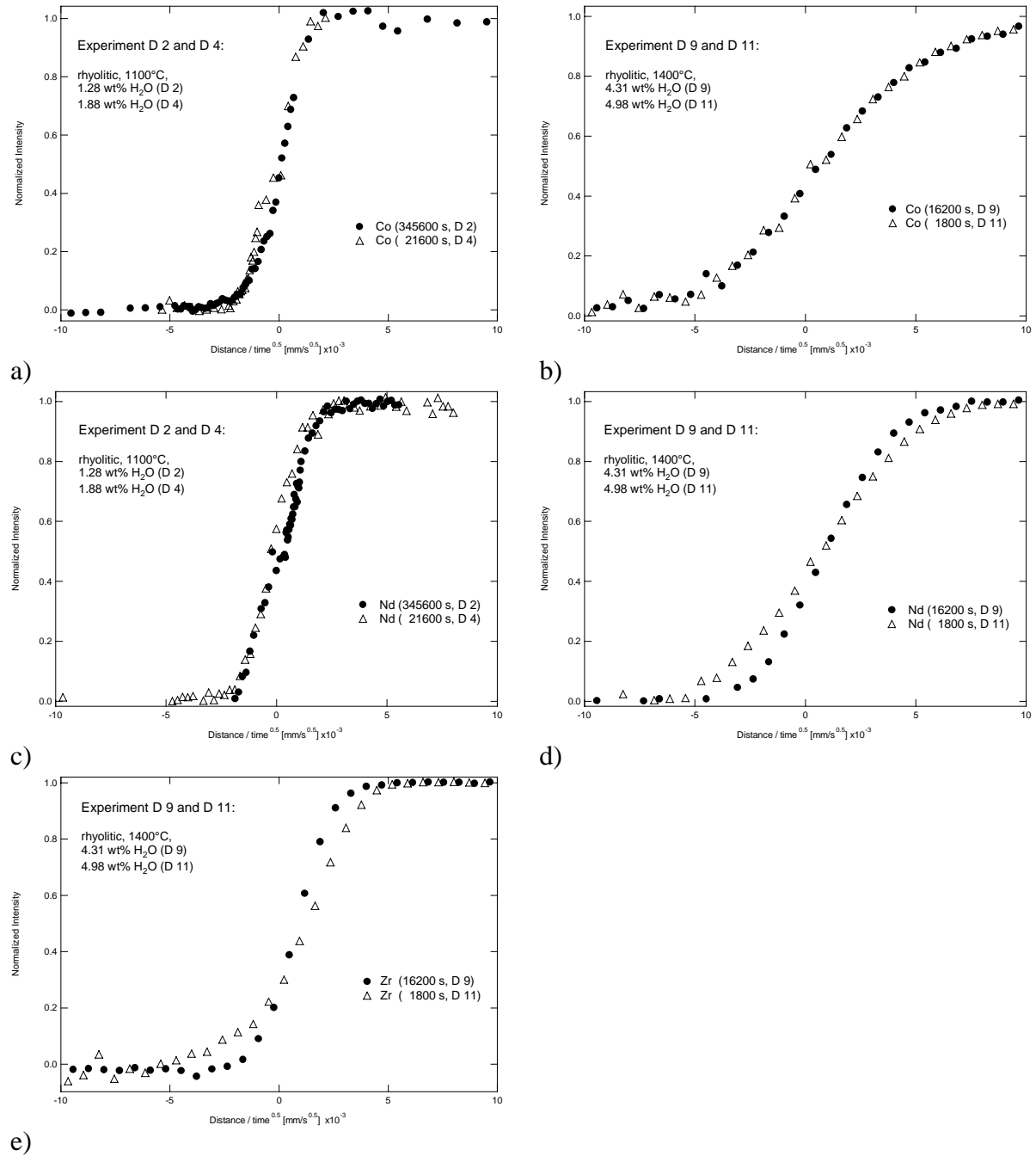


Fig. 5: Normalized diffusion profiles of Co, Nd and Zr for short- (open triangles) and long- (filled circles) term runs at identical P-T conditions. Intensity is normalized to 1 and the distance is scaled by the square root of time to make the profiles invariant in time.

In the case of Co, the normalized profiles of the long- and short term run matches very good, both at 1100°C and 1400°C, for melts containing about 5 wt% H₂O. In contrast, the normalized profiles of Nd and Zr are significantly longer for the short term than for the long term run at 1400°C. On the other hand, at 1100°C short and long term runs are in good agreement for Zr. It can be infer from these results that because of the higher H₂O content of the short term run an enhancing effect on diffusion by water is more pronounced for Zr than for Co.

Also a non-diffusive transport could affect the diffusion data especially for slowly moving cations in very short runs at high temperature. An apparently enhanced diffusion was observed also in zero-time experiments on water diffusion in haplogranitic melts (Nowak and Behrens 1997) and on trace element diffusion in andesitic melts (Koepke and Behrens 2001). A possible explanation is locally restricted mixing at the contact of the diffusion couple during heating from glass to melt state. Diffusion data which are affected by non-diffusive mixing are not included in Tab. 2, 3 and 5.

4.3. Trace Element Diffusion

Selected diffusion profiles of trace elements are shown for rhyolitic and dacitic melts in Fig. 6 a-f for different water contents (0.20-4.91 wt% H₂O) and temperatures (1100-1400°C). Provided the boundary condition of semi-infinite media is fulfilled, normalized concentration profiles of the elements with different mobilities (corresponding to different profile lengths) intersect at the interface of the two halves of diffusion couple. In some long term diffusion runs the intersection points of mobile cations are shifted compared to the other elements (e.g. Ba in Fig. 6 b) indicating reflection of the profile at the doped end of the sample. When diffusional exchange did not proceed to much (less than 10% decrease in concentration at the doped end), these profiles could be evaluated using the solution of Fick's second law for finite media (Crank 1975, eq 2.17).

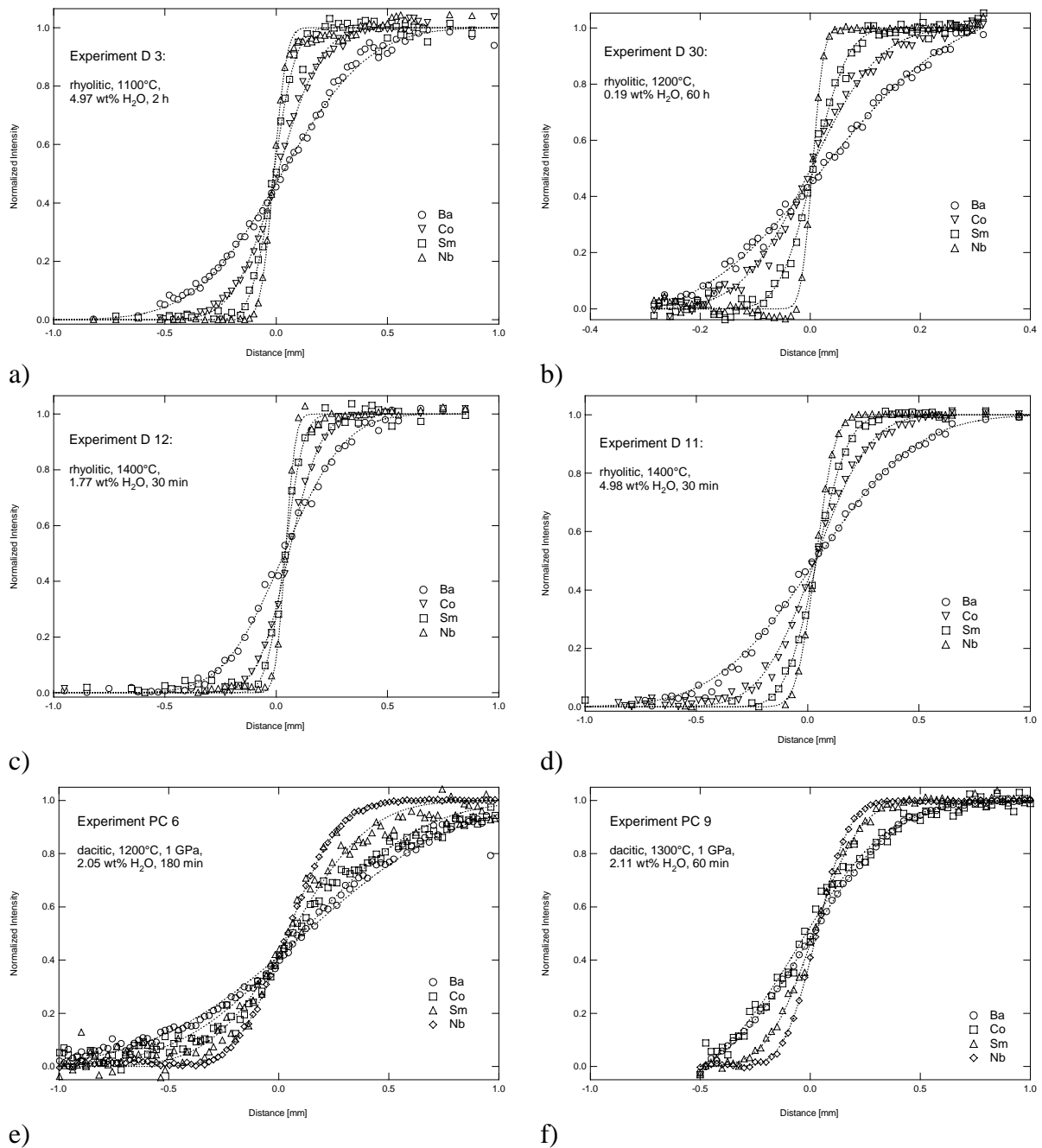


Fig. 6: Selected diffusion profiles of Ba, Co, Sm and Nb for different water contents (0.19, 1.77 and 4.98 wt % H₂O) and temperatures (1100, 1200 and 1400°C) in rhyolitic at 500 MPa and dacitic melts at 1 GPa. Maximum intensities are normalized to 1 for comparison. An error function fit for each element is shown by a curve through the measured data points.

A basic assumption in the evaluation of the trace element profiles has been that diffusion coefficients are independent on concentration of the trace element because concentrations are low. This assumption is supported by the symmetry of concentration distance profiles. The variation of gradients at the intersection point demonstrate that the LFSE Ba diffuses faster than the TME Co, the REE Sm and the HFSE Nb, independent of temperature and water

content. In general, concentration profiles for cations with higher valence such as REE and HFSE (i.e. Sm and Nb) are more steep than those with lower valence such as LFSE (i.e. Ba). From Tab. 2, 3 and 5 it is evident that at constant pressure, temperature and water content the diffusion coefficients decrease with increasing ionic charge from monovalent Rb to tetravalent Zr and Ge. For instance, at 500 MPa, 1200 °C, 5wt% H₂O the tracer diffusivity in rhyolitic melts decreases from $\log D_{\text{Rb}} = -9.99$ to $\log D_{\text{Ba}} = -10.66$ to $\log D_{\text{Nd}} = -11.59$ to $\log D_{\text{Zr}} = -12.47$ (D in m²/s). In dacitic melts at 1 GPa, 1200 °C, 2 wt% H₂O tracer diffusivity decreases from $\log D_{\text{Rb}} = -10.80$ to $\log D_{\text{Ba}} = -11.32$ to $\log D_{\text{Nd}} = -11.51$ to $\log D_{\text{Zr}} = -12.26$. The decrease of diffusion coefficients from the LFSE (Rb) to the HFSE (Zr) in rhyolitic melts is about 3.5 log units at 800 °C for melts containing ca. 5 wt% H₂O, about 2 log units at 1100 °C for melts with 2 wt% H₂O and about 3.5 to 4 log units at 1200 °C for the water-poor melt. A much smaller decrease is found for dacitic melts at 1 GPa of about 1.5 log units at 1200 °C for melts with 2 wt% H₂O and about 0.7 log unit at 1400 °C in the water-rich melt. Diffusion of cations is about 0.1 (LFSE) to 1 log units (HFSE) faster at 2 wt% H₂O, 1200 °C and about 0.4 (LFSE) to 2 (HFSE) log units faster at 5 wt% H₂O, 1400 °C in dacitic melts than in rhyolitic melts.

Shown in a plot $\log D$ vs elements (Fig. 7) no simple relationship between diffusivity and ionic radius can be applied to all cations with the same charge. Whereas Sr²⁺ (ionic radius = 1.26 Å) always was found to migrate faster than Ba²⁺ (1.42 Å) the smaller Ni²⁺ (0.69 Å) is slower than both with a mobility close to the REE. The diffusion coefficients of the various REE are almost identical except of Eu, for which D is 0.2 orders of magnitude higher for rhyolitic melts at 1400 °C and 5 wt% H₂O and even 2 orders of magnitude higher at 1200 °C in water-poor rhyolitic melts. In dacitic melts the diffusion of Eu is almost identical to the diffusion of the other REE. Sn always migrates significant faster than Ge in rhyolitic and dacitic melts. Nb is faster than its neighbor element Zr and Co is faster than the other TME's Ni and Cu. Surprisingly, the determined diffusivities of Cu, which is expected to be in mono-

or divalent are slower than all the other TME and its diffusion coefficient is close to the HFSE.

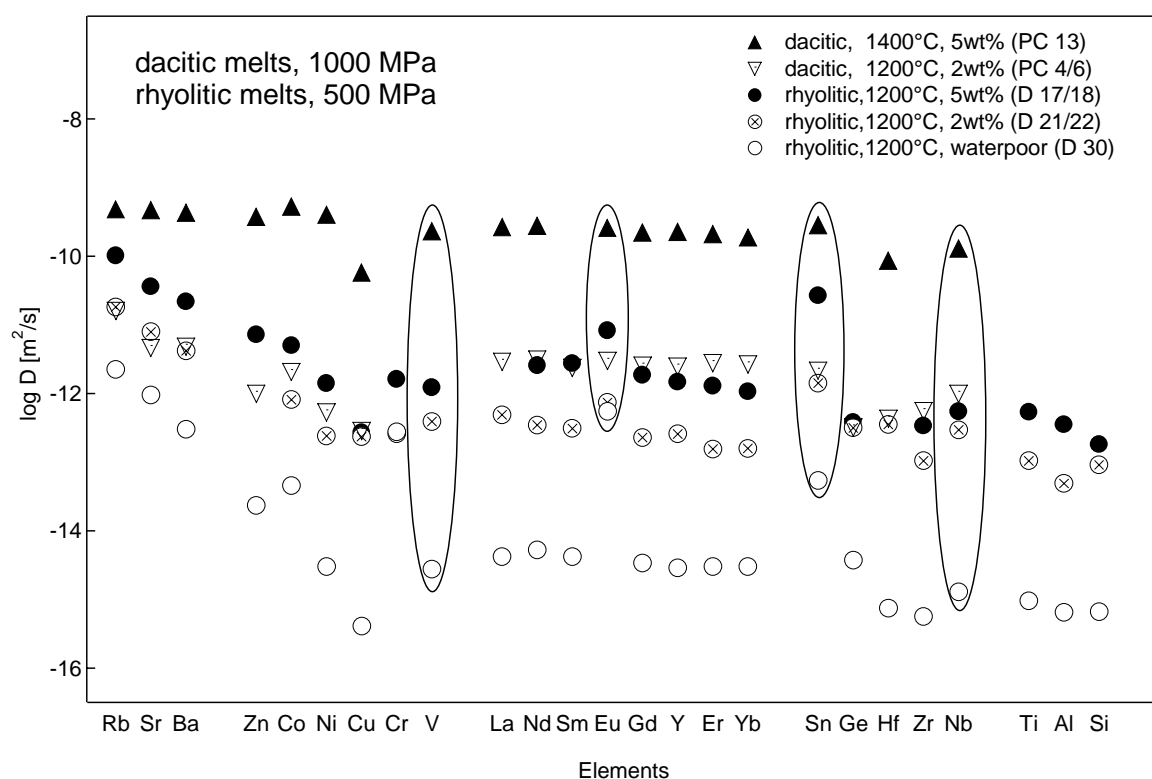


Fig. 7: Comparison of diffusion coefficients in a log D vs element plot for water-poor and hydrous rhyolitic melts at 1200 °C and 500 MPa.

4.4. Diffusion Profiles evaluated by SYXRF and SIMS

SYXRF was routinely used to determine diffusion coefficients by the analysis of concentration distance profiles. In order to compare results and analytical methods, SIMS was also used to determine the diffusion of trace elements on the samples D18 and D22 (Tab. 7). In Fig. 8 a normalized concentration distance profiles determined by SYXRF and SIMS are presented for Ba, Gd and Zr. Diffusion profiles for V and Sn could not be analyzed by SIMS because of the overlapping of V with NaSi molecule (which are highly concentrated in the used glass matrix) and a very low intensity signal of Sn. Although Ni is found to be problematic element to measure with SIMS because Ni intensity signals overlap with CaO molecule of the glass matrix, a much higher scattering is observed from the SYXRF profiles

for Ni (see normalized Ni profiles in Fig. 8 b). Diffusivities of Ni evaluated from SIMS profiles are about 1 log unit smaller for identical experimental runs.

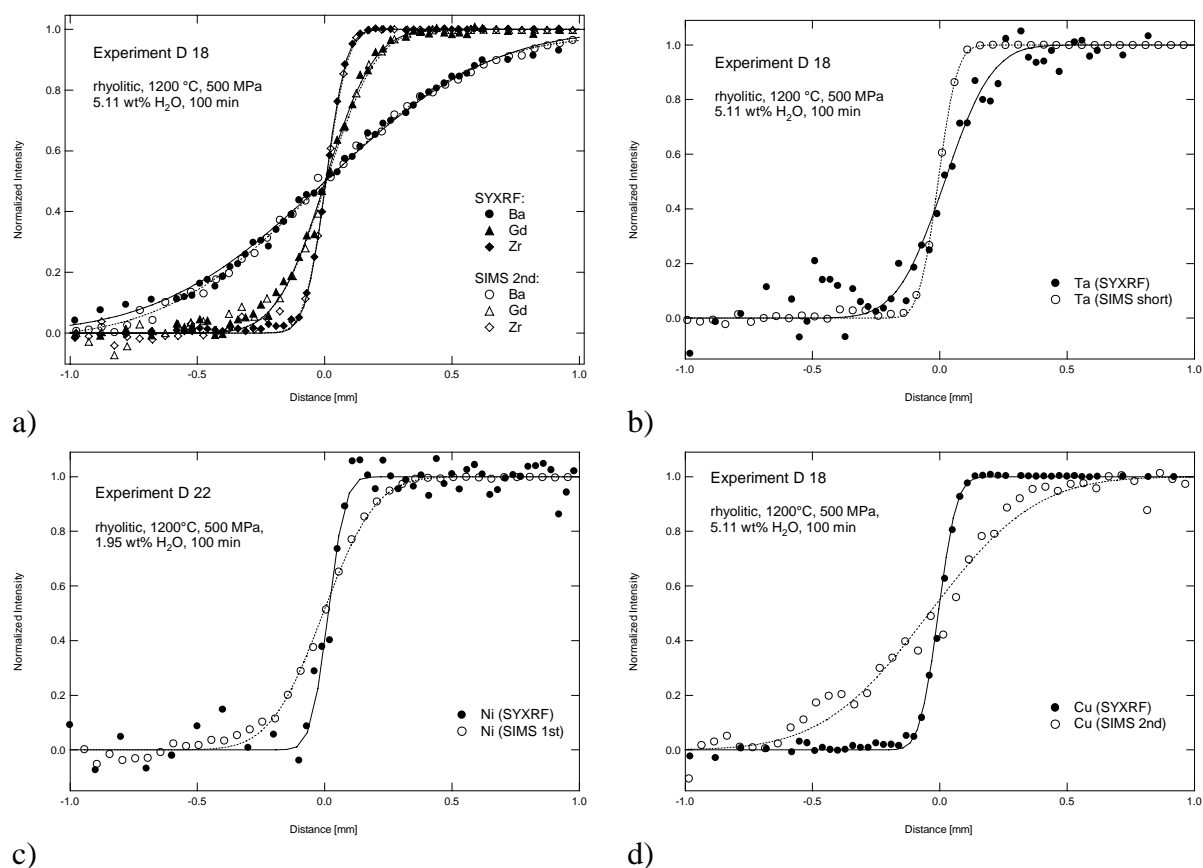


Fig. 8: Comparison of concentration distance profiles measured with SYXRF (filled symbols) and SIMS (open symbols).

Since Ta is used as a material of the cross slit system at the SYXRF beamline the high discrepancy in diffusivities for Ta (1 to 1.6 log units) and the large scattering of the SYXRF measurements can be explained by the presence of an intensive Ta background signal in SYXRF analyses (Fig. 8 c). The scattering of Ce profiles measured with SYXRF is even so high that because of the low quality of the fit the resulting standard error of D is unacceptably high (0.45-0.55 log units). From quantitative determinations of trace element concentrations by Rickers, Ce was found to be much lower concentrated (50-70 ppm, pers. comm. by Rickers) than the other elements in the glasses (300-500 ppm). This is too low to measure well-resolved diffusion profiles with SYXRF but still high enough to determine Ce profiles with SIMS. Experimental problems while doping the starting glasses could have caused this low

concentration in Ce. Since Ce_2O_3 is a very hygroscopic and sticky material it cannot be excluded that some of the material is lost during grinding and mixing before synthesis. Diffusivities of Ce and Ta evaluated from SYXRF measurements received no further consideration in this study because of the mentioned problems and are not presented in Tab. 2, 3 and 5. Profiles of Cu (Fig. 8 d) show a smoother profile from SYXRF than SIMS measurements. However, the diffusivity of $\log D = -10.43$ calculated from the SIMS is more compatible to diffusivities of the other TME than the diffusivity of $\log D = -12.47$ evaluated from the SYXRF profile.

4.5. Chemical Diffusion

An example of concentration profiles of SiO_2 , Al_2O_3 and TiO_2 measured in a chemical diffusion couple is shown in Fig. 9. Since all chemical diffusion profiles display an error-function shape, it can be concluded that the compositional dependence of the diffusion coefficients is negligible in the range of composition studied. No indication for uphill diffusion was found in any of the experiments. Therefore the model of the EBDC (Cooper, 1968) is a suitable approach to the experiments and EBDC's were determined by fitting the profiles to the solution for a diffusion couple with constant diffusivity (eq. 5). Chemical diffusion of Ti in rhyolitic melts is found to be systematically 0.2 – 0.8 log units faster than diffusion of network formers Al and Si except for run D3 in which the profiles are too short for discrimination of chemical diffusivities. In general, the EBDC of Si, Al and Ti are close to trace element diffusivities of HFSE (Tab. 2 and 3).

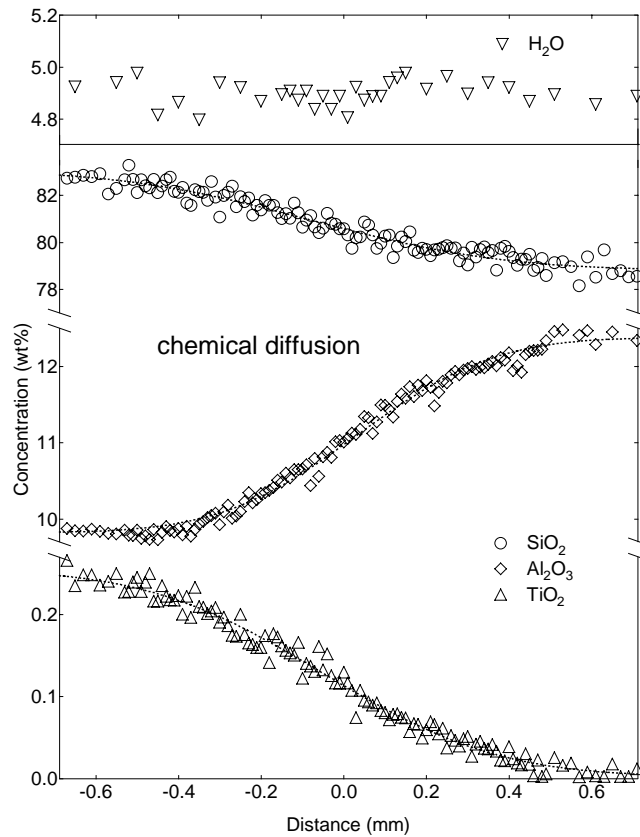


Fig. 9: An example of concentration profiles of SiO_2 , Al_2O_3 and TiO_2 measured in a chemical diffusion couple for an experiment at 1100 °C in a rhyolitic melt containing about 5 wt % H_2O . The profiles do not reach the ends of the couple and no indication of uphill diffusion is found.

4.6. Precision of Diffusion Data

Reproducibility of data collection and evaluation was tested by duplicated measurements of profiles on the same sample (e.g. run D1, D15, D12 and D30). Differences in the diffusion coefficients are within the uncertainties derived from error calculations. Calculation of errors of the diffusion coefficient follows Behrens and Koepke (2001) considering uncertainties in run duration, temperature and water content as well as the spatial resolution of SYXRF, the intensity of the fluorescence signal of the SYXRF and the quality of the fit. In the short term experiments the uncertainty in the run duration due to heating up and cooling down can have a systematic influence on diffusivity data. The time ($t_{\text{heat/cool}}$) required at run temperature to produce the same profile length as generated in the heating/cooling period was calculated for

each element using the individual activation energies for diffusion. $t_{\text{heat/cool}}$ decreases with increasing activation energy and is the largest for Rb and the smallest for HFSE's (Zr). Estimated uncertainties due to run duration range from 1% for 800°C to 6% at 1400°C for short term runs (50 h-30 min) and from 0.02% to 3% for long term runs (15 d-4.5 h). The error of diffusivity due to uncertainty of temperature increases with the activation energy of diffusion and decreases with temperature. HFSE have a contribution of temperature to the error in diffusivities of about 15% at 1100 °C and LFSE of about 5 % at 1400 °C. Uncertainties in the determination of water contents by IR measurements is estimated to be 2% (relative). Variation of water content along the diffusion profiles are within 0.2 wt% for short term runs and 0.4 wt% for the long term runs. The quality of the concentration distance profiles (lower signal to noise ratio) increases with increasing intensity of the fluorescence signal of the SYXRF. Based on fit quality, elements of high quality (Ge, Rb, Sr, Y, Zr, Nb) with 3-5 % standard error of D, intermediate quality (Co, Ni, Cu, V, Sn, Ba, La, Nd, Sm, Eu, Gd) with 10-15 % standard error of D and low quality (Er, Yb, Hf, Ta) with 30-50 % standard error of D can be distinguished (Koepke and Behrens (2001)). The resulting total errors of diffusivity are included in Tab. 2, 3 and 5.

4.7. Enhancement of Diffusivities by adding H₂O

In Fig. 10 diffusion coefficients of various cations in rhyolitic melts at 1200 °C as a function of dissolved water in the melt are presented. The data show an enhancement of diffusion by 1.5 to 3.5 log units when adding 5 wt% H₂O to the water-poor melt.

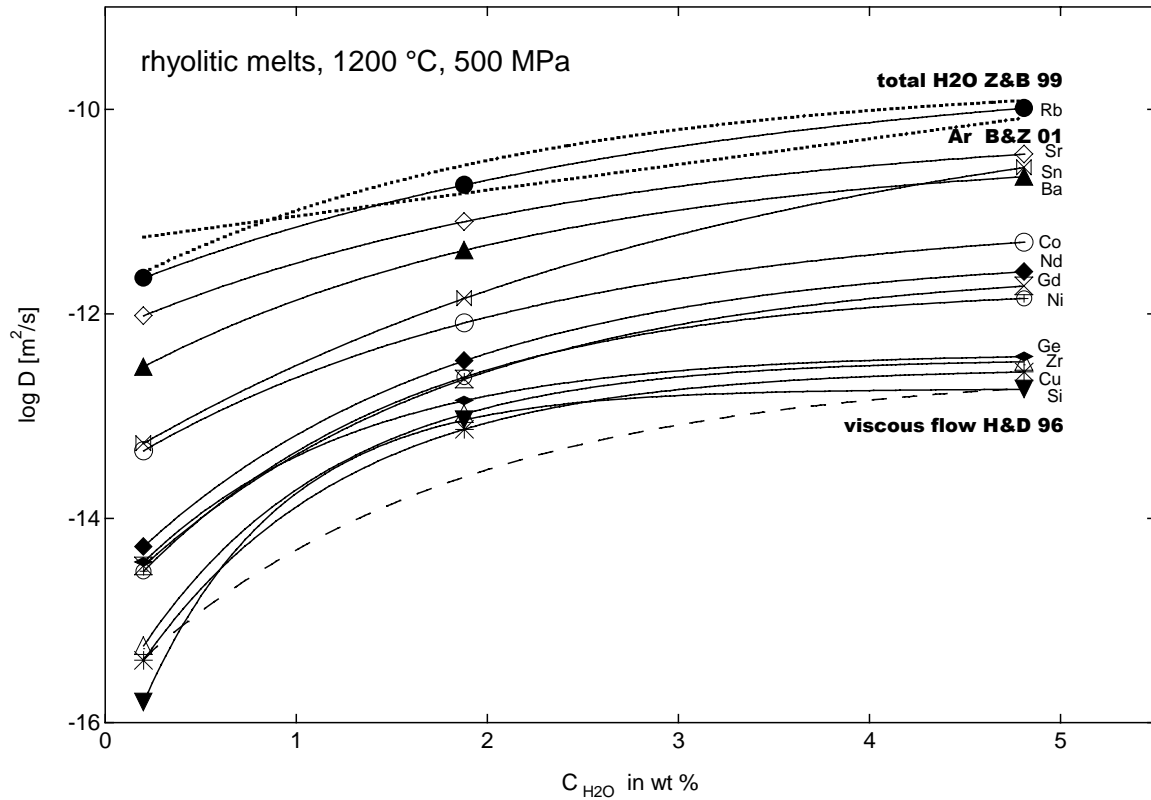


Fig. 10: Dependence of diffusivities upon the H₂O content in rhyolitic melts at 1200 °C.

The dependence on water content decreases with water content and it is larger for the HFSE's and the major elements Si and Al than for the LFSE's Rb and Sr. Diffusivities of Rb and Zr increase by 1 and 2 log units, respectively, from 0.2 to 1.9 wt% H₂O and by 1 log unit from 1.9 to 4.9 wt% H₂O. A relatively large variation with water content is observed for Sn which may indicate a change in redox state with hydration. In excellent agreement are diffusivities for the HFSE Zr and Si with the chemical diffusivity D_{η} derived from the viscous flow modelled after Hess and Dingwell (1996) at low and high water content. The total water diffusion in rhyolitic melts (Zhang and Behrens, 1999) and also the Ar diffusion (Behrens and Zhang, 2001) in hydrous silicate melts with similar compositions to melts used in the present study are close to the diffusion of the LFSE Rb.

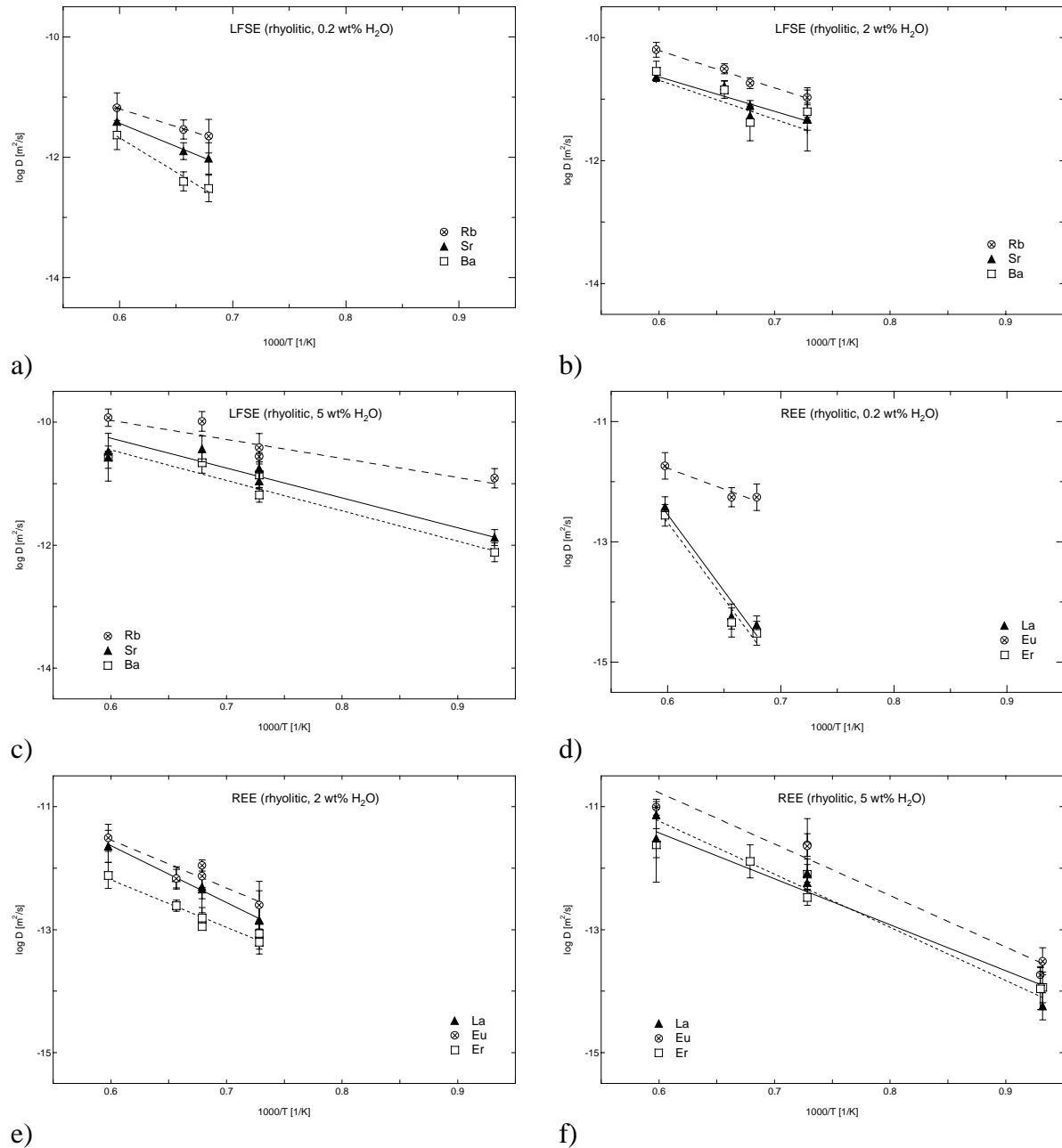
4.8. Temperature Dependence of Diffusion in Rhyolitic Melts

To investigate the temperature dependence of cation diffusion, experiments were performed at least at three to four different temperatures in the temperature range of 800-1400°C, depending on water content. With the anhydrous composition, experiments are limited to temperatures $\geq 1200^\circ\text{C}$ because of partial crystallization at lower temperatures. Diffusion coefficients with an error of more than 0.35 log units were not considered for calculations of activation energies for rhyolitic melts (see Tab. 2, 3 and 4). At constant pressure the temperature dependence of diffusivity can be described by an Arrhenius law (Glasstone et al., 1941):

$$D = D_0 \cdot e^{\frac{-E_a}{RT}}, \quad (6)$$

where R is the gas constant, T the absolute temperature in Kelvin, D_0 a pre-exponential factor and E_a the activation energy for diffusion. Fig. 11 a-j show the Arrhenius plots for selected elements of the different geochemical elemental groups. The activation energy for trace element diffusion increases from 116 kJ/mole for monovalent Rb to 231 kJ/mole for tetravalent Ge in rhyolitic melts with 2 wt% H_2O and from 59 kJ/mole for Rb to 161 kJ/mole for Ge in rhyolitic melts containing about 5 wt% H_2O . For the REE's the activation energies are intermediate between those of LFSE's and HFSE's. The TME Co has a relatively low activation energy for diffusion similar to those of the LFSE's. Activation energies for chemical diffusion of the major components Al_2O_3 and SiO_2 (197 and 207 kJ/mole for melts with 2 wt% H_2O and 156 and 160 kJ/mole for melts with 5 wt% H_2O) are in the same range than activation energies for the HFSE's. The increase of E_a from the LFSE to HFSE is about 100 kJ/mole at both 2 and 5wt% H_2O . Activation energies for diffusion in melts with 2 wt% H_2O are higher by about 20 kJ/mole for LFSE and by up to 60 kJ/mole for HFSE compared to melts with 5 wt% H_2O . Activation energies for the water-poor melts increase from 112 – 218 kJ/mole for Rb – Ba and further to 464 – 467 kJ/mole for Hf – Zr. Since the temperature range

of 1200-1400°C is very small and only one data point for each temperature is available, errors in E_a resulting from the Arrhenian fits are higher for E_a in water-poor than for E_a in the hydrous melts.



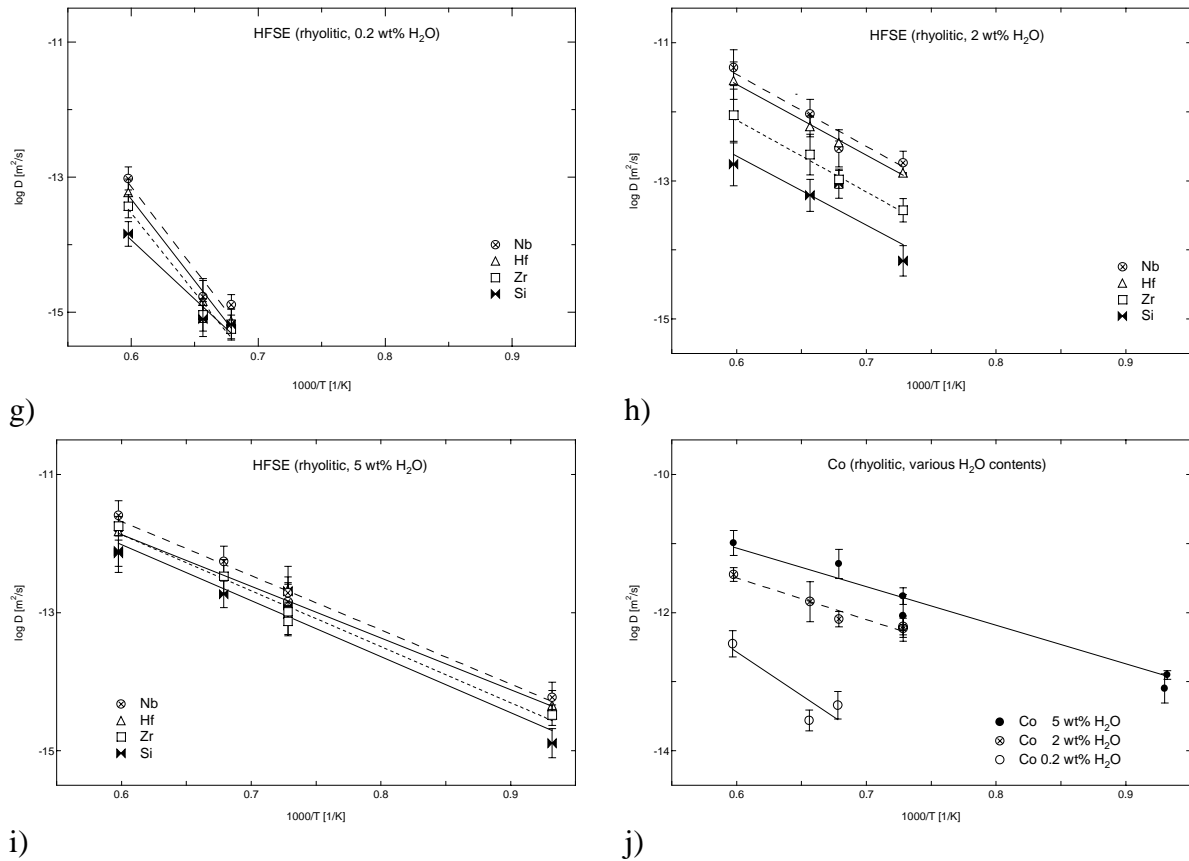


Fig. 11: Temperature dependence of the elemental groups in Arrhenius plots of $\log D$ as a function of $1/T$. From the slope of Arrhenius plots activation energies E_a in kJ/mole were calculated.

4.9. Pressure Dependence of Diffusion in Dacitic Melts

Diffusion experiments with dacitic melts containing about 5 wt% H_2O were performed in the IHPV at three different pressures at 1200°C in the pressure range of 100 – 500 MPa to investigate the pressure dependence on cation diffusion. The experiment performed with the same melt composition at 1 GPa in the PCA (PC11) is not taken into account because this sample showed deformation after the run. The apparent diffusion coefficients of all elements evaluated from these experiments are quite similar. This indicates transport by flow of the melt and these samples were not considered for evaluating the pressure dependence. From Tab. 5 it is evident that the pressure effect on the diffusion of the LFSE is negligible (diffusivities are almost identical for Rb, Sr and Ba in the pressure range 100-500 MPa) but

for higher valenced cations such as REE and HFSE diffusivities decrease with increasing pressure by 0.4-0.6 and even 1.2 log units, respectively.

Since the solubility of water in dacitic melts at 100 MPa is about 4 wt% at 1200 °C (pers. comm. by Ohlhorst) the measured water content after the experimental run is only 4.5-4.7 (PCH14), which is 0.2-0.5 wt% lower than of runs at 250 and 500 MPa. This might also caused the small variation in diffusivities of the cations in PCH14, which is only 0.5 log units from Rb to Hf. Most likely are diffusive processes of the cations influenced by an mixing process of the unsoluted water during the experiment.

However, at constant temperature the pressure dependence of diffusion can be expressed analog to the Arrhenius-type equation:

$$D_{T,P} = D_T \cdot e^{\frac{-PV_a}{RT}}, \quad (7)$$

where R is the gas constant, T the absolute temperature in Kelvin, D_T is the diffusivity at one bar and V_a is the apparent activation volume diffusion. Fig. 12 shows the Arrhenius plots for selected elements of the different geochemical elemental groups.

Activation volumes were determined by linear regressions for each element for the water-rich dacitic melt composition (Tab. 6). It is noteworthy that pressure not only affects the mobility of cations but also the structure of the melt. Thus, the activation volume can not be directly related to the local expansion required for a jump of a cation as in the case of crystals. The apparent activation volume increases from 12 cm³/mole for Ni over 18 cm³/mole for Ba over 43 cm³/mole the REE's and Sn to about 80 cm³/mole for Hf. The TME Co has the lowest V_a comparable with those for Ni and Ba.

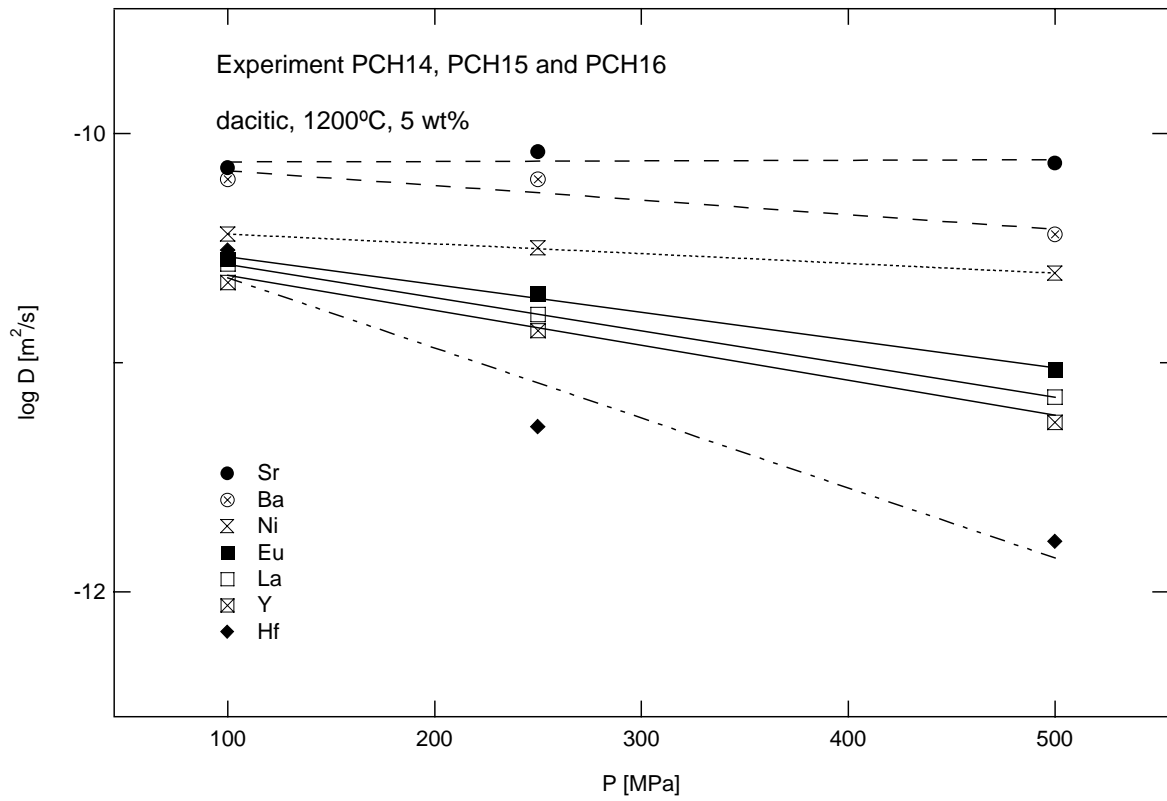


Fig. 12: Pressure dependence of various elements. Apparent activation volumes are calculated from the slopes.

5. DISCUSSION

5.1. Comparison of SYXRF and SIMS Analyses

The two analytical techniques are reliable and convenient for analysing trace elements with detection limits under the ppm limit. With the SYXRF it is possible to analyze simultaneously elements (multi-element spectra) with atomic numbers between 20 and 92 using the K_{α} lines as analytical signal at a very small spatial resolution and with no damage of the sample material. In contrast to SIMS analysis of glasses (Koepke et al., 1998) matrix effects due to water in the glasses are negligible in SYXRF analysis. An easy analysis and quantification of the X-ray spectra due to a fundamental and detailed knowledge about the physics of X-rays enables automatically processing of a great number of X-ray spectra within a short time, whereas for SIMS analysis magnets have to be calibrated for every session with special metal standards and for every element. However, due to the X-ray penetration and negligible absorption of synchrotron radiation inside the samples, a cylindric volume is analysed in SYXRF. For that reason the lateral resolution depends on thickness and orientation of the sample and can only be kept with a small section thickness of 50-80 μm , which is very difficult to prepare and to mount on the sample holder.

An important advantage of SIMS is its high sensitivity and the ability to count individual ions results in detection limits in the parts-per-billion range for many elements. Also the fact that ions released from the sample are separated by their mass-over-charge ratio means that isotopic analyses can be performed on very small sample volumes. However, no simultaneous analysis of the elements is possible and especially for the short profiles such as Zn, Ge, Hf, Zr, Nb and Ta counting times of about 20 min for one point of the diffusion profile are necessary to observed sufficient secondary ions because of working with a smaller beam size in contrast to SYXRF measurements of 4 min for one point. Since the bombarding with the primary

beam damages the sample with crater-like spots, reproducibility measurements can not be done on the same point.

Diffusion profiles determined by SYXRF and SIMS are in excellent agreement for the most elements. However, each method has disadvantages with respect to selected elements out of the given trace element data set, which is already discussed in detail with the results (chap. 4.4). Problematic elements for SIMS are V (overlapping with NaSi molecule), Sn (intensity too low), and Ni (overlapping with CaO molecule). Problematic elements for SYXRF are Ta (material of the cross slit system at the SYXRF) and Ce (too low concentrated in the glasses). Fluorescence signals of the heavier elements such as Er, Yb, Ta and Hf have very low intensities, which lead to a large scattering in the analyzed diffusion profiles.

In this study diffusivities of Cu determined by SYXRF deviates strongly from other TME's. Diffusion coefficients of Cu are more in the order of diffusivities of major components SiO₂ and Al₂O₃. This is an unexpected slow diffusion for Cu¹⁺ or Cu²⁺ and could demonstrate a strong coupling on the network dynamics, possibly be caused by the d-electrons and the tendency to form strong complex structure of Cu. On the other hand the diffusion of the TME's Co and Ni evaluated from SYXRF profiles are slower than the other divalent cations Sr and Ba it could be a systematically analytical effect in SYXRF measurements as well. Results from SIMS analyses for the TME's are more compatible to the divalent cations but there were no peakoverlaps found for TME's in SYXRF analysis. It might be difficult to separate the peak position of each TME because fluorescence peaks of the TME are very close together.

5.2. Effect of H₂O on Diffusion

The new experimental study presents diffusion coefficients for a large variety of important cations in rhyolitic and dacitic melts in order to evaluate the effect of dissolved water on diffusion. To constrain and quantify how H₂O contents affect cation diffusion, homogeneity

of H₂O in diffusion couples and triple plays an important role. Concentration of H₂O vary at most by 0.25 wt% within a couple or triple (see Fig. 9, Tab. 2, 3 and 5). Except of two long term runs (D2, D9) the water content after experiment was close to the nominal water content of the starting glasses indicating that water loss or gain during the experiment is negligible. Diffusion data obtained from the runs D2 an D9 are similar to data from the corresponding short term runs. This suggest that water loss in these particular runs mainly occurred in the final stage of the experiments. To estimate whether an initial inhomogeneity in water distribution may affect the diffusion of cations in the rhyolitic samples, bulk water diffusivities in rhyolitic melts at various conditions were calculated (Zhang and Behrens, 2000). As shown in Fig. 10 water migrates much faster than most of the cations at 1200 °C and 500 MPa. Thus an initial inhomogeneity of water is rapidly equilibrated in the regime of diffusion of all elements except of the LFSE's. On the other hand, the LFSE's are not very sensitive to the water content, especially at high c_{water} . Therefore, it can be concluded that small initial differences in water content of the constituents of the diffusion couples or triples had no significant influence on the experiments.

5.3. Effect of Pressure on Diffusion

Since no detailed studies has been obtained for the diffusion mechanisms in hydrous dacitic melts, the effect of pressure on transport of mater only in rhyolitic melts or simple analog compositions is briefly reviewed. Mungall and Dingwell (1997) observed an increase of Th and U diffusivity in haplogranitic melts containing 0.02–0.3 wt% water by a factor of 4 at 1400°C, when the pressure was increased by 1 GPa. In contrast, diffusion of the noble gas Ar in rhyolitic melts with <0.5 wt% H₂O strongly decreases with pressure at 600°C but it is almost independent on pressure at 1000°C for melts containing up to 5 wt% H₂O (Behrens and Zhang, 2001). Baker and Watson (1988) found that an increasing pressure enhances the diffusion for Al, Fe, Si, Mn, and Y but slows the diffusion for the HFSE's Zr and Nb in a

complex silica rich melt. The effect of pressure on cation diffusion may be correlated to the melt viscosity. Kushiro (1976) found a negative dependence of the viscosity of anhydrous albitic melt. On the other hand, the viscosity of a hydrous haplogranitic melt (6 wt% H₂O) is independent on pressure in the range 0.3–1 GPa (Schulze et al. 1996). The viscosity reduction in the polymerized albitic melts was interpreted as the result of a disruption of the three-dimensional network of silicon-aluminum-oxygen tetrahedral (Mysen and Virgo, 1985). With increasing depolymerization of the melt (e.g., by incorporation of H₂O) this effect becomes less important and melt viscosity change towards a positive pressure dependence. The conclusion from these result is that applying this diffusivity data to pressures differing by \pm 500 MPa from the experimental pressure of 500 MPa used in this study has no significant error for hydrous rhyolitic melts (2-5 wt% H₂O) but may have an error of up to 0.3 log units for water-poor melts.

5.3.1. Comparison to other Diffusion Studies on Rhyolitic Melts

Tracer diffusion in natural or dehydrated obsidians was extensively studied at ambient pressure twenty years ago using radiotracers and etching techniques (Jambon, 1982). The diffusivities of the LFSE's Rb, Sr and Ba extrapolated to 1200 °C are $\log D_{\text{Rb}} = -11.4$ and $\log D_{\text{Ba}} = -11.5$ (Jambon, 1982) and $\log D_{\text{Sr}} = -11.6$ and $\log D_{\text{Ba}} = -12.1$ (Margaritz and Hofmann, 1978 a). Considering the uncertainty of the diffusion data due to the extrapolation from the experimental range ($T < 950^\circ\text{C}$) and the poorly constrained water content (H₂O profiles were not measured after the runs in both studies), the agreement with data of this study is very good (within one log unit). The Eu diffusivity determined by Jambon (1982) is half an order of magnitude faster than measured by Margaritz and Hofmann (1978 b), which may be explained by differences in water content and/or redox state of europium. Extrapolated Ce diffusivity at 1200°C is close to REE data of this study, the extrapolation to lower temperatures such as 800 °C differ by about 2 log units compared to results of Mungall et al. (1999) for Nd in

anhydrous melts. This could be likely affected by the error in extrapolation. Diffusivities of this study and the study of Mungall et al. (1999) are determined at higher temperatures than those of Jambon (1982). Activation energy for Ce is about 490 kJ/mole (875-1300°C), which is comparable with E_A 's for REE's in nominally anhydrous melts of this study at 1200-1400°C.

Activation energies for cation diffusion in obsidians summarized by Jambon (1982) are in the trend of results for rhyolitic hydrous melts of this study showing an increase of E_a with decreasing water content (Tab. 4). Diffusion data for a large set of trace elements in a haplogranitic melt were determined by Mungall et al. (1999) using SIMS to measure concentration-distance profiles after diffusion couple experiments (see Fig. 13 and Fig. 14).

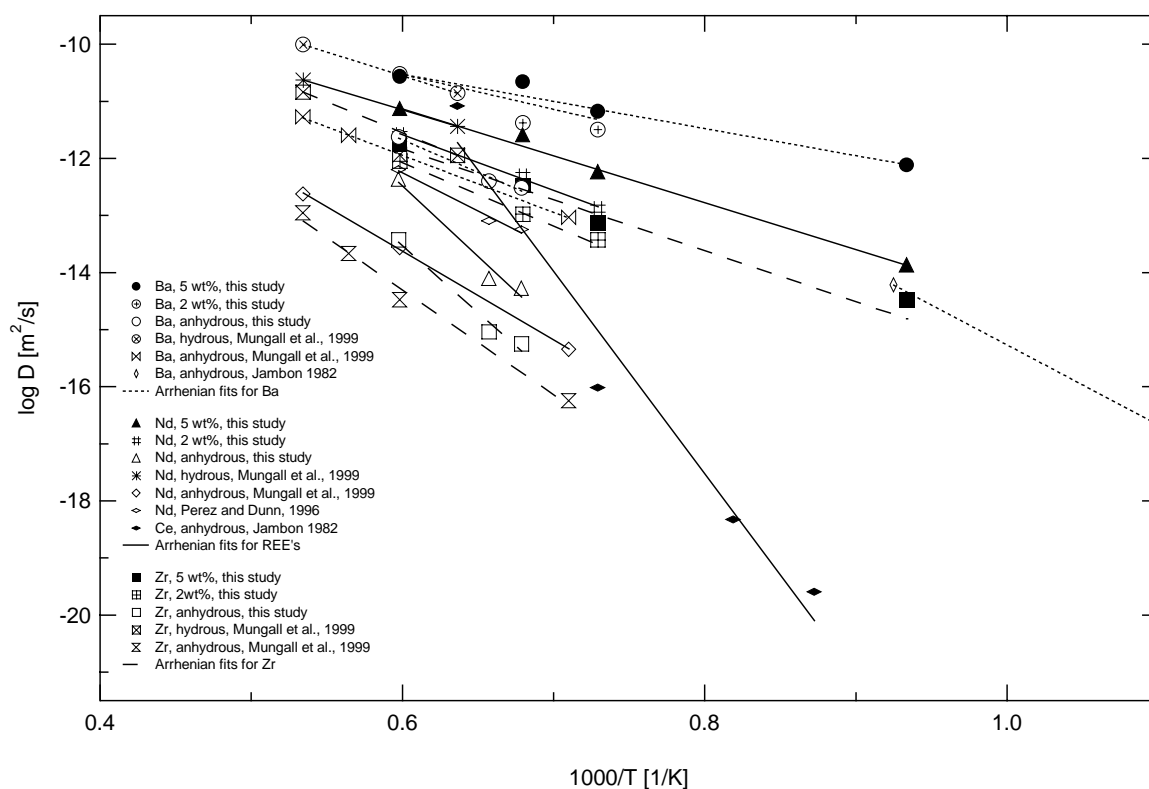


Fig. 13: Arrhenian plot of results of Mungall et al. (1999) and Jambon (1982) for granites compared to our results. Circled lines represent Arrhenian plots for Ba, solid lines for Nd and dashed lines for Zr. Jambon (1982) only measured Ce as a representative REE in his study.

Compared to results of this study at 500 MPa, diffusivities in the anhydrous haplogranitic melts at 1 atm melt are slower by 0.2 to 0.5 log units for the LFSE Ba, by 0.3 – 1.5 log units

for the REE Nd and by 0.2 to 1.0 log units for the HFSE. An explanation for the lower diffusivity in the study of Mungall et al. (1999) might be a lower water content of the samples, because diffusivity in rhyolitic melts is very sensitive to c_{water} at low water content. Anhydrous samples used for this study contain about 0.15 wt% H₂O. The water content of the nominally anhydrous haplogranitic melts of Mungall et al. (1999) is not known, but a water content about 0.1 wt% lower than in melts of this study would explain the lower diffusivities. However, differences in experimental and analytical procedures, anhydrous melt composition and run pressure may also contribute to the difference in the diffusion data. Sr and Nd diffusivities in nominally dry rhyolitic melts at 10 GPa were determined by Perez and Dunn (1996) using electron microprobe to analyze profiles in diffusion couples. Perez and Dunn only measured the water content of selected diffusion samples by IR spectroscopy. These measurements indicate a higher c_{water} (0.5-0.7 wt%) than in water-poor samples used in this study. In the range 1200-1250°C their data are in excellent agreement with measurements presented here (within 0.3 log units).

5.3.2. Hydrous Melts (> 0.5 wt% H₂O)

Jambon et al. (1978) firstly demonstrated the large effect of dissolved water on cation diffusion in rhyolitic melts for Cs. It is difficult to interpret quantitatively the results of their pioneering study because experiments were performed in an open capsule under Ar pressure, so that water partly diffused out of the melt. Watson (1981) confirmed the dramatic enhancement of Cs diffusion by dissolved water and found an increase by 2.5 to 3.5 log units when 6 wt% H₂O were added to an anhydrous melt at 700–900°C. His results indicate that the enhancing effect of water is related to the mobility of the cation. For the faster diffusing Ca the effect is smaller than for Cs and diffusion of the mobile Na is nearly independent of water content of the melt. Data of this study in Fig. 10 support the correlation between the enhancing effect of H₂O and the cation mobility, but the effect of H₂O is less pronounced at

1200°C than at 700-900°C. Diffusivity of Rb and Sr increases by 1.6 log units and diffusivity of Si by 2.7 log units when 5 wt% water are added to the melt at 1200°C. The studies of Mungall and Dingwell (1997) and Mungall et al. (1997) on diffusion in haplogranitic melts indicates that the enhancement by dissolved H₂O becomes even smaller at 1400°C. Diffusivities of Th and U increased only by about 2 log units when 5 wt% H₂O were added (Mungall and Dingwell 1997) and diffusivity of the LFSE Ba did not vary noticeably with water content (Mungall et al. 1999).

In general, the data of Mungall et al. (1999) for trace element diffusion in hydrous haplogranitic melts (3.7 wt% H₂O) at 1 GPa are in excellent agreement to data of this study (Fig. 13 and Fig. 14). So combination of both data sets can be used to describe trace element diffusion for a wide range of elements at various temperatures and water contents. However, there are some differences in detail, e.g. in variation of diffusivity of alkaline Earth elements, which will be discussed later on.

5.4. Comparison to other Melt Compositions

The diffusion behavior of cations depend on the matrix composition of the melt and therefore it is interesting to compare diffusion data of dacitic and rhyolitic melts of this study to different compositional systems such as andesite and basalt (see Fig. 14).

In general, the trace element diffusion coefficients in anhydrous rhyolitic melt (high-viscous) are smaller than in andesitic and basaltic (low-viscous) melts, especially at low temperature. Trace element diffusivities of Ba and Zr in anhydrous rhyolitic melts at 1200-1250 °C and 500 MPa are 1.2 and 3.3 log units slower than in an haplobasaltic melts at 1 atm (extrapolated data from LaTourrette et al. (1996)). This data indicate that for the LFSE Sr the diffusivity is also about one log unit slower in rhyolitic melts than in basaltic melts like determined by Leshner (1994) but more than 3 log units smaller for the REE such as Nd. Tracer diffusion coefficients for rhyolitic melts of this study are lower than for andesitic melts studied by Koepke and

Behrens (2001), e.g., by 0.2 log units for Rb and Ba and 1.0 log units for Zr and Nb at 1200 °C for a melt containing 5 wt% H₂O. In andesitic melts Eu is also faster than the other REE but the difference in mobility compared to the neighbor elements is more pronounced in rhyolitic melts (experiments were performed at similar redox conditions in both studies).

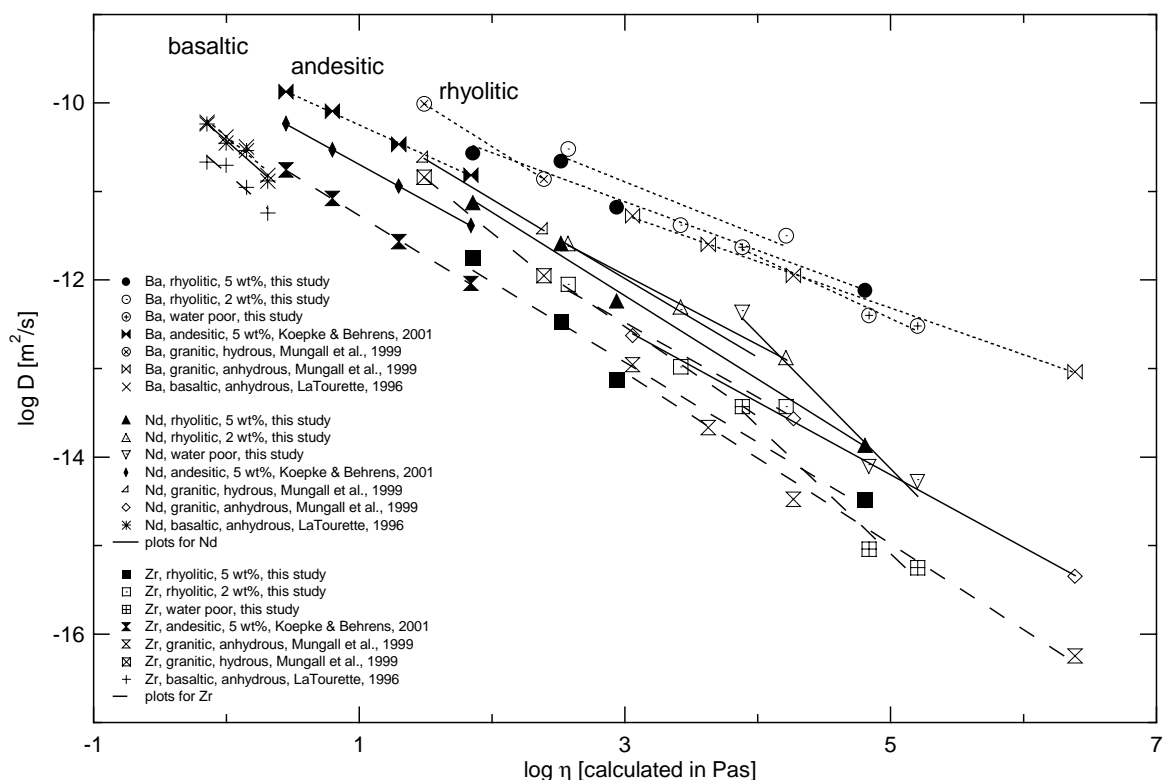


Fig. 14: Variation of trace element diffusion for Zr, Nd, and Ba with viscosity in melts of different compositions. Andesite: Koepke and Behrens (2001), Granite: Mungall et al. (1999); Basalt: LaTourrette et al. (1996). Circled lines represent linear regressions of the data points for Ba, solid lines for Nd and dashed lines for Zr.

5.5. Speciation and Effect of Redox Conditions on Trace Element Diffusion

Our experimental data of diffusivities and results of the other studies discussed above indicate that the mobility of cations at any given temperature and melt composition relate in some way to ionic properties such as radius or/and charge. Especially charge and coordination numbers of many elements depend strongly on experimental conditions and melt composition, but spectroscopic data for this systems are still little investigated. Available spectroscopic data known from the literature are summarized:

Transition elements Ni and Zn are usually in a divalent state in silicate glasses (Brown et al., 1995). Results of Farges et al. (2001) show that in sodiumtrisilicate and albite glasses dissolved water increases the coordination number of Ni from 5 to 6. From wet-chemical analysis (titration against KI by Johnston, 1965) of andesitic melts Co is found to be predominantly (94%) divalent. Under very reducing conditions Cr is usually divalent (Schreiber et al., 1978; Keppler, 1992). Wilke and Behrens, (1999) found Eu to be di- and trivalent under intrinsic conditions of the IHPV. In hydrous haplogranitic melts Sn changes from divalent under reducing conditions to tetravalent under oxidizing conditions in CSPV's (Linnen et. al, 1996). Nb is usually considered to be Nb⁵⁺ (e.g., Keppler, 1993; Horng et al., 1999).

Experimental data on the effect of redox conditions on diffusion of heterovalent elements in silicate melts are obtained by LaTourette and Wasserburg (1997). They studied the effect of oxygen fugacity on the diffusion of some elements including Eu in a haplobasaltic system at 1 atm. Decreasing oxygen fugacity from air to Fe-FeO buffer conditions at 1400°C increased the Eu diffusivity by a factor of two whereas the Nd diffusivity remains unchanged.

Comparing the diffusion data of Eu with its neighbour elements Sm and Gd, which are both present only in the trivalent state, and with Sr, which is divalent and has a similar radius as Eu. Therefore the diffusion flux of Eu could be described with the diffusion of Eu²⁺ and Eu³⁺ (see Koepke and Behrens, 2001). Assuming that the diffusion of Sr²⁺ is comparable with the diffusion of Eu²⁺ and an average of the diffusion of Sm³⁺ and Gd³⁺ with the diffusion of Eu³⁺, Eu²⁺/Eu_{total} ratios from the diffusion coefficients listed in Tab. 2, 3 and 5 were calculated with

$$X_{\text{Eu}^{2+}} = \frac{(D_{\text{Eu}} - (D_{\text{Sm}} + D_{\text{Gd}})/2)}{(D_{\text{Sr}} - (D_{\text{Sm}} + D_{\text{Gd}})/2)}. \quad (8)$$

Experiments in this study were performed in three different pressure apparatus with different redox conditions, which vary from very oxidizing ($\Delta\text{NNO}+3.5$ at 1100 °C, 500 MPa in the IHPV) to very reducing ($\Delta\text{NNO}-2$ at 1200°C, 1 GPa in the PCA).

The ratio of $\text{Eu}^{2+}/\text{Eu}_{\text{total}}$ depends not only on the intrinsic conditions of the IHPV or PCA but also on the water content in and the composition of the melt. Ratios of dacitic melts performed in the PCA are calculated to be 0.11-0.25 for water contents of 2 wt% H_2O , whereas ratios of dacitic melts performed in the IHPV with 5 wt% H_2O are only 0.04-0.11. With increasing water content the conditions become more oxidizing and Eu^{3+} clearly dominates in water-rich melts. This could also be affected by the preoxidated starting materials synthesized in the IHPV. It is not clear, if an equilibrium is reached for the redox reaction during the experimental run in the PCA or if the permeability of H_2 affects the oxygen fugacity.

In the water-poor rhyolitic melts the calculated ratios of $\text{Eu}^{2+}/\text{Eu}_{\text{total}}$ are 0.42-0.57, whereas ratios in hydrous rhyolitic melts containing about 2 wt% H_2O reach a minimum at 0.01-0.13 and increase to 0.02-0.24 for melts with up to 5 wt% H_2O . Since the diffusion of H_2O and H_2 is faster than diffusion of di- and trivalent cations (Chekmir et al., 1985, Behrens and Nowak, 1997) a rapid oxidation and reduction can be achieved in hydrous melts by the redox reaction of H_2O and H_2 . Since in water bearing glasses at low water contents (<4 wt% of total H_2O) hydroxyl groups are the dominant species next to molecular H_2O (Nowak and Behrens, 2001; Zhang et al., 1997 and Stolper, 1982), the minimum of $\text{Eu}^{2+}/\text{Eu}_{\text{total}}$ for melts with about 2 wt% H_2O could possibly be caused by the stabilization of the trivalent Eu species by OH groups. $\text{Eu}^{2+}/\text{Eu}_{\text{total}}$ ratios estimated from diffusion data of Koepke and Behrens (2001) are at all temperatures in the hydrous (around 5 wt% H_2O) andesitic melt lower than in the here presented rhyolitic melts with the same water content. Eu^{3+} clearly dominates in their hydrous melts. The $\text{Eu}^{2+}/\text{Eu}_{\text{total}}$ ratio of 0.06 of their anhydrous andesitic melt is close to unity, whereas in rhyolitic melts the $\text{Eu}^{2+}/\text{Eu}_{\text{total}}$ ratio is 0.2. Since experimental conditions are identical to experiments of this study, it can be assumed that compositional effects have an influence on the $\text{Eu}^{2+}/\text{Eu}_{\text{total}}$ as well.

Linnen et al. (1995) studied the effect of f_{O_2} on the solubility, diffusion and speciation of tin in haplogranitic melts adjacent to cassiterite crystals at 850 °C and 2 kbar. They found the fastest

diffusion for tin at the most reducing conditions ($f_{O_2} = \text{NNO} - 1.8$) and a decrease in diffusivity with increasing oxygen fugacity concluding that Sn^{2+} behaves as a network modifier at reducing conditions and Sn^{4+} as a HFSE at oxidized conditions ($f_{O_2} = \text{NNO} + 2.5$). The activation energy for diffusion of tin in rhyolitic melts with 2 wt% H_2O (183 kJ/mole) is found to be in the same order than activation energies of the HFSE (see Tab. 4), whereas the activation energy for tin in melts with 5 wt% H_2O (99 kJ/mole) is more close to activation energies for divalent cations such as Sr and Ba. That means in rhyolitic melts with 2 wt% H_2O tin is dominantly present as Sn^{4+} , whereas in melts with 5 wt% H_2O tin is more stable as Sn^{2+} . The stabilization of Sn^{2+} in the melt structure could be caused by complexation with H_2O species in this study.

Since the diffusivity of Nb in rhyolitic melts is always higher than diffusivity of the tetravalent cations Zr and Hf which have almost identical diffusivity, is inconsistent with Nb being exclusively Nb^{5+} . A portion of Nb^{3+} in the melt could explain the relative high diffusivity of Nb also found in andesitic melts by Koepke and Behrens (2001).

5.6. Predicting Trace Element Diffusivity

Difficulties in finding a quantitative prediction of diffusion coefficient and their relation to cation properties are the not well defined ionic radii of the cations in the melt structure and uncertainties in clarifying of the coordination number. Additionally radius and charge can not be clearly defined for some elements because they exist in more than one oxidation state.

To study the relation between diffusivity and ionic size, Jambon (1982) determined diffusivities for alkalis in natural and dehydrated obsidian at 300 to 1300 °C and 0-400 MPa and Roselieb and Jambon (1997) measured diffusivities of the alkalis K, Rb and Cs in supercooled jadeite melt at temperatures between 800 and 1020 °C at 1 bar. They found a clear decrease of diffusivities with increasing cation size. This is also observed for alkalis in the system $\text{SiO}_2\text{-NaAlSi}_2\text{O}_6$ by Rothman et al. (1982). Diffusivities for the LFSE Sr and Ba in

this study show also a decrease of diffusivity with increasing cation size. Nakamura and Kushiro (1998) found higher diffusivities for Sr in comparison with Ba both in a jadeite and in a diopside melt at high pressure. Surprisingly, Mungall et al. (1999) observed an opposite trend for alkaline earth elements in haplogranitic melts. They found a positive correlation to cation size for Sr and Ba.

In this study, no simple relationship between diffusivity and ionic radius applies to cations with the same charge. On one hand Sr^{2+} (ionic radius = 1.26 Å) diffuses faster than Ba^{2+} (1.42 Å), on the other the smaller Ni^{2+} (0.69 Å) diffuses slower than both. Therefore this relationship does not apply for all melt compositions and care is needed when using it especially for TME. This could prove the diffusion data of Cu, Co and Ni indicating strong bondings of d-elements in complex structures with oxygen species.

For diffusing species with similar size and different cationic charge (He , Na^+ , Ca^{2+} , Ce^{3+}) a depressing effect of charge on diffusivity and a negative correlation between cation radius and diffusivity for alkalis was found in granitic melts for temperatures up to 1000°C (Jambon, 1979).

Hofmann (1980) found a linear decrease of $\log D$ with the ionic field defined as z^2/r (z = atomic number, r = ionic radius) for monovalent Na to pentavalent V in basaltic melts at 1300°C. In order to find correlations of diffusion with cation charge and size for results of this study diffusion data versus the ionic field strength are plotted in Fig. 15 defined as the ratio of charge to the squared distance between cation and oxygen (Dietzel, 1942). Coordination number, charge and radius of the diffusing cations are discussed in Koepke and Behrens (2001) assuming that the large sized LFSE and most REE are 8-coordinated and the smaller sized REE Er and Yb as well as the TME and HFSE are 6-coordinated. For calculations of the ionic field strength corresponding ionic radii from Shannon (1976) were used and coordination numbers and charge for each cation follows Brown et al. (1995).

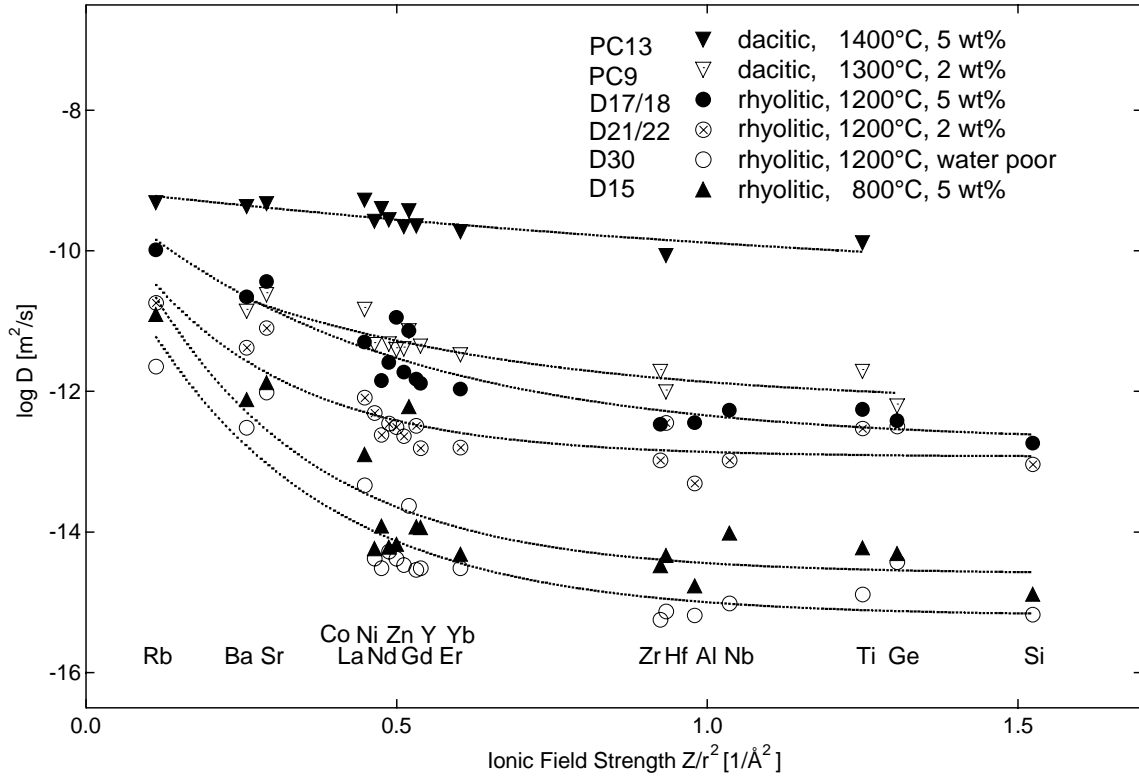


Fig. 15: Correlation between cation diffusivity in hydrous rhyolitic melts and ionic field strength (z / r_{M-O}^2) defined as the ratio of charge to the squared distance between cation and oxygen. Only cations with a well defined oxidation state are plotted. Diffusivities show a negative correlation to the ionic field strength at any temperature.

A general relation between $\log D$ and ionic field strength is not valid for all elements in the presented system (Fig. 15). Such a relation is only expected for elements diffusing by the same mechanisms. Diffusion coefficients of this study lead to the conclusion that diffusion mechanisms of the elemental groups are different. To understand diffusion mechanisms of the different elemental groups trace element diffusion of LFSE, TME, REE and HFSE is compared with the chemical diffusion of major components Si and Al. In this study tracer diffusivities and also the activation energies of HFSE are for all temperatures and water contents similar to the EBDCs of Si and Al. Since diffusivities for LFSE are much faster it can be suggested that diffusion mechanisms for the LFSE can be described with individual jumps in the melt structure, whereas the diffusion of higher valenced cations is more controlled by viscosity and relaxation of the melt structure. Also Nakamura and Kushiro (1998) suggested that the diffusion behavior of trace elements is correlated with that of major

elements in jadeite and diopside melts. Mono- and divalent cations behave like network modifying cations (such as Na, Ca and Mg) and tri and higher valenced cations behave similarly to network forming elements (such as Si and Al).

5.7. Relation of Diffusivities to Viscosity

The influence of H₂O on the viscosity of haplogranitic melts is well investigated by Schulze et al. (1996) for high temperatures and high water contents. They found a strong decrease of viscosity with the addition of water to the melt, which is more pronounced at lower water contents. Hess and Dingwell (1996) presented an equation for the calculation of shear viscosity's in leucogranitic melts for different water contents and temperatures. Their model is based on Vogel-Fulcher-Tammann fit of 111 viscosity data from the literature. Both models were used to calculate diffusion data from viscosity's using the Eyring equation:

$$D_{\eta} = \frac{k T}{\lambda \eta} \quad (9)$$

where k is the Boltzmann constant, T the absolute temperature in Kelvin, λ is the characteristic jump distance and η the viscosity of the melt in Pas. The calculated viscous flow of Schulze et al (1996) is nearly identical to calculated viscosities of Hess and Dingwell (1996) at 1100 °C and above. At lower temperatures e.g 800 °C viscosities of Schulze et al (1996) are about 0.2 log units higher for water contents of 4-6.5 wt% H₂O. The error in calculation is given by Hess and Dingwell (1996) of about 0.4 log units and the jump distance is set as a constant of 0.5 nm in both models. To compare the EBDC's of this study with Eyring diffusivities D_{η} a jump distance of 0.3 nm as in the study of Koepke and Behrens (2001) is used for calculations. The evaluated EBDC's of Al and Si are in excellent agreement with the calculated D_{η} (see Tab. 2 and 3) with the model after Hess and Dingwell (1996).

In the log D versus log η plot (Fig. 14) most of the investigated elements of the hydrous rhyolite system show a roughly linear relation. For different compositions relevant to nature

(basaltic, andesitic, granitic) only data sets for trace elements including examples for LFSE, REE, and HFSE were used. The viscosity's were either measured (Mungall et al., 1999 for an anhydrous granitic system; Nakamura and Kushiro, 1998 for an anhydrous jadeite system) or calculated (this study using the model of Hess and Dingwell, 1996; LaTourrette et al., 1996 for an anhydrous basaltic system using a model of Shaw, 1972; Mungall et al., 1999 for a hydrous granitic system using the model of Hess and Dingwell, 1996 and Koepke and Behrens, 2001 for andesitic composition using the model of Richet et al., 1996).

As representatives for different geochemical groups, the elements Ba (LFSE), Nd (REE), and Zr (HFSE) were plotted. For all elements a raw correlation between viscosity and diffusivity can be demonstrated which roughly fits independently of melt compositions. E.g., the mobile elements Rb, Sr and Ba show parallel trends with a nearly constant slope. The REE and Y also show parallel trends, but with a slightly steeper slope. The trend of Zr with the slowest diffusivity shows a further small increase in the slope. The different slopes correlate with the activation energies for diffusion of the elements. The covered range in diffusion coefficients is large in highly viscous melts and decreases significantly for less viscous melts. In case of the high-viscous anhydrous granitic melt the diffusivity of Ba is more the 3 decades higher than Zr (this study, Mungall et al., 1999), whereas in a low-viscous melt the difference in diffusivity of these elements is less than an order of magnitude (LaTourrette et al., 1996). The study of Mungall et al. (1999) for the granitic system and this study cover a viscosity range wide enough for evaluating reliable trends. Since pressure dependencies on diffusion is known to be very small and negligible for hydrous granitic melts (Schulze et al., 1996) variation in diffusion could be caused by influences of water species on the melt structure or a variable jump distance depending on water content could explain systematic variation for the diffusion. To set the jump distance as a constant is may be not a universal method to calculate diffusivities or viscosities with the Eyring equation.

For a better understanding of the effect of water on the melt structure in more detail further investigations on the mechanisms of diffusion in hydrous melts are needed in a more broader viscosity range and higher water contents as well. However, the defined relations in the log-log plot open interesting perspectives for prediction of trace element diffusivities in silicate melts. A similar study of Mungall et al. (1999) and Koepke and Behrens (2001) presenting an internally consistent diffusion data set in a granitic and andesitic melt led to the same conclusion.

6. CONCLUSION

With the combination of a new experimental arrangement of diffusion triples and the analytical techniques such as SYXRF or SIMS (trace element diffusion), electron microprobe (chemical diffusion) and IR (H_2O analysis), an internally consistent set of trace element diffusion coefficients and EBDC's for nominally anhydrous and hydrous rhyolitic and dacitic melts could be obtained in a broad temperature (800-1400°C) and pressure range (0.1-1 GPa).

At constant temperature, pressure and water content, diffusivities systematically decrease with ionic charge of the cation. The range of diffusivities in rhyolitic melts is about 3.5 log units at 800 °C and 5 wt% H_2O , about 2 log units at 1100 °C and 2 wt% H_2O and up to 4 log units at 1200 °C in the water-poor melt. A smaller decrease for dacitic melts at 1 GPa (1.5 log units at 1200 °C and 2 wt% H_2O , 0.7 log unit at 1400 °C and 5 wt% H_2O) is found. At constant temperature and water content cations in dacitic melts diffuses at 1200 °C about 0.1 (LFSE) to 1 log units (HFSE) faster with 2 wt% H_2O and at 1400 °C about 0.4 (LFSE) to 2 (HFSE) log units faster with 5 wt% H_2O than in rhyolitic melts. On the other hand, no simple relationship between diffusivity and ionic radius applies to cations with the same charge. Diffusivities of Eu, Sn, V and Nb are always smaller compared to diffusivities of cations with similar cation properties, especially in rhyolitic melts. This may be explained by varying oxidation states during the experiments under intrinsic conditions of the IHPV.

The generally lower diffusivity of the TME than other divalent cations indicates either strong bondings of d-elements in complex structures with oxygen species or profiles are affected by systematically analytical problems at SYXRF which could not be clarified so far.

In general, the enhancing effect of water is stronger for network former (HFSE, Si, Al) than for network modifier (LFSE, TME, REE). Most of the increase in mobility occurs in the first added 0 to 2 wt% H_2O . For H_2O contents from 1.88 wt% to 4.85 wt% the enhancement is only about 0.5 –1.2 log units. The overall enhancement of diffusion by dissolved H_2O is about 1.5-

3.5 log units for nominally anhydrous rhyolitic melts to melts containing about 5 wt%. The minimum of calculated of $\text{Eu}^{2+}/\text{Eu}_{\text{total}}$ for melts with about 2 wt% H_2O could possibly be caused by stabilization of the Eu^{3+} by OH-groups. A relatively large variation with water content is observed for Sn which may indicate a change in valence of Sn from 4+ at low water to 2+ at high water contents.

Chemical diffusion of Ti is found to be systematically 0.2–0.8 log units faster than diffusion of network formers Al and Si in rhyolitic melts. In general, the EBDC of Si, Al and Ti are close to trace element diffusivities of HFSE and in excellent agreement with calculated Eyring diffusivities after Hess and Dingwell (1996). Also activation energies of Al_2O_3 and SiO_2 are in the same range than activation energies for the HFSE's. The increase of E_a from the LFSE to HFSE is 100 kJ/mole at both 2 and 5 wt% H_2O . Activation energies for the water-poor rhyolitic melts increase from about 100 kJ/mole for LFSE to 470 kJ/mole for HFSE in the temperature range of 1200-1400°C. Apparent activation volumes increase from 12 cm^3/mole for Ni to 18 cm^3/mole for Ba to 43 cm^3/mole for the REE's and Sn to about 80 cm^3/mole for Hf in dacitic melts with 5 wt% H_2O in the pressure range of 100-500 MPa at 1200 °C.

No general fitting to the relation between log D and ionic field strength is found for all elements in the used melt system. Therefore diffusion mechanisms of the elemental groups are expected to be different. Diffusion mechanisms for the LFSE can be described with individual jumps in the melt structure, whereas the diffusion of higher valenced cations is controlled by the viscosity of the melt.

7. REFERENCES CITED

- Allen C. M. (1991) Local equilibrium of mafic enclaves and granitoids of the Turtle pluton, southeast California: Mineral, chemical, and isotopic evidence. *Am. Mineral.* **76**, 574-588.
- Bagdassarov N.S. and Dingwell D.B. (1993) Frequency dependent rheology of vesicular rhyolite. *Jour. Geophys. Res.* **98**, 6477 - 6487.
- Baker, D.R. and Vaillancourt, J. (1995) The low viscosities of F+H₂O-bearing granitic melts and implications for melt extraction and transport. *Earth Planet. Sci. Lett.* **132**, 199-211.
- Baker D. R. (1993) The effect of F and Cl on the interdiffusion of peralkaline intermediate and silicic melts. *Am. Mineral.* **78**, 316-329.
- Baker D. R. (1992) Tracer diffusion of network formers and multicomponent diffusion in dacitic and rhyolitic melts. *Geochim. Cosmochim. Acta.* **56**, 617-631.
- Baker D. R. (1991) Interdiffusion of hydrous dacitic and rhyolitic melts and the efficacy of rhyolite contamination of dacite enclaves. *Contrib. Mineral. Petrol.* **106**, 462-473.
- Baker D. R. (1990) Chemical interdiffusion of dacite and rhyolite: Anhydrous measurements at 1 atm and 10 kbar, application of transition state theory, and diffusion in zoned magma chambers. *Contrib. Mineral. Petrol.* **104**, 407-423.
- Baker D. R. (1989) Tracer versus trace element diffusion: Diffusional decoupling of Sr concentration from Sr isotope composition. *Geochim. Cosmochim. Acta* **53**, 3015-3023.
- Baker D. R. and Watson E. B. (1988) Diffusion of major and trace elements in compositionally complex Cl- and F-bearing silicate melts. *J. Non-Cryst. Solids* **102**, 62-70.
- Becker A., Holtz F. and Johannes W. (1998) Liquidus temperatures and phase compositions in the system Qz-Ab-Or at 5 kbar and very low water activities. *Contrib. Mineral. Petrol.* **130**, 213-224.
- Behrens H. and Zhang Y. (2001): Ar-diffusion in hydrous silicic melts: Implications for volatile diffusion mechanisms and fractionation. *Earth Planet. Sci. Lett.* **192**, 363-376.

- Behrens H., Schmidt M.O. (1998): Infrared spectroscopy of hydrous silicic glasses at temperatures up to 600°C and implications for the incorporation and dynamics of water in the glasses. *N. Jb. Mineral. Abh.* **172**, 203-226.
- Behrens H. and Nowak M. (1997) The mechanisms of water diffusion in polymerized silicate melts. *Contrib. Mineral. Petrol.* **126**, 377-385.
- Behrens H., Romano C., Nowak M., Holtz F., Dingwell D.B. (1996) Near-infrared spectroscopic determination of water species in glasses of the system $MAISi_3O_8$ (M = Li, Na, K): an interlaboratory study. *Chem. Geol.* **128**, 41-64.
- Berndt, J., Liebske, C., Holtz, F., Freise, M., Nowak, M., Ziegenbein, D., Hurkuck, W., and Koepke, J. (submitted) A combined rapid-quench and H₂-membrane setup for internally heated pressure vessels: Description and application for water solubility in basaltic melts.
- Blank J. G., Stolper E. M. and Carroll M. R. (1993) Solubility of carbon dioxide and water in rhyolitic melt at 850 °C and 750 bars. *Earth Planet Sci. Lett.* **119**, 27-36
- Blichert-Toft J., Leshner, C. E., and Rosing M. T. (1992) Selectively contaminated magmas of the Tertiary East Greenland macrodike complex. *Contrib. Mineral. Petrol.* **110**, 154-172.
- Brady J. B. (1995) Reference frames and diffusion coefficients. *Am. Jour. Sci.* **275**, 954-983.
- Brown G. E., Farges F., and Calas G. (1995) X-ray scattering and X-ray spectroscopy studies of silicate melts. In *Structure, Dynamics and Properties of Silicate Melts*, (eds. J. F. Stebbins, P. F. McMillan, and D. B. Dingwell), *Rev. Mineral.* **32**, 317-410.
- Burnham, C.W. (1979) The importance of volatile constituents. In *The evolution of the igneous rocks*, **16**. Princeton University Press.
- Chakraborty S. (1995) Diffusion in silicate melts. In *Structure, Dynamics and Properties of Silicate Melts*, (eds. J. F. Stebbins, P. F. McMillan, and D. B. Dingwell), *Rev. Mineral.* **32**, 411-503.

- Chakraborty S., Dingwell D. B. and Rubie D. C. (1995a) Multicomponent diffusion in ternary silicate melts in the system $K_2O-Al_2O_3-SiO_2$: 1. Experimental measures. *Geochim. Cosmochim Acta*, **59**, 255-264.
- Chakraborty S., Dingwell D. B. and Rubie D. C. (1995b) Multicomponent diffusion in ternary silicate melts in the system $K_2O-Al_2O_3-SiO_2$: II. Mechanisms, systematics, and geological applications. *Geochim. Cosmochim. Acta*, **59**, 265-277.
- Chakraborty S. and J. Ganguly (1992) Cation diffusion in aluminosilicate garnets: experimental determination in spessartine-almandine diffusion couples, evaluation of effective binary diffusion coefficients and applications. *Contrib. Mineral. Petrol.* **111**, 74-86.
- Chekmir A. S., Persikov E. S., Epel'baum M. B., and Bukhtiyarov P. G. (1985) Hydrogen transport through a model magma. *Geokhimiya* **5**, 594-598.
- Chen, C.-H., DePaolo, D. J., Nakada, S. and Shieh, Y. N. (1993) Relationship between eruption volume and neodymium isotopic composition at Unzen volcano. *Nature*, **362**, 831-834.
- Cooper A. R. (1968) The use and limitations of the concept of an Effective Binary Diffusion Coefficient for multicomponent diffusion. In *Mass Transport in Oxides* (eds. J. Wachtman Jr. And A. D. Franklin); *NBS Spec. Publ.* **196**, 79-84.
- Crank J. (1975) The mathematics of diffusion, 2nd edition. *Clarendon press, Oxford* 414pp.
- Dalpe C. and Baker, D. R. (1995) Synchrotron X-ray fluorescence and Laser-Ablation ICP-MS microprobes: useful instruments for analysis of experimental run-products. *Can. Min.* **33**, 481-498.
- Dietzel A. (1942) Die Kationenfeldstärken und ihre Beziehungen zu Entglasungsvorgängen, zur Verbindungsbildung und zu den Schmelzpunkten von Silikaten. *Z. Elektrochem.* **48**, 9-23.
- Doremus R.H. (1995) Diffusion of water in silica glasses. *J. Mater. Res.* **10**, 2379-2389.

- Farges F., Munoz M., Siewert R., Malavergne V., Brown G. E. Jr., Behrens H. and Nowak M., Petit P. E. (2001): Transition elements in water-bearing silicate glasses/melts. Part II. Ni in water-bearing glasses. *Geochim. Cosmochim. Acta* **65**, 1679-1693.
- Fogel R. A. and Rutherford M. J. (1990) The solubility of carbon dioxide in rhyolitic melts: A quantitative FTIR study. *Am. Mineral.* **75**, 1311-1326.
- Ghiorso M. S. (1987) Chemical mass transfer in magmatic processes. III. Crystal growth, chemical diffusion and thermal diffusion in multicomponent silicate melts. *Contrib. Mineral. Petrol.* **96**, 291-313.
- Glasstone S., Laidler K. J. and Eyring H. (1941) Theory of Rate Processes. *McGraw-Hill, New York*.
- Grove T. L., Kinzler R. J., Baker M. B., Donnelly-Nolan J. M. and Lesher C. E. (1988) Assimilation of granite by basaltic magma at Burnt Lava flow, Medicine Lake volcano, northern California: Decoupling of heat and mass transfer. *Contrib. Mineral. Petrol.* **99**, 320-343.
- Gupta P. K. and Cooper A. R. (1971) The [D] matrix for multicomponent diffusion. *Physica*, **54**, 39-59.
- Haller M. and Knöchel A. (1996) X-ray fluorescence analysis using synchrotron radiation (SYXRF). *J. Trace Microprobe Techniques* **14**, 461-488.
- Hess K.-U. and Dingwell D. B. (1996) Viscosities of hydrous leucogranitic melts: A non-Arrhenian model. *Am. Mineral.* **81**, 1297-1300.
- Hinton R. W. (1995) Ion microprobe analysis in geology. In *Microprobe techniques in the Earth sciences* (eds. Potts P. J., Bowles J. W., Reed S. J. B. and Cave M. R.). Chapman and Hall, London pp. 235-289.
- Hofmann A. W. (1980) Diffusion in natural silicate melts: A critical review. In *Physics of magmatic processes* (ed. Hargraves R. B.), Princeton University Press, Princeton, New Jersey pp. 385-417.

- Holtz F., Roux J., Behrens H., Pichavant M. (2000) Water solubility in silica and quartzofeldspathic melts. *Am. Mineral.* **85**, 682-686.
- Hornig W., Hess P. C., and Gan H. (1999) The interactions between M^{+5} cations (Nb^{+5} , Ta^{+5} , or P^{+5}) and anhydrous haplogranite melts. *Geochim. Cosmochim. Acta* **63**, 2419-2428.
- Jambon A. (1982) Tracer diffusion in granitic melts: Experimental results for Na, K, Rb, Cs, Ca, Sr, Ba, Ce, Eu to 1300°C and a model of calculation. *J. Geophys. Res.* **87**, 10,797-10,810.
- Jambon A. (1979) Diffusion of water in a granitic melt: an experimental study. *Carnegie Inst. Washington, Year Book*, 352-355.
- Jambon A., Carron J. P. and Delbove F. (1978) Données préliminaires sur la diffusion dans les magmas hydratés : le césium dans un liquide granitique à 3 kbar. *C. R. Hebd. Séances Acad. Sci. Ser. D*, **287**, 404-406.
- Johannes W. and Bode B. (1978) Loss of iron to the Pt-container in melting experiments with basalts and a method to reduce it. *Contrib. Mineral. Petrol.* **67**, 221-225.
- Johnston W. D. (1965) Oxidation-reduction equilibria in molten $Na_2O \cdot 2SiO_2$ glass. *J. Am. Ceram. Soc.* **48**, 184-190.
- Keppler H. (1993) Influence of fluorine on the enrichment of high field strength trace elements in granitic rocks. *Contrib. Mineral. Petrol.* **114**, 479-488.
- Keppler H. (1992) Crystal field spectra and geochemistry of transition metal ions in silicate melts and glasses. *Am. Mineral.* **77**, 62-75.
- Khodzher, T.V., Obolkin, V. A., Potemkin, V. L., Bufetov, N. S., Tomza, U., Rahn, K. A. (2000) A study of trace elements in atmospheric aerosols of the Eastern Siberia using neutron activation and synchrotron radiation X-ray fluorescence analysis. *Nuc. Instr. and Meth. in Phys. Res.* **A448**, 413-418.
- Koepke J. and Behrens H. (2001) Trace element diffusion in andesitic melts: An application of synchrotron X-ray fluorescence analysis. *Geochim. Cosmochim. Acta* **65**, 1481-1498.

- Koepke J., Rocholl A., and Jantos N. (1998): Trace element microanalysis of hydrous silicate melts: The influence of water on SIMS and synchrotron-XRF analysis. *Terra Nova* **10**, Abstract Supplement 1, 31.
- Kress V. C. and Ghiorso M. S. (1993) Multicomponent diffusion in MgO-Al₂O₃-SiO₂ and CaO-MgO-Al₂O₃-SiO₂ melts. *Geochim. Cosmochim. Acta* **57**, 4453-4466.
- Kubicki, J. D., Muncill, G. E. and Lasaga, A. C. (1990) Chemical diffusion in melts on the CaMgSi₂O₆-CaAl₂Si₂O₈ join under high pressures. *Geochim. Cosmochim. Acta* **54**, 2709-2715.
- Kushiro I. (1976) Changes in viscosity and structure of melt of NaAlSi₂O₆ composition at high pressures. *J. Geophys. Res.* **81**, 6347-6350.
- Lange, R. A. (1994) The effect of H₂O, CO₂, and F on the density and viscosity of silicate melts. In *Volatiles in Magmas* (eds. M. R. Carroll and J. R. Holloway); *Rev. Mineral.* **30**, 331-369.
- Lapham, K. E., Holloway, J. R., Delaney, J. R. (1994) Diffusion of H₂O and D₂O in obsidian at elevated temperatures and pressures. *J. Non-Cryst. Solids* **67**, 179-191.
- Lasaga A. C. (1982) Toward a master equation in crystal growth. *Amer. J. Sci.* **282**, 1264-1288.
- LaTourette T. and Wasserburg G. J. (1997) Self diffusion of europium, neodymium, thorium, and uranium in haplobasaltic melt: The effect of oxygen fugacity and the relationship to melt structure. *Geochim. Cosmochim. Acta* **61**, 755-764.
- LaTourette T., Wasserburg G. J., and Fahey A. J. (1996) Self diffusion of Mg, Ca, Ba, Nd, Yb, Ti, Zr, and U in haplobasaltic melt. *Geochim. Cosmochim. Acta* **60**, 1329-1340.
- Lechtenberg, F., Garbe, S., Bauch, J., Dingwell, D. B., Freitag, J., Haller, M., Hansteen, T. H., Ippach, P., Knöchel, A., Radtke, M., Romano, C., Sachs, P. M., Schmincke, H.-U., and Ullrich, H.-J. (1996) The X-ray fluorescence measurement place at beamline L of HASYLAB. *J. trace and microprobe techniques*, **14(3)**, 561-587.

- Leshner C. E. (1994) Kinetics of Sr and Nd exchange in silicate liquids: Theory, experiments, and applications to uphill diffusion, isotopic equilibration, and irreversible mixing of magmas. *J. Geophys. Res.* **99**, 9585-9604.
- Liang Y., Richter F. M., Davis A. M. and Watson E. B. (1996) Diffusion in silicate melts: I. Self diffusion in CaO-Al₂O₃-SiO₂ at 1500°C and 1GPa. *Geochim. Cosmochim. Acta* **60**, 4353-4367.
- Linnen R. L., Pichavant M., and Holtz F. (1996) The combined effects of f_{O₂} and melt composition on SnO₂ solubility and tin diffusivity in haplogranitic melts. *Geochim. Cosmochim. Acta* **60**, 4965-4976.
- Linnen R.L., Pichavant M., Holtz F., Burgess S. (1995) The effect of f(O₂) on the solubility, diffusion and speciation of tin in haplogranitic melt at 850 °C and 2 kbar. *Geochim. Cosmochim. Acta*, **59**, 1579-1588.
- Magaritz M. and Hofmann A. W. (1978a) Diffusion of Sr, Ba, and Na in obsidian. *Geochim. Cosmochim. Acta* **42**, 595-605.
- Magaritz M. and Hofmann A. W. (1978b) Diffusion of Eu and Gd in basalt and obsidian. *Geochim. Cosmochim. Acta* **42**, 847-858.
- Metson, J. B., Tui, D. C., Muir, I. J. and Bancroft, G. M. (1988) High secondaries for the quantitative secondary ion mass spectrometric analysis of minerals. *Scanning microscopy*, **2**, 663-670.
- Mungall J. E., Dingwell D. B., and Chaussidon M. (1999) Chemical diffusivities of 18 trace elements in granitoid melts. *Geochim. Cosmochim. Acta* **63**, 2599-2610.
- Mungall J. E., Romano C. and Dingwell D. B. (1998) Multicomponent diffusion in the molten system K₂O-Na₂O-Al₂O₃-SiO₂-H₂O. *Am. Mineral.* **83**, 685-699.
- Mungall J. E. and Dingwell D. B. (1997) Actinide diffusion in a haplogranitic melt: Effects of temperature, water content, and pressure. *Geochim. Cosmochim. Acta* **61**, 2237-2246.

- Mysen, B. O. and Virgo, D. (1985) Structure and properties of fluorine-bearing aluminosilicate melts: The system $\text{Na}_2\text{O}-\text{Al}_2\text{O}_3-\text{SiO}_2-\text{F}$ at 1 atm. *Contrib. Mineral. Petrol.* **91**, 205-220.
- Mysen, B. O. and Virgo, D. and Scarfe, C. (1980) Relation between the anionic structure and viscosity of silicate melts: A Raman spectroscopic study. *Am. Min.* **65**, 900-914.
- Nakamura E. and Kushiro I. (1998) Trace element diffusion in jadeite and diopside melts at high pressures and its geochemical implication. *Geochim. Cosmochim. Acta* **62**, 3151-3160.
- Nickel, K. G., Brey, G. P. and Kogarko L. (1985) Orthopyroxene-clinopyroxene equilibria in the system $\text{CaO}-\text{MgO}-\text{Al}_2\text{O}_3-\text{SiO}_2$ (CMAS): new experimental results and implications for two-pyroxene thermometry. *Contrib. Mineral. Petrol.* **91**, 44-53.
- Nowak M. and Behrens H. (2001): Water in magmas: a slippery problem gets more grip. *Earth Planet. Sci. Letters* **184**, 515-522.
- Nowak M. and Behrens H. (1997) An experimental investigation on diffusion of water in haplogranitic melts. *Contrib. Mineral. Petrol.* **126**, 365-376.
- Ochs F. and Lange R. (1999) The density of hydrous magmatic liquids. *Science* **283**, 1314-1317.
- Ohlhorst S., Behrens H. and Holtz F. (2001) Compositional dependence of molar absorptivities of near-infrared OH and H_2O bands in rhyolitic to basaltic glasses. *Chem. Geol.* **174**, 5-20.
- Perez W. A. and Dunn T. (1996) Diffusivity of strontium, neodymium, and lead in natural rhyolite melt at 1.0 GPa. *Geochim. Cosmochim. Acta* **60**, 1387-1397.
- Persikov E. S., Zharikov V. A., Bukhtiyarov P. G. and Pol'skoy S. F. (1990) The effect of volatiles on the properties of magmatic melts. *Eur. J. Mineral.* **2**, 621-642.

- Pouchou J. L. and Pichoir F. (1991) Quantitative analysis of homogeneous or stratified microvolumes applying the model "PAP". In *Electron probe quantification* (eds. K. F. J. Heinrich and D. E. Newbury), Plenum Press, New York. pp. 31-75.
- Puziewicz J. and Johannes W. (1988) Phase equilibria and composition of Fe-Mg-Al minerals and melts in water-saturated peraluminous granitic systems. *Contrib. Mineral. Petrol.* **100**, 156-168.
- Ratajeski K. and Sisson T.W. (1999) Loss of iron to gold capsules in rock melting experiments. *Am. Mineral.* **84**, 1521-1527.
- Richet P., Whittington A., Holtz F., Behrens H., Ohlhorst S., Wilke M. (2000) Water and the density of silicate glasses. *Contrib. Mineral. Petrol.* **138**, 337-347.
- Richet P., Lejeune A. M., Holtz F. and Roux J. (1996) Water and the viscosity of andesite melts. *Chem. Geol.* **128**, 185-197.
- Roselieb K. and Jambon A. (1997) Tracer diffusion of Potassium, Rubidium and Cesium in a supercooled jadeite melt. *Geochim. Cosmochim. Acta* **61**, 3101-3110.
- Rothman S. J., Marcuso T. L. M., Nowicki L. J., Baldo P. M. and McCormick A. W. (1982) Diffusion of alkali ions in vitreous silica. *J. Amer. Ceram. Soc.* **65**, 578-582.
- Roux, J. and Lefevre, A. (1992) A fast rapid quench device for internally heated pressure vessel. *Eur. J. Mineral.* **4**, 279-281.
- Schreiber H. D., Thanyasari T., Lach J. J., and Legere, R. A. (1978) Redox equilibria of Ti, Cr, Eu in silicate melts: Reduction potentials and mutual interactions. *Phys. Chem. Glasses*, **9**, 126-139.
- Schulze F., Behrens H., Holtz F., Roux J., and Johannes W. (1996) The influence of H₂O on the viscosity of a haplogranitic melt. *Am. Miner.* **81**, 1155-1165.
- Shannon R. D. (1976) Revised effective ionic radii and systematic studies of interatomic distances in halides and chalcogenides. *Acta Crystallogr. A* **32**, 751-767.

- Shaw H. R. (1972) Viscosities of magmatic silicate liquids: An empirical method of prediction. *Amer. Jour. Sci.* **272**, 870-893.
- Sisson T. W. and Grove T. L. (1993a) Experimental investigations of the role of H₂O in calc-alkaline differentiation and subduction zone magmatism. *Contrib. Mineral. Petrol.* **113**, 143-166.
- Smith J. V. and Rivers M. L. (1995) Synchrotron X-ray microanalysis. In *Microprobe techniques in the Earth sciences* (eds. P. J. Potts, J. F. W. Bowles, S. J. B. Reed, and M. R. Cave), Chapman & Hall, London. pp. 163-233.
- Snyder D. and Tait S. (1998) The imprint of basalt on the geochemistry of silicic magmas. *Earth Planet. Sci. Lett.* **160**, 433-445.
- Stevenson R. J., Dingwell D. B., Webb S. L. and Bagdassarov N. S. (1995) The equivalence of enthalpy and shear stress relaxation in rhyolitic obsidians and quantification of the liquid-glass transition in volcanic processes. *J. Volcanol. Geotherm. Res.* **68**, 297-306.
- Stolper, E. (1982) The speciation of water in silicate melts. *Geochim. Cosmochim. Acta* **46**, 2609-2620.
- Tamic N., Behrens H., and Holtz F. (2001) The solubility of H₂O and CO₂ in rhyolitic melts in equilibrium with a mixed CO₂-H₂O fluid phase. *Chem. Geol.* **174**, 333-347.
- Tarasov, L. S., Kudryashova, A. F., Ulyanov, A. A., Baryshev, V. B., Zolotarev, K. V. (1998) Geochemistry of trace elements in the highland lunar rocks based on SRXFA data. *Nuc. Instr. and Meth. in Phys. Res. A* **405**, 590-598.
- Taylor, J.R., Wall, V.J., and Pownceby, M.I. (1992) The calibration and application of accurate redox sensors. *Am. Min.* **77**, 284-295.
- Trial A. F. and Spera F. J. (1990) Mechanisms for the generation of compositional heterogeneities in magma chambers. *GSA Bulletin* **102**, 353-367.

- Vanko, D. A., Bonnin-Mosbah, M., Philippot, P., Roedder, E., Sutton, S. R. (2001) Fluid inclusions in quartz from oceanic hydrothermal specimens and the Bingham, Utah porphyry-Cu deposit: a study with PIXE and SXRF. *Chem. Geol.* **173**, 227-228.
- Van der Laan S., Zhang Y., Kennedy A. K. and Wyllie P. J. (1994) Comparison of element and isotope diffusion of K and Ca in multicomponent silicate melts. *Earth Planet. Sci. Lett.* **123**, 155-166.
- Van Espen P. J., Nullens H., and Adams F. (1977) A computer analysis of X-ray fluorescence spectra. *Nucl. Instr. Meth.* **145**, 579-582.
- Wasserburg G. J. (1988) Diffusion of water in silicate melts. *Jour. Geol.* **96**, 363-367.
- Watson E. B. (1994) Diffusion in volatile-bearing magmas. In *Volatiles in Magmas* (eds. M. R. Carroll and J. R. Holloway); *Rev. Mineral.* **30**, 371-411.
- Watson E. B. (1991) Diffusion of dissolved CO₂ and Cl in hydrous silicic and intermediate magmas. *Geochim. Cosmochim. Acta* **55**, 1897-1902.
- Watson E. B. and Baker D. R. (1991) Chemical diffusion in magmas: an overview of experimental results and geochemical implications. In: *Advances in Physical Geochemistry, Springer, 6, I: Kusiro and L. Perchuk, eds.*, 120-151
- Watson E. B. (1982) Basalt contamination by continental crust: some experiments and models. *Contrib. Mineral. Petrol.* **80**, 73-87.
- Watson E. B. (1981) Diffusion in magmas at depth in the earth: The effects of pressure and dissolved H₂O. *Earth Planet. Sci. Lett.* **52**, 291-301.
- White B. S. and Montana A. (1990) The effect of H₂O and CO₂ on the viscosity of sanidine liquid at high pressures. *Jour. Geophys. Res.* **95**, 15683-15693.
- Wilke M. and Behrens H. (1999) The dependence of the partitioning of iron and europium between plagioclase and hydrous tonalitic melt on oxygen fugacity. *Contrib. Mineral. Petrol.* **137**, 102-114.

- Withers A. C. and Behrens H. (1999) Temperature induced changes in the NIR spectra of hydrous albitic and rhyolitic glasses between 300 and 100 K. *Phys. Chem. Minerals* **27**, 119-132.
- Zhang Y. and Behrens H. (2000) H₂O diffusion in rhyolitic melts and glasses. *Chem. Geol* **169**, 243-262.
- Zhang Y. (1999) H₂O in rhyolitic glasses and melts: Measurement, speciation, solubility, and diffusion. *Rev. Geophys.* **37**, 493-516.
- Zhang Y. and Behrens H. (1998) H₂O diffusion in silicate glasses and melts. *Min. Mag.* **62A**, 1695-1696.
- Zhang Y., Belcher, R., Ihnger, P. D., Wang L., Xu Z. and Newman S. (1997) New calibration of infrared measurements of water in rhyolitic glasses. *Geochim. Cosmochim. Acta* **61**, 3089-3100.
- Zhang Y. (1993) A modified effective binary diffusion model. *J. Geophys. Res.* **11**, 901-11, 920
- Zhang Y., Walker D. and Lesher C. E. (1989) Diffusive crystal dissolution. *Contrib. Mineral. Petrol.* **102**, 492-513.

8. TABLES

Table 1a: Chemical composition of anhydrous starting materials.

	EDF (Rhyolite)	Al ¹	A2 ²	A3 ³	Unzen (Dacite)	AD1 ⁴	AD2	AD3
SiO ₂	77.04 ± 0.77	76.44 ± 0.61	83.31 ± 0.51	77.85 ± 0.55	65.19 ± 0.67	67.15 ± 0.27	72.04 ± 0.50	67.31 ± 0.28
TiO ₂	0.11 ± 0.01	n.a.	0.26 ± 0.07	n.a.	0.65 ± 0.15	0.69 ± 0.04	0.81 ± 0.05	0.68 ± 0.03
Al ₂ O ₃	12.76 ± 0.13	13.22 ± 0.29	10.77 ± 0.16	12.85 ± 0.22	15.29 ± 0.49	15.47 ± 0.21	13.23 ± 0.12	15.10 ± 0.16
FeO ⁵	0.68 ± 0.07	0.62 ± 0.06	0.51 ± 0.04	0.84 ± 0.06	4.68 ± 0.19	2.63 ± 0.18	2.35 ± 0.25	2.54 ± 0.30
MnO	0.07 ± 0.01	0.09 ± 0.04	0.07 ± 0.05	0.04 ± 0.03	n.a.	0.13 ± 0.07	0.09 ± 0.06	0.09 ± 0.06
MgO	0.08 ± 0.01	0.07 ± 0.02	0.07 ± 0.05	0.06 ± 0.02	2.11 ± 0.15	1.84 ± 0.06	1.58 ± 0.05	1.82 ± 0.13
CaO	0.58 ± 0.06	0.63 ± 0.04	0.42 ± 0.02	0.63 ± 0.04	4.84 ± 0.28	4.88 ± 0.09	4.28 ± 0.09	4.84 ± 0.27
Na ₂ O	4.07 ± 0.02	4.05 ± 0.17	1.53 ± 0.22	2.83 ± 0.19	3.65 ± 0.16	3.02 ± 0.23	2.79 ± 0.33	3.40 ± 0.20
K ₂ O	4.79 ± 0.24	4.67 ± 0.15	2.84 ± 0.08	4.05 ± 0.11	2.52 ± 0.13	2.34 ± 0.11	2.00 ± 0.10	2.36 ± 0.13
Total	100.18	99.79	99.78	99.15	99.01	98.15	99.17	98.14
NBO/T ⁶	0.02	0.01	0.04	0.03	0.14	0.11	0.11	0.13

Notes:

Compositions were analysed by electron microprobe. H₂O contents were measured by IR.

Standard deviation corresponds to 10 – 20 analysis for each sample.

n.a. = not analysed.

EDF = natural obsidian from Erivan Dry Fountain Armenia.

Unzen = natural dacite from the Unzen Volcano.

¹ Al1 = Synthesised glass with EDF-like composition.

² A2 = Synthesised glass enriched with about 5 wt% SiO₂ and 0.3 wt% TiO₂.

³ A3 = Synthesised glass doped with 300-500 ppm of trace elements.

⁴ AD1-3 = Synthesised glass with Unzen-like composition.

⁵ All iron as FeO.

⁶ NBO/T = 2 (O-2H) / T, with H as netforming cations and O as oxygen after Mysen et al. (1980).

Table 1b: Chemical composition of hydrous starting materials

	A1_2 ¹	A2_2	A3_2	A1_5 ²	A2_5	A3_5	AD1_2	AD2_2	AD3_2
SiO ₂	75.92 ± 0.42	85.87 ± 0.47	74.91 ± 0.38	72.59 ± 0.58	80.08 ± 0.40	74.86 ± 0.31			
TiO ₂	n.a.	0.15 ± 0.04	n.a.	n.a.	0.23 ± 0.31	n.a.			
Al ₂ O ₃	12.23 ± 0.22	8.19 ± 0.83	12.49 ± 0.07	11.68 ± 0.12	10.16 ± 0.35	12.38 ± 0.11			
FeO ³	0.73 ± 0.10	0.46 ± 0.05	0.63 ± 0.15	0.65 ± 0.11	0.55 ± 0.11	0.75 ± 0.09			
MnO	0.08 ± 0.01	0.02 ± 0.01	0.12 ± 0.01	0.13 ± 0.03	0.03 ± 0.01	0.07 ± 0.03			
MgO	0.07 ± 0.02	0.04 ± 0.01	0.06 ± 0.03	0.04 ± 0.01	0.04 ± 0.01	0.05 ± 0.01			
CaO	0.52 ± 0.03	0.32 ± 0.05	0.52 ± 0.06	0.54 ± 0.03	0.35 ± 0.07	0.58 ± 0.04			
Na ₂ O	4.00 ± 0.17	1.45 ± 0.03	2.91 ± 0.06	3.74 ± 0.20	1.55 ± 0.04	2.70 ± 0.04			
K ₂ O	4.15 ± 0.07	2.00 ± 0.22	3.78 ± 0.02	3.90 ± 0.04	2.41 ± 0.40	3.82 ± 0.09			
H ₂ O ⁴	1.76	1.95	2.06	5.03	4.76	4.12			
H ₂ O ⁵	1.96	2.15	2.45	5.15	5.15	4.94			
Total	99.64 ± 0.18	100.6 ± 0.32	97.91 ± 0.78	98.43 ± 0.36	100.2 ± 1.32	100.2 ± 0.40			
NBO/T	0.14	0.13	0.16	0.41	0.34	0.35			

¹ A1-3_2 correspond to hydrous glasses containing 2 wt% H₂O

² A1-3_5 correspond to hydrous glasses containing 5 wt% H₂O

³ Iron as FeO.

⁴ H₂O analysed using KFT-analysis.

⁵ H₂O analysed using IR-spectroscopy.

Table 2: Diffusion coefficients in $\log D$ (D in m^2/s) for rhyolitic melts at 500 MPa with up to 2 wt % H_2O .

Run	D_30 long	D_29short	D_31 long	D_4 short	D_2 long	D_22 short	D_21 long	D_24 short	D_12 short
T [°C]	1200	1250	1400	1100	1100	1200	1200	1250	1400
t_{dwell} [min]	3600	1200	1440	420	5760	100	7200	70	30
$t_{\text{heat/cool}}$ [min] ¹	1.68-4.48	1.79-4.76	2.15-5.65	2.3-3.8	2.3-3.8	2.6-4.3	2.6-4.3	2.9-5.1	3.3-5.5
$\text{Eu}^{2+}/\text{Eu}_{\text{total}}$ ²	0.57	0.43	0.42	-	0.02	0.06	0.13	0.01	0.05
$a_{\text{H}_2\text{O}}$ ³	0.020	0.020	0.020	0.212	0.212	0.216	0.216	0.218	0.225
ΔNNO ⁴	-1.6	-1.6	-1.6	+2.4	+2.4	+2.5	+2.5	+2.5	+2.5
$\text{H}_2\text{O}[\text{wt}\%]^{\text{A3/A1/A2}}$	0.21/0.19/0.18	0.17/0.16/0.17	0.23/0.18/0.23	1.83/1.88/1.83	1.15/1.28/1.57	1.83/1.91/1.95	1.93/1.86/1.88	1.88/1.91/1.91	1.83/1.77/1.86
Trace element diffusion coefficient (tracer diffusion)									
Rb	-11.65±0.28	-11.54±0.16	-11.18±0.25	-10.97±0.12	-10.74±0.09	-10.74±0.09	-10.74±0.09	-10.51±0.08	-10.21±0.12
Sr	-12.02±0.26	-11.90±0.14	-11.41±0.23	-11.33±0.13	-11.33±0.32	-11.10±0.08	-11.27±0.25	-10.79±0.09	-10.64±0.13
Ba	-12.52±0.22	-12.40±0.16	-11.63±0.24	-11.20±0.14	-11.38±0.07	-11.38±0.07	-11.64±0.25*	-10.85±0.14	-10.55±0.17
Zn	-13.63±0.18	-13.61±0.24	-	-	-	-	-	-	-
Co	-13.34±0.20	-13.56±0.15	-12.45±0.19	-12.20±0.12	-12.23±0.19	-12.09±0.11	-12.64±0.13	-11.84±0.29	-11.45±0.10
Ni	-14.52±0.22	-12.50±0.20	-12.50±0.20	-12.85±0.23	-12.84±0.28	-12.62±0.23	-12.64±0.13	-12.00±0.15	-12.00±0.15
Cu	-15.39±0.18	-15.13±0.24	-13.57±0.21	-12.82±0.25	-12.88±0.24	-13.13±0.45*	-12.63±0.14	-12.32±0.18	-12.32±0.18
Cr	-12.56±0.31	-13.01±0.28	-13.01±0.28	-13.01±0.36*	-12.87±0.29	-12.59±0.21	-12.63±0.14	-11.61±0.31	-11.61±0.31
V	-14.56±0.27	-14.50±0.19	-14.50±0.19	-12.76±0.27	-12.60±0.28	-12.41±0.19	-12.34±0.18	-12.13±0.18	-11.54±0.26
La	-14.38±0.15	-14.24±0.21	-12.42±0.17	-12.85±0.23	-12.84±0.28	-12.31±0.16	-12.34±0.18	-12.16±0.16	-11.64±0.16
Nd	-14.28±0.17	-14.11±0.22	-12.37±0.18	-12.82±0.25	-12.88±0.24	-12.46±0.24	-12.31±0.16	-12.19±0.19	-11.59±0.24
Sm	-14.38±0.14	-14.26±0.19	-12.45±0.15	-13.01±0.36*	-12.87±0.29	-12.51±0.19	-12.35±0.19	-12.21±0.15	-11.68±0.22
Eu	-12.26±0.22	-12.26±0.16	-11.74±0.22	-12.26±0.19	-12.60±0.19	-12.13±0.15	-11.96±0.23	-12.17±0.12	-11.51±0.25
Gd	-14.47±0.15	-14.35±0.23	-12.50±0.15	-13.07±0.28	-12.78±0.27	-12.64±0.18	-12.35±0.25	-12.19±0.15	-11.71±0.19
Y	-14.54±0.12	-14.40±0.19	-12.52±0.14	-12.99±0.27	-12.69±0.19	-12.59±0.27	-12.49±0.12	-12.31±0.29	-11.81±0.21
Er	-14.52±0.20	-14.34±0.24	-12.56±0.18	-13.06±0.22	-13.20±0.26	-12.81±0.23	-12.95±0.27	-12.61±0.18	-12.12±0.29
Yb	-14.52±0.22	-14.45±0.27	-12.61±0.21	-13.09±0.26	-13.20±0.26	-12.80±0.28	-12.35±0.22	-11.89±0.22	-11.89±0.22
Sn	-13.27±0.25	-13.09±0.22	-12.28±0.20	-12.07±0.10	-12.39±0.36	-11.85±0.19	-11.51±0.15	-11.51±0.15	-11.51±0.15
Ge	-14.43±0.17	-14.48±0.27	-13.11±0.15	-12.89±0.17	-12.89±0.17	-12.85±0.26*	-12.50±0.13	-12.41±0.25	-11.70±0.27
Hf	-15.13±0.18	-14.84±0.31	-13.23±0.20	-12.89±0.17	-12.89±0.17	-12.85±0.26*	-12.45±0.13	-12.21±0.29	-11.55±0.38
Zr	-15.25±0.14	-15.04±0.24	-13.43±0.17	-13.43±0.17	-13.43±0.17	-13.43±0.17	-12.98±0.17	-12.62±0.21	-12.05±0.26
Nb	-14.89±0.15	-14.77±0.27	-13.02±0.17	-13.43±0.17	-12.74±0.15	-12.53±0.19	-12.53±0.19	-12.03±0.21	-11.36±0.36
Al	-15.19±0.14	-15.08±0.22	-13.87±0.15	-14.15±0.20	-14.15±0.20	-14.15±0.20	-13.31±0.18	-13.24±0.20	-12.82±0.25
Si	-15.18±0.23	-15.10±0.26	-13.84±0.18	-14.16±0.22	-14.16±0.22	-14.16±0.22	-13.04±0.21	-13.21±0.23	-12.76±0.31
Ti	-15.02±0.17	-14.73±0.20	-13.25±0.15	-13.88±0.17	-13.88±0.17	-13.88±0.17	-12.98±0.18	-13.14±0.19	-12.71±0.29
$\log D_{\text{H}}$ ⁶	-15.45	-15.10	-13.92	-14.21	-14.36	-13.56	-13.59	-13.32	-12.66

¹ $t_{\text{heat/cool}}$ [s] were calculated individually for each cation using activation energies summarized in Tab.4. (lowest value = Si, highest value = Rb.)

² $\text{Eu}^{2+}/\text{Eu}_{\text{total}}$ ratios were calculated with D of Sr and an average of D of Sm and D of Gd. See also in the text.

³

⁴

⁵ Three values of total H_2O were measured by IR at the contact planes A3/A1, in the middle part of A1 and at the contact plane A1/A2 of the diffusion triple after the experiments.

⁶ $\log D_{\text{H}}$ is calculated by the viscosity model of Hess and Dingwell (1996) using the Eyring equation with a jump distance of 3 Å and H_2O contents at the contact plane A1/A2.

Table 3: Diffusion coefficients in $\log D$ (D in m^2/s) for hydrous rhyolitic melts with nominal 5 wt % H_2O .

Run	D_15 short	D_16 long	D_3 short	D_1 long	D_18 short	D_17 long	D_11 short	D_9 long
T [°C]	800	800	1100	1100	1200	1200	1400	1400
t _{dwell} [min]	3000	21600	120	5760	100	2700	30	270
t _{heat/cool} [min]	1.8-4.2	1.8-4.2	2.9-6.6	2.9-6.6	3.3-7.5	3.3-7.5	4.2-9.3	4.2-9.3
Eu ²⁺ /Eu _{total}	-	-	0.19	0.09	-	0.17	0.24	-
a _{H₂O}	0.540	0.540	0.563	0.563	0.574	0.574	0.598	0.598
Δ NNO	+3.2	+3.2	+3.3	+3.3	+3.3	+3.3	+3.4	+2.0
H ₂ O[wt %]	5.14/5.07/4.99	5.15/4.97/4.86	5.05/4.97/4.99	4.55/4.67/4.79	5.01/4.98/5.11	4.99/4.84/4.93	4.92/4.98/5.15	4.21/4.31/3.99
%[A3/A1/A2]								
Trace element diffusion coefficient (tracer diffusion)								
Rb	-10.91±0.16	-11.73±0.41*	-10.56±0.12	-10.42±0.23	-9.99±0.16	-13.43±0.31*	-9.93±0.14	-10.55±0.42*
Sr	-11.88±0.13	-13.49±0.53*	-10.96±0.13	-10.75±0.25	-10.44±0.21	-10.70±0.23*	-10.48±0.17	-10.57±0.39
Ba	-12.12±0.15	-13.99±0.42*	-11.18±0.12	-10.86±0.21	-10.66±0.17	-11.47±0.31*	-10.57±0.18	-11.22±0.38*
Zn	-12.22±0.15	-	-	-	-11.14±0.15	-	-	-
Co	-12.90±0.16	-13.10±0.21	-11.76±0.12	-12.05±0.21	-11.30±0.21	-10.75±0.41*	-10.99±0.18	-10.95±0.22
Ni	-13.92±0.30	-13.92±0.34	-	-9.11±0.48*	-	-11.85±0.25	-	-
Cu	-14.71±0.19	-	-	-12.57±0.16	-	-12.29±0.26	-	-
Cr	-13.37±0.44	-13.45±0.52	-	-11.79±0.26	-	-13.59±0.47*	-	-
V	-13.89±0.28	-13.55±0.31	-12.35±0.19	-12.18±0.25	-11.91±0.27	-11.63±0.15	-	-11.62±0.21
La	-14.24±0.22	-	-12.24±0.12	-12.08±0.14	-	-11.19±0.17	-11.13±0.22	-11.52±0.31
Nd	-14.22±0.24	-13.87±0.20	-12.24±0.15	-12.08±0.18	-11.59±0.19	-10.95±0.41*	-11.13±0.18	-11.37±0.24
Sm	-14.18±0.26	-13.93±0.32	-12.37±0.20	-12.07±0.22	-	-10.95±0.36	-11.53±0.12	-12.00±0.41*
Eu	-13.52±0.22	-13.74±0.24	-11.62±0.18	-11.64±0.35	-	-11.08±0.31	-11.01±0.13	-13.30±0.47*
Gd	-14.26±0.21*	-13.56±0.36	-12.38±0.15	-12.17±0.15	-11.73±0.15	-11.66±0.26	-11.24±0.21	-11.58±0.22
Y	-13.93±0.16	-14.06±0.21	-	-12.27±0.19	-11.83±0.21	-11.22±0.31	-11.23±0.18	-11.91±0.31*
Er	-13.94±0.25	-13.96±0.34	-12.48±0.13	-12.10±0.24	-11.89±0.27	-11.43±0.31	-11.62±0.13	-12.50±0.41*
Yb	-13.92±0.43	-14.32±0.35	-12.57±0.17	-12.23±0.33	-	-11.97±0.32	-11.54±0.25	-12.32±0.44*
Sn	-12.67±0.19	-11.79±0.38*	-11.70±0.15	-12.17±0.31	-	-10.57±0.40	-10.82±0.17	-11.13±0.21
Ge	-14.31±0.22	-11.14±0.37*	-13.27±0.24	-13.18±0.14	-11.62±0.29*	-12.42±0.29	-12.16±0.42	-11.34±0.31
Hf	-14.34±0.21	-13.43±0.29*	-13.03±0.31	-12.67±0.24	-11.62±0.29	-	-11.83±0.32	-12.16±0.22
Zr	-14.48±0.15	-	-13.13±0.19	-12.99±0.14	-12.47±0.24	-12.00±0.31*	-11.75±0.24	-12.16±0.21
Nb	-14.23±0.22	-12.58±0.38*	-12.84±0.25	-12.71±0.15	-12.26±0.22	-11.71±0.39*	-11.59±0.31	-12.22±0.23
Effective binary diffusion coefficients (chemical diffusion)								
Al	-14.77±0.18	-	-13.02±0.22	-13.01±0.16	-	-12.45±0.17	-12.13±0.26	-12.15±0.17
Si	-14.89±0.21	-	-12.89±0.24	-12.69±0.21	-	-12.74±0.19	-12.11±0.31	-12.14±0.19
Ti	-14.02±0.20	-	-12.77±0.21	-12.79±0.19	-	-12.27±0.25	-12.12±0.26	-12.02±0.19
log D _n	-15.11	-15.17	-13.14	-13.18	-12.67	-12.70	-11.95	-12.13

Table 4: Arrhenian parameters for rhyolitic melts.

elements	Charge	anhydrous nominal (0.16-0.23 wt% H ₂ O) 1200 – 1400°C			2 wt% H ₂ O nominal (1.15-1.93 wt% H ₂ O) 1100 – 1400°C			5 wt% H ₂ O nominal (3.99-5.15 wt% H ₂ O) 800 – 1400°C		
		E _a [KJ/mol]	log D ₀	profiles	E _a [KJ/mol]	log D ₀	profiles	E _a [KJ/mol]	log D ₀	profiles
Tracer Diffusion										
Rb	+1	112±5	-7.68±0.16	3	116±10	-6.57±0.35	4	59 ±14	-8.11±0.54	5
Sr	+2	147±12	-6.83±0.41	3	107±22	-7.28±0.80	6	83 ±18	-7.74±0.68	7
Ba	+2	218±32	-4.84±1.07	3	121±23	-6.89±0.54	4	94 ±15	-7.49±0.57	5
Co	+2/+3	241±119	-5.01±3.99	3	111±15	-8.02±0.53	5	107±13	-7.81±0.50	6
V	+3/+5	-	-	2	165±18	-6.44±0.66	5	127±11	-7.49±0.43	6
La	+3	489±102	-2.77±3.42	3	177±7	-6.08±0.25	6	165±18	-6.05±0.68	6
Nd	+3	474±90	-2.37±3.05	3	175±14	-6.14±0.51	6	165±11	-5.97±0.44	7
Sm	+3	483±105	-2.55±3.53	3	185±13	-5.87±0.47	5	153±16	-6.57±0.65	6
Eu	+2/+3	132±36	-7.64±1.23	3	149±23	-6.87±0.15	5	160±17	-5.75±0.71	6
Gd	+3	493±107	-2.81±3.62	3	180±26	-6.07±0.92	6	164±16	-6.13±0.61	7
Y	+3	504±106	-3.15±3.57	3	150±21	-7.15±0.76	6	161± 4	-6.18±0.18	6
Er	+3	486±91	-2.56±3.08	3	148±18	-7.56±0.62	6	143±12	-6.95±0.50	7
Yb	+3	481±116	-2.32±3.91	3	174±46	-6.45±0.63	4	163±19	-6.30±0.74	6
Sn	+2/+4	240±23	-4.81±0.79	3	183±23	-5.30±0.93	4	99 ±21	-8.00±0.78	6
Ge	+4	339±105	-2.60±3.55	3	231±20	-4.50±0.72	3	161±20	-6.73±0.60	5
Hf	+4	464±59	-1.21±1.99	3	196±9	-5.44±0.32	4	144±14	-7.37±0.57	6
Zr	+4	449±74	-0.53±2.49	3	205±13	-5.65±0.44	4	155±12	-7.03±0.46	5
Nb	+3/+5	467±100	-1.50±3.38	3	210±37	-4.86±0.29	4	150± 8	-6.99±0.32	5
Chemical Diffusion										
Al	+3	328± 64	-3.67±2.17	3	197±30	-6.61±1.05	4	156±12	-7.10±0.47	6
Si	+4	335± 73	-3.42±2.48	3	207±31	-6.23±1.06	4	160±21	-6.94±0.80	6
Ti	+4	431± 50	-0.16±1.69	3	172±17	-7.32±0.58	4	119±9	-8.24±0.35	6

Table 5: Diffusion coefficients in $\log D$ (D in m^2/s) for hydrous dacitic melts with nominal 2 or 5 wt % H_2O .

Run	PCH14	PCH16	PCH15	PC13	PC_6 short	PC_4 long	PC_9 short	PC_10 long
P [MPa]	100	250	500	1000	1000	1000	1000	1000
T [°C]	1200	1200	1200	1400	1200	1200	1300	1300
t dwell [min]	45	30	30	5	180	3600	60	720
Eu ²⁺ /Eu _{total}	0.11	0.09	0.04	-	0.24	0.25	0.11	-
H ₂ O[wt%] _{A3/A1/A2}	4.78/5.01/4.96	4.66/4.97/4.93	4.81/5.05/4.85	4.75/4.98	2.32/2.05	2.03/1.89	2.25/2.11	1.99/1.87
Rb	-10.14±0.21	-9.91±0.13	-9.99±0.20*	-9.32±0.19	-10.80±0.17	-11.41±0.28	-10.24±0.13	-10.86±0.31
Sr	-10.15±0.20	-10.08±0.10	-10.13±0.24	-9.33±0.16	-11.34±0.18	-11.41±0.28	-10.63±0.08	-10.86±0.31
Ba	-10.20±0.19	-10.20±0.12	-10.44±0.23	-9.37±0.14	-11.32±0.14	-12.01±0.24	-10.86±0.14	-10.86±0.31
Zn	-10.36±0.18	-10.32±0.20		-9.43±0.29	-11.68±0.31	-11.93±0.29	-11.14±0.27	-11.23±0.25
Co	-10.60±0.20	-10.61±0.14	-10.71±0.21	-9.28±0.25	-11.69±0.19	-12.28±0.24	-10.84±0.23	-10.83±0.29
Ni	-10.44±0.23	-10.50±0.19	-10.61±0.18	-9.40±0.31				
Cu		-11.61±0.26	-11.94±0.20	-10.24±0.33	-12.00±0.32	-12.55±0.21	-12.14±0.33	
Cr	-9.70±0.24	-10.63±0.25					-11.68±0.36	
V	-10.42±0.22	-10.71±0.24		-9.64±0.22				
La	-10.57±0.20	-10.79±0.17	-11.15±0.19	-9.58±0.18	-11.54±0.17	-11.73±0.23	-11.34±0.19	-11.35±0.21
Nd	-10.66±0.21	-10.72±0.18	-11.05±0.18	-9.56±0.21	-11.51±0.13	-11.71±0.22	-11.33±0.10	-11.37±0.20
Sm	-10.62±0.24	-10.80±0.17	-11.11±0.19		-11.63±0.19	-11.78±0.25	-11.41±0.14	-11.39±0.21
Eu	-10.55±0.20	-10.70±0.14	-11.03±0.21	-9.59±0.19	-11.53±0.15	-11.65±0.31	-11.21±0.17	-11.24±0.28
Gd	-10.67±0.23	-10.83±0.17	-11.27±0.18	-9.66±0.24	-11.60±0.19	-11.77±0.21	-11.40±0.17	-11.41±0.17
Y	-10.65±0.19	-10.86±0.14	-11.26±0.19	-9.65±0.26	-11.61±0.22	-11.69±0.18	-11.39±0.14	-11.39±0.14
Er	-10.67±0.25	-10.89±0.20	-11.26±0.21	-9.68±0.29	-11.56±0.21	-11.79±0.25	-11.36±0.18	-11.46±0.22
Yb	-10.74±0.28	-10.87±0.21	-11.17±0.22	-9.73±0.29	-11.58±0.24	-11.85±0.26	-11.48±0.26	-11.46±0.25
Sn	-10.55±0.19	-10.58±0.17	-11.13±0.20	-9.55±0.18	-11.67±0.18		-11.05±0.15	-11.08±0.27
Ge		-11.58±0.24	-12.02±0.17			-12.50±0.16	-12.21±0.29	-12.23±0.17
Hf	-10.51±0.29	-11.28±0.26	-11.78±0.20	-10.07±0.33		-12.37±0.21	-12.01±0.31	-11.95±0.19
Zr		-11.36±0.23	-11.83±0.14			-12.26±0.17	-11.72±0.27	-11.87±0.15
Nb		-11.22±0.24	-11.62±0.17	-9.89±0.34		-12.01±0.19	-11.72±0.25	-11.72±0.19

¹ PCH experiments were run as diffusion triples in the IHPV. Chemical diffusion was not analyzed so far.

Table 6: Apparent activation volumes (V_a) for dacitic melts.

element	charge	ionic radius	5 wt% H ₂ O nominal (4.66-5.05 wt% H ₂ O) 100 -500 MPa (1200°C)	profiles
		$r_{ion}[pm]$	$V_a[cm^3/mol]$	$\log D_0$
Rb	+1		-7.08±1.44	-10.09±0.17
Sr	+2	126	-0.69±0.49	-10.13±0.06
Ba	+2	142	17.96±7.18	-10.10±0.08
Co	+2/+3	65 (2+)	8.12±2.49	-10.56±0.03
Ni	+2	69	12.03±0.30	-10.40±0.00
La	+3	116	40.87±0.20	-10.43±0.00
Nd	+3	114	28.49±6.88	-10.52±0.08
Sm	+3	108	34.60±0.30	-10.50±0.00
Eu	+2/+3	107 (3+)	34.19±2.39	-10.42±0.03
Gd	+3	105	43.06±5.18	-10.49±0.06
Y	+3	102	43.23±1.50	-10.49±0.02
Er	+3	100	41.62±0.10	-10.52±0.00
Yb	+3	99	30.68±2.49	-10.62±0.03
Sn	+2/+4	45 (4+)	43.06±14.96	-10.32±0.17
Hf	+4	83	86.17±23.43	-10.32±0.27

Table 7: Tracer diffusion data determined by SIMS analysis in comparison to SYXRF.

Run	D_22				D_18			
	(rhyolitic, 1200°C, 2 wt % H ₂ O, 100min)		(rhyolitic, 1200°C, 5 wt % H ₂ O, 100min)		(rhyolitic, 1200°C, 2 wt % H ₂ O, 100min)		(rhyolitic, 1200°C, 5 wt % H ₂ O, 100min)	
Method Profile ¹	SIMS 1 st 50 μm	SIMS 2 nd 50 μm	SIMS Short 25 μm	SYXRF 30 μm	SIMS 1 st 50 μm	SIMS 2 nd 50 μm	SIMS Short 25 μm	SYXRF 30 μm
¹³³ Cs	-11.36±0.11	n.a.	n.a.		-10.41±0.18	n.a.	n.a.	
⁸⁵ Rb	n.a.	-10.78±0.09	n.a.	-10.74±0.09	-10.29±0.21	-10.13±0.21	n.a.	-9.99±0.16
⁸⁸ Sr	-12.60±0.17	-11.15±0.07	n.a.	-11.10±0.08	-11.50±0.25	-10.56±0.09	n.a.	-10.44±0.21
¹³⁸ Ba	-12.42±0.24	-11.38±0.11	n.a.	-11.38±0.07	-11.28±0.24	-10.71±0.10	n.a.	-10.66±0.17
⁶⁴ Zn	n.a.	n.a.	-11.81±0.16		n.a.	n.a.	-11.09±0.17	-11.14±0.15
⁶⁶ Zn	n.a.	n.a.	-11.76±0.28		n.a.	n.a.	-12.32±0.19	
⁵⁹ Co	n.a.	n.a.	-11.71±0.19	-12.09±0.11	n.a.	n.a.	-10.93±0.22	-11.30±0.21
⁵⁸ Ni	-11.65±0.21	n.a.	n.a.	-12.62±0.23	-10.77±0.21	-10.71±0.21	n.a.	
⁶³ Cu	-12.23±0.25	n.a.	n.a.	-11.04±0.26	-11.04±0.26	-10.43±0.28	n.a.	-12.57±0.16
¹³⁹ La	n.a.	n.a.	-12.40±0.16	-12.31±0.16	n.a.	n.a.	-11.53±0.08	
¹⁴⁰ Ce	-12.42±0.30	-12.33±0.21	n.a.		-11.30±0.27	-11.63±0.15	n.a.	
¹⁴⁷ Sm	-12.42±0.33	-12.41±0.14	n.a.	-12.51±0.19	-11.37±0.30	-11.70±0.20	n.a.	
¹⁵¹ Eu	-11.86±0.15	-11.95±0.20	n.a.	-12.13±0.15	-10.97±0.20	-11.24±0.17	n.a.	
¹⁵³ Eu	-12.49±0.14	-11.92±0.24	n.a.		-11.37±0.30	-11.27±0.15	n.a.	
¹⁵⁸ Gd	-11.48±0.24	-12.53±0.24	n.a.	-12.64±0.18	-11.39±0.27	-11.70±0.23	n.a.	-11.73±0.15
⁸⁹ Y	n.a.	n.a.	-12.60±0.16	-12.59±0.27	n.a.	n.a.	-11.90±0.05	-11.83±0.21
¹⁷⁴ Yb	-12.85±0.28	-12.58±0.24	n.a.	-12.80±0.28	-11.60±0.27	-11.78±0.24	n.a.	
⁷⁴ Ge	n.a.	n.a.	-13.29±0.18		n.a.	n.a.	n.a.	
¹⁸⁰ Hf	-13.29±0.25	-13.34±0.25	-13.44±0.22		-12.37±0.18	-12.61±0.24	n.a.	-11.62±0.29
⁹⁰ Zr	-13.53±0.25	-13.36±0.19	-13.39±0.24		-12.19±0.19	-12.43±0.20	n.a.	-12.47±0.24
⁹³ Nb	-13.28±0.26	-12.99±0.27	-13.02±0.23		-12.26±0.20	-12.26±0.23	n.a.	-12.26±0.22
¹⁸¹ Ta	-12.68±0.17	-13.33±0.27	-13.43±0.22		-11.46±0.21	-12.54±0.20	-12.90±0.22	-10.83±0.34

¹ For reproducibility two different sessions at SIMS were done on each sample with a profile distance of 30 μm. Short profiles were analyzed in a third session with a smaller beam spot and longer counting time. (details see text).

Lebenslauf:

Name: Astrid Sabine Tegge-Schüring

Geburtsdatum: 19. Juli 1971

Staatsangehörigkeit: deutsch

Familienstand: verheiratet seit 06.07.1995

Kinder: Ben Luca Schüring, geb. 11.02.2002
Carla Louise Schüring, geb. 11.02.2002

Schulbildung:

1978 - 1982 Grundschule in Twistringen

1982 - 1988 Gymnasium Liebfrauenschule in Vechta
Abschluß: Erweiterter Sekundarabschluß 1

1988 - 1992 Berufsfachschule in Minden
Abschluß: Ingenieurassistentin für Chemietechnik
und Allgemeine Hochschulreife

Hochschulstudium

1992 – 1998 Studium der Mineralogie an der Universität Hannover
Schwerpunkt: Experimentelle Petrologie und Geochemie
Abschluß: Diplom-Mineralogin

1997 - 1998 Thema der Diplomarbeit:
Dehydration-Melting Experimente mit synthetisiertem Monazit zur
Untersuchung von Spurenelementverteilungen in den Granat- und
Schmelzphasen.

1998 – 2001 Wissenschaftliche Mitarbeiterin am Institut für Mineralogie,
Universität Hannover mit Anfertigung der Dissertation

1999 – 2001 Mitarbeit in der Arbeitsgruppe um Prof. Dr. Y. Zhang am
Department of Geology,
University of Michigan in Ann Arbor, USA

10. Juli 2002 Tag der Promotion

